Heat and Mass Transfer during Solid-Liquid Phase Transition of *n*-Alkanes in the C_{16} to C_{19} Range

Rune Holmen

Thesis submitted in partial fulfillment
of the requirements for the degree of

Doktor Ingeniør

Dept. of Applied Mechanics, Thermodynamics and Fluid Dynamics
The Norwegian University of Science and Technology

URN:NBN:no-3317

Preface

This work was accomplished at the Department of Applied Mechanics, Thermodynamics and Fluid Dynamics at the Norwegian University of Science and Technology (NTNU). The study started in January 1998 and ended in February 2001. The thesis was financed by STATOIL and the Research Council of Norway(NFR).

While carrying out this work, I have been employed by the Foundation of Scientific and Industrial Research, SINTEF.

I am indepted to my supervisors Associate Professor Ole Melhus, NTNU and PhD. Harald Førdedal, STATOIL for their guidance. Professor B.F. Magnussen was appointed as assisting supervisor.

The guidance of Professor Magne Lamvik was instrumental in the realization of the experimental work. Without him this work would not have been feasible.

Thanks to all my colleges at NTNU-SINTEF for making the department an interesting place to spend time. A special thank to Erling Mikkelsen, who gladly assisted me in the laboratory.

Thanks to Mette Løvås, who not only helped proofread the manuscript but also became my wife.

Abstract

The main goal of this project has been to study heat and mass transfer during solid-liquid phase transition of *n*-alkanes in the in the C_{16} to C_{19} range. Phase transitions of both mixtures and pure components have been investigated.

All experiments and simulations have been performed without any convection.

Thermal conductivities have been determined at the melting point for solid and liquid unbranched alkanes ranging from C_{16} to C_{19}. An assessment of the error of the method has been performed.

The measurements of solid conductivities are in accordance with measurements reported previously and confirm the applicability of the method. Liquid conductivities are higher than extrapolated values from the literature. The enhanced conductivity is believed to be caused by structural changes close to the melting point which is not taken into account when extrapolating values from the literature.

Experiments have been performed for the purpose of investigating the freezing of mixtures of *n*-alkanes in the C_{16}-C_{19} range. The positions of the solid-liquid interfaces have been measured as freezing occured.

Calculations of the ratio of liquid and solid conductivities show that the solid structure of mixtures of the investigated *n*-alkanes is predominantly in a rotator structure at the temperatures investigated. There are indications of a transformation into an orthorhombic structure at lower temperatures.

The temperatures on the solid-liquid interface have been measured, and compared with calculated values from chapter 4. The temperature of the interface

is represented better by the measured interfacial temperatures than by the calculated interfacial temperatures.

The experimental results indicate that the diffusion of heat is the limiting mechanism of phase transition. This result in a homogeneous liquid composition.

A numerical model has been developed in order to simulate the experimental freezing of mixtures. The model represents the results of the experiments within the limit of the uncertainties of the physical properties and the interfacial temperature.

Also the numerical model suggests that the solid structure is predominantly in a rotator structure at the temperatures investigated. The properties of the rotator phase are represented better by the physical properties of solid C_{17} than by molar averages.

The results from the simulations support the hypothesis that the limiting mechanism of deposition is the diffusion of heat to the interface. This implies that further work should focus on the determination of the thermophysical properties of solid wax instead of further development of models for the solid-liquid equilibrium.

Contents

Symbols

Latin Symbols

Symbol	Description	Dimension
a	variable used in calculations	
C	Concentration	mol m^{-3}
C_{no}	number of carbon atoms	
C_p	heat capacity at constant pressure	J kg^{-1} K^{-1}
D	diffusion coefficient	m^2 s^{-1}
f	fugacity	Pa
F	amount of feed	mol
g	specific Gibbs energy	J mol^{-1}
G	Gibbs energy	J
h	enthalpy	J mol^{-1}
H	total height of experimental cell	m
J	Flux of species	mol s^{-1} m^{-2}
k	thermal conductivity	W K^{-1} m^{-1}
K	ratio between solid and liquid mole fraction at equilibrium	
l	parameter used in calculation of the interaction energy	
L	amount of liquid	mol
Le	Lewis number	
Li^n	position of liquid calculation volume number n	m
Li^n_B	position of bottom of liquid calculation volume number n	m
LT	total number of liquid calculation volumes	

Latin Symbols, cont.

Symbol	Description	Dimension
M_r	molar mass	kg mol^{-1}
n	amount of substance	mol
P	pressure	Pa
Ph	Stephan number	
R	gas constant	8.314 J mol^{-1} K^{-1}
s	specific entropy	J mol^{-1} K^{-1}
s^i	mole fraction of component i in the solid phase	
S	amount of solid	mol
Si^n	position of solid calculation volume number n	m
Si^n_B	position of bottom of solid calculation volume number n	m
ST	total number of solid calculation volumes	
t	time	s
T	temperature	K
U	interaction energy	J mol^{-1}
v	molar volume	m^3 $mol^{-}1$
v_w	van der waals volume	m^3 $mol^{-}1$
x	height/position	m
x^i	mole fraction of component i in the liquid phase	
x_{mp}	height of solid-liquid interface	m
z^i	mole fraction of component i in the feed	

Greek Symbols

Symbol	Description	Dimension
α	parameter used in determination of the interaction energy	
γ	activity coefficient	
Δi	change of property i	
θ	parameter used in determination of the liquid activity coefficient	
λ	parameter used in determination of the interaction energy	
μ	chemical potential	J mol^{-1}
ρ	density	kg m^{-3}
σ	standard deviation	
Φ	fugacity coefficient	
ω	mass fraction	

Subscript

Symbol	Description
0	at the bottom of the regarded area
B	at the bottom of the calculation volume
c	critical property
$excess$	difference between ideal and real
H	at the top of the regarded area
$ideal$	ideal contributions
inf	infinite dilution
l	liquid
liq	liquidus
m	mass fixed reference system
mix	at mixing of components
mp	at melting point, i.e. solid-liquid phase border
r	reduced property
s	solid
ss	solid-solid phase transition
sub	sublimation
t	at the triple point
v	volume fixed reference system
w	van der Waals volume
vap	at evaporation

Superscript

Symbol	Description
*	ideal gas
^{0}	pure component
^{calc}	calculated property
$^{C_{16}}$	unbranched hexadecane
$^{C_{17}}$	unbranched heptadecane
$^{C_{18}}$	unbranched octadecane
$^{C_{19}}$	unbranched nonadecane
^{i}	component i
^{j}	component j
^{long}	the longest molecule of a pair
^{LT}	top liquid calculation volume
^{meas}	measured property
^{n}	calculation volume number n
^{p}	at previous timestep
^{short}	the shortest molecule of a pair
ST	top solid calculation volume
^{tot}	total i.e: sum of all components

Chapter 1

Introduction

1.1 Background and Purpose

During transportation and production of crude oils, heavy components, i.e. wax, tend to deposit on the walls of pipelines and process equipment. This deposition of wax may induce reduced capacity and eventually plugging of pipelines. This problem is particularly present during transportation of crude oils in a cold environment, as in the North Sea.

Different measures are taken against this deposition. One approach has been to develop wax interaction modifiers [1], another suggestion [2] is to let the oil go through heat and cooling cycles in order to develop wax crystals which can easily be pumped. However, the most common remedy is to increase the frequency of the pigging.

The deposited wax is a mixture of different hydrocarbons, but a substantial part [3],[4], consists of n-paraffinic waxes. Among these waxes are the components studied in this work.

Solidification/melting of equivalent components has also found applications as heat carriers or thermal storage materials. More exotic utilizations are temperature regulated clothes [5] and heat storage aboard space vehicles [6]. Since the melting points of the studied components are close to room temperature, they are often used as model substances in fundamental experiments

on solid-liquid phase transitions [7].

Much work has been carried out to model the solid-liquid equilibria of petroleum waxes. A review of such models can be found in Pauly, Dauphin and Daridon [8] or in Coutinho, Andersen and Stenby [9].

The main goal of this project has been to study heat and mass transfer during solid-liquid phase transition of *n*-alkanes in the in the C_{16} to C_{19} range. Phase transitions of both mixtures and pure components have been investigated.

Thermal conductivities of the pure components have been measured during solidification/melting, and the experiments done on mixtures have been tested against numerical simulations. All experiments and simulations have been performed without any convection.

1.2 Basic Concepts and Conditions

The definition of wax depends on the point of view. Basic textbooks of organic chemistry, such as Hart [10], define wax as lipids that differ from fats and oils in being simple monoesters. In the petroleum industry, everything with a waxy feel and look is termed wax, and it is this latter definition which will be applied in this work.

Saturated unbranched hydrocarbons i,e: n-$C_{16}H_{34}$, n-$C_{17}H_{36}$ etc., will be referred to as C_{16} and C_{17}.

SI-units are used throughout this work. Energy units are on a molar basis.

All symbols which are not explained in the running text will be found in the list of symbols.

1.3 Organization of the Thesis

1.3.1 Overview

The thesis is organized in chapters which may be read independently, but references to other chapters may occur.

1.3.2 Chapter 2 : Theory

In this chapter the basic physical models required to explain heat and mass transfer during solid-liquid phase transition are presented. In addition, a brief discussion on the solid structure of wax is presented.

1.3.3 Chapter 3: Thermal Conductivities of Pure Solid and Liquid *n*-Alkanes during Phase Transition

This chapter presents thermal conductivities for both solid and liquid unbranched alkanes ranging from C_{16} to C_{19}. The thermal conductivities are measured with a method giving both liquid and solid thermal conductivities at the temperature of phase transition.

An assessment of the error of the method is performed. The measurements of solid conductivities are in accordance with measurements reported previously. Liquid conductivities are higher than extrapolated values from the literature. This is believed to be caused by incipient solidification.

1.3.4 Chapter 4: Calculation of Solid-Liquid Equilibrium

In general, equilibrium is assumed when studying solid-liquid phase transitions. Even though the main topic of this thesis is transport processes which are not at equilibrium, models for the equilibria are required.

Since the phase envelopes for the mixtures studied here are not available, the solid-liquid equilibria must be calculated. Equations for the liquidus are necessary in subsequent work and will also be presented in this chapter.

1.3.5 Chapter 5: Experimental Investigation of Wax Deposition from Mixtures

After having dealt with wax deposition from pure components without convection in chapter 3 the next natural step on the path toward a model for deposition of wax from crude oils is the introduction of mixtures.

In this chapter the experimental results will be reported. The experimental setup used here is the same as used in chapter 3. The apparatus is described in detail in appendix B.

The results from the experiments preformed will not only be used to verify numerical models of transient freezing, but also to determine which solid structure is formed when mixtures crystallize. This can be done by calculating the ratio between the solid and liquid conductivities.

1.3.6 Chapter 6: Numerical Modeling

The final topic in this thesis is to simulate freezing of mixtures of *n*-alkanes in the C_{16}-C_{19} range. The initial and boundary conditions will be chosen in order to imitate the conditions of the experiments reported in chapter 5.

The basis of the numerical procedure is described by Versteeg and Malalasekera [11] and Patankar[12].

The simulations will be used to test different hypothesis regarding physical properties and mechanisms.

Chapter 2

Theory

2.1 Introduction

In this chapter the basic physical models required to explain heat and mass transfer during solid-liquid phase transition are presented.

In addition to the physical models, a brief discussion on the structure of solid wax and mixtures of solid wax is presented.

Even though some of the formulations found in this chapter may be new for the reader, all the material in this chapter is based on previously published work. If a more detailed explanation is desired, one should consult these references.

2.2 Heat Transfer

2.2.1 Heat Transfer During Solid-Liquid Phase Transition

Considering a situation as illustrated in Fig. 2.1, Lamvik and Zhou [13] gave Neumann's general condition at the phase interface as:

$$-k_s \frac{\partial T_s}{\partial x} + k_l \frac{\partial T_l}{\partial x} + \rho \frac{\Delta h_{mp}}{M_r} \frac{dx_{mp}}{dt} = 0 \tag{2.1}$$

This equation, Eq. (2.1), is simply derived from a heat balance across the control volume marked with a broken line in Fig. (2.1).

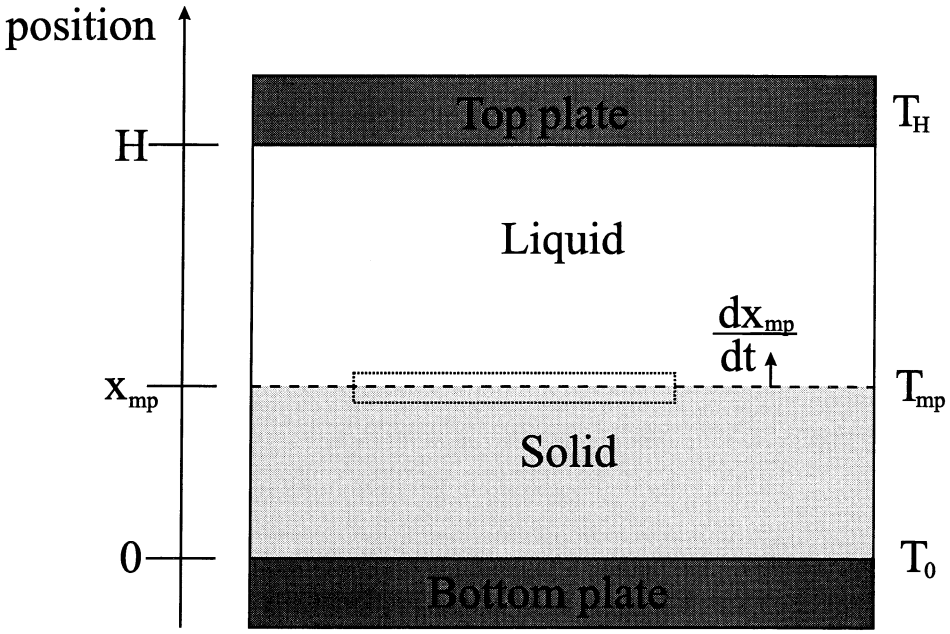

Figure 2.1: Schematic illustration of phase transition

where ρ is the density of the disappearing phase, k_s and k_l are solid and liquid conductivity respectively and Δh_{mp} is the enthalpy of phase transition. Assuming that the temperature at the bottom, T_0 is lower than at the top, T_H, the temperature gradients in the solid, $\frac{\partial T_s}{\partial x}$, and in the liquid, $\frac{\partial T_l}{\partial x}$, are both positive. During freezing the position of the interface, x_{mp}, is moving upward, i.e: the speed of the interface, $\frac{dx_{mp}}{dt}$ is positive.

Eq. (2.1) can be simplified by choosing proper experimental conditions, i.e. melting or freezing with temperature gradient only in the appearing phase.

No thermal gradient in the liquid phase gives:

$$k_s = \rho_l \frac{\Delta h_{mp}}{M_r} \frac{dx_{mp}}{dt} \left(\frac{\partial T_s}{\partial x} \right)^{-1} \tag{2.2}$$

Assuming melting and no thermal gradient in solid phase, one finds:

$$k_l = -\rho_s \frac{\Delta h_{mp}}{M_r} \frac{dx_{mp}}{dt} \left(\frac{\partial T_l}{\partial x} \right)^{-1} \tag{2.3}$$

Introducing steady state in Eq. (2.1), the ratio of the conductivities appears as:

$$\frac{k_l}{k_s} = \frac{\frac{\partial T_s}{\partial x}}{\frac{\partial T_l}{\partial x}} \tag{2.4}$$

2.2.2 Heat Transfer in a Single Phase

Assuming no fluid flow and only one dimension, the equation for heat flow as given by White [14], can be formulated as:

$$\rho \frac{\partial \frac{h}{M_r}}{\partial t} = \frac{\partial}{\partial x} k \frac{\partial T}{\partial x} \tag{2.5}$$

Assuming no phase change and constant heat capacity, $\partial h = C_p \partial T$, gives:

$$\rho \frac{C_p}{M_r} \frac{\partial T}{\partial t} = \frac{\partial}{\partial x} k \frac{\partial T}{\partial x} \tag{2.6}$$

2.3 Composition

2.3.1 Solid-Liquid Equilibrium

2.3.1.1 Solid-Liquid Equilibrium Ratio

On the solid-liquid interface, the compositions at equilibrium can be found by calculating the solid-liquid equilibrium ratio. Since the expression for this ratio is expressed differently by different investigators, a derivation of this ratio is carried out here.

It is an ordinary starting point for equilibrium that the chemical potential of the components are equal in both phases:

$$\mu_s^i = \mu_l^i \tag{2.7}$$

The chemical potential can be defined as:

$$\mu^i = \frac{\partial G^{tot}}{\partial n^i}|_{T,P,n^j} \tag{2.8}$$

Where G^{tot} can be expressed as:

$$G^{tot} = (G^0 - G^{*,0}) + G^{*,0} + \underset{mix}{\Delta} G_{ideal} + \underset{mix}{\Delta} G_{excess} \tag{2.9}$$

Using that:

$$\frac{\partial \underset{mix}{\Delta} G_{ideal}}{\partial n^i} = RT \ln x^i \tag{2.10}$$

and the definitions :

$$RT \ln \Phi^{i,0} = \frac{\partial (G^0 - G^{*,0})}{\partial n^i} \tag{2.11}$$

and

$$RT \ln \gamma^i = \frac{\partial \underset{mix}{\Delta} G_{excess}}{\partial n^i} \tag{2.12}$$

One finds that μ^i can be expressed as:

$$\mu^i = g^{i,*} + RT \ln \gamma^i \Phi^{i,0} x^i \tag{2.13}$$

Returning to the starting point, Eq. (2.7), using the above expression, a solution for the fraction between the pure component fugacity coefficients is:

$$\frac{s^i \gamma_s^i}{x^i \gamma_l^i} = \frac{\Phi_l^{i,0}}{\Phi_s^{i,0}} \tag{2.14}$$

Using the definition of the fugacity coefficient and differentiating:

$$RT \ln \frac{\Phi_l^{i,0}}{\Phi_s^{i,0}} = g_l^{i,0} - g_s^{i,0} \tag{2.15}$$

The liquid state referred to here, a subcooled liquid, is normally not a physically viable state and should consequently be considered as a hypothetical state used only in calculations.

The difference in Gibbs energy can be calculated following a path as shown in Fig. (2.2) outlined by Prausnitz [15].

The change in Gibbs energy going from pure solid at temperature T (point A) to pure liquid at the same temperature (point D) can be expressed as:

$$g_l^{i,0} - g_s^{i,0} = \underset{A \to D}{\Delta g^{i,0}} = \underset{A \to D}{\Delta h^{i,0}} - T \underset{A \to D}{\Delta s^{i,0}} \tag{2.16}$$

Assuming that the solid does not change phase, and that the effect of pressure on the properties of the solid and the liquid can be neglected, one obtains for the enthalpy change:

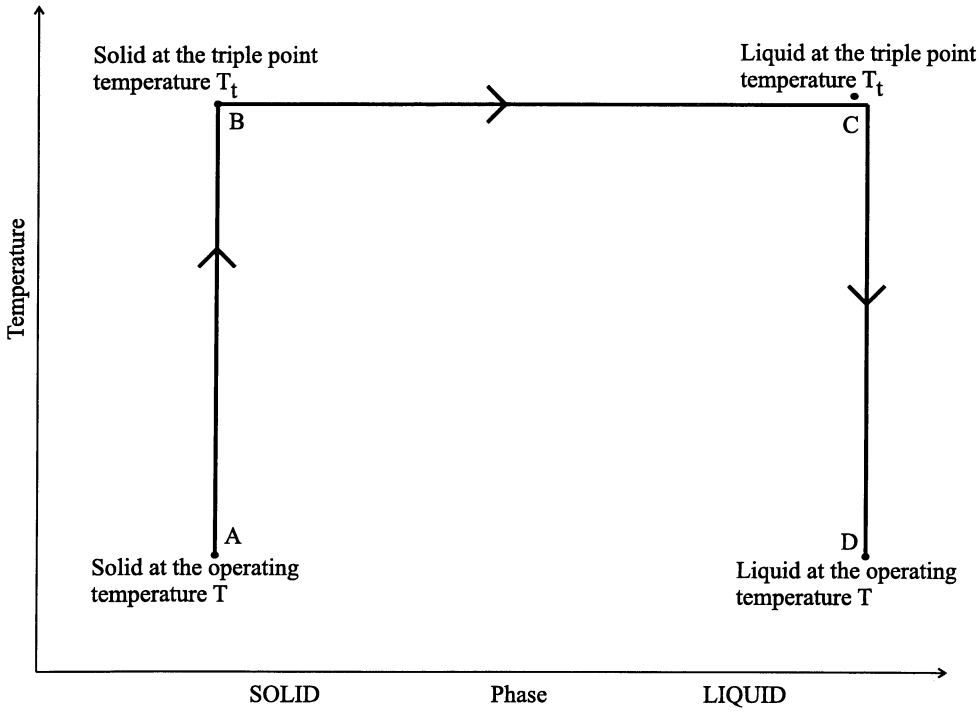

Figure 2.2: Thermodynamic cycle for calculating the fugacity of a pure subcooled liquid. (from Prausnitz [15])

$$\underset{A\to D}{\Delta h^{i,0}} = \underset{A\to B}{\Delta h^{i,0}} + \underset{B\to C}{\Delta h^{i,0}} + \underset{C\to D}{\Delta h^{i,0}} = \Delta h^{i,0}_{mp} + \int_{T_t}^{T} \Delta C_p^{i,0} dT \tag{2.17}$$

where $\Delta C_p^{i,0} = C_{p,l}^{i,0} - C_{p,s}^{i,0}$.

The change in entropy is calculated equivalently:

$$\underset{A\to D}{\Delta s^{i,0}} = \underset{A\to B}{\Delta s^{i,0}} + \underset{B\to C}{\Delta s^{i,0}} + \underset{C\to D}{\Delta s^{i,0}} = \frac{\Delta h^{i,0}_{mp}}{T_t} + \int_{T_t}^{T} \frac{\Delta C_p^{i,0}}{T} dT \tag{2.18}$$

Introducing the last two equations (2.18) and (2.17) into (2.16), one finds:

$$\underset{A\to D}{\Delta g^{i,0}} = \Delta h^{i,0}_{mp} + \int_{T_t}^{T} \Delta C_p^{i,0} dT - T\left(\frac{\Delta h^{i,0}_{mp}}{T_t} + \int_{T_t}^{T} \frac{\Delta C_p^{i,0}}{T} dT\right) \tag{2.19}$$

Eq. (2.19) used in Eqs. (2.14,2.15) gives:

$$K^i = \frac{s^i}{x^i} = \frac{\gamma_l^i}{\gamma_s^i} \exp\left[\frac{\Delta h_{mp}^{i,0}}{RT_t}\left(\frac{T_t}{T} - 1\right) + \frac{\Delta C_p^{i,0}}{R}\left(1 - \frac{T_t}{T} + \ln\frac{T_t}{T}\right)\right] \tag{2.20}$$

2.3.1.2 Liquid Activity Coefficient

In order to solve Eq.(2.20) one needs a model for γ_s^i and γ_l^i. Coutinho Andersen and Stenby [9] present a model for the liquid activity coefficient based on a Flory free-volume model, which can be described as:

$$\ln \gamma_l^i = \ln\frac{\theta^i}{x^i} + 1 - \frac{\theta^i}{x^i} \tag{2.21}$$

where

$$\theta^i = \frac{x^i((v^i)^{\frac{1}{3}} - (v_w^i)^{\frac{1}{3}})^{3.3}}{\sum_j x^j((v^j)^{\frac{1}{3}} - (v_w^j)^{\frac{1}{3}})^{3.3}} \tag{2.22}$$

2.3.1.3 Solid Activity Coefficient

The activity coefficient is defined in Eq.(2.12):

$$RT \ln \gamma^i = \frac{\partial \overset{\Delta}{_{mix}} G_{excess}}{\partial n^i} \tag{2.23}$$

Wilson's model for excess energy can be presented as:

$$\overset{\Delta}{_{mix}} G_{excess} = -RT \sum_i s^i \ln \sum_j s^j e^{\frac{-U^{ij}}{RT}} \tag{2.24}$$

giving :

$$\ln \gamma^i = -\ln(\sum_j s_j e^{\frac{-U^{ji}}{RT}}) - \sum_j \frac{s_j(e^{\frac{-U^{ji}}{RT}} - \sum_k x_k e^{\frac{-U^{jk}}{RT}})}{(\sum_k x_k e^{\frac{-U^{jk}}{RT}})} \tag{2.25}$$

Coutinho et al. [16] have developed a model for U^{ij} for mixtures of solid wax.

Since U^{ij} is a measure of the interaction energy, i.e. the energy to separate two different molecules:

$$U^{ii} = 0 \tag{2.26}$$

But U^{ij} is modeled as:

$$U^{ij} = \lambda^{ij} - \lambda^{ii} \tag{2.27}$$

where:

$$\lambda^{ii} = -\frac{1}{3}(\Delta h_{sup} - RT) \tag{2.28}$$

Δh_{sup} refers to the enthalpy connected to a transition from an orthorhombic structure to vapor. λ^{ij} is found as:

$$\lambda^{ij} = \lambda^{ji} = \lambda^{short,short}(1 - \alpha^{short-long}) \tag{2.29}$$

The superscripts *short* and *long* refer to the relative lengths of the molecules in question.

$$\alpha^{short-long} = -73,98\frac{(l^{long} - l^{short})^2}{(l^{short})^3} + 0.01501 \tag{2.30}$$

Finally the expression for l^i is given as:

$$l^i = 1.270 * C^i_{no} + 1.98 \tag{2.31}$$

2.3.2 Diffusion

The term diffusion is not a precise term. It can refer to transport of heat or mass induced by gradients in pressure, temperature, external force field or chemical potential.

Only diffusion in liquids will be discussed in this work.

Excellent discussions of diffusion are presented by Reid and Prausnitz [17] and Dysthe [18].

2.3.2.1 Diffusion Coefficients

Reid and Prausnitz [17] define the diffusion coefficient as the proportionality constant between the flux and the diffusion potential. One must also define which flux and diffusion potential to use.

One of the most confusing aspects of diffusion is the choice of reference frame. For binary mixtures, Dysthe [18] shows that the diffusion flux, assuming a mass fixed reference system, can be calculated using:

$$J_m^i = -D^{ij} \frac{\rho}{M_r} \frac{\partial \omega^i}{\partial x} \tag{2.32}$$

The diffusion coefficient in this expression is chosen such that it is equivalent to the diffusion coefficient in the usual definition, which is a volume fixed reference system:

$$J_v^i = -D^{ij} \frac{\partial C^i}{\partial x} \tag{2.33}$$

Reid and Prausnitz [17] denote D^{ij} introduced in Eq. (2.32) as the mutual diffusion coefficient which is a measure of the diffusion, or rate of mixing, of one component in a binary system.

The tracer diffusion coefficient, D_{inf}^i, of a component is a measure of the diffusion of a labeled molecule within a homogenous mixture. The tracer

diffusion of component i in pure i is also called self-diffusion coefficient, $D_{inf}^{i,0}$.

The relation between the different coefficients is shown in Fig.. (2.3). One should note that the tracer diffusion of component i in pure j is equal to the mutual diffusion coefficient, $D^{i,j}$.

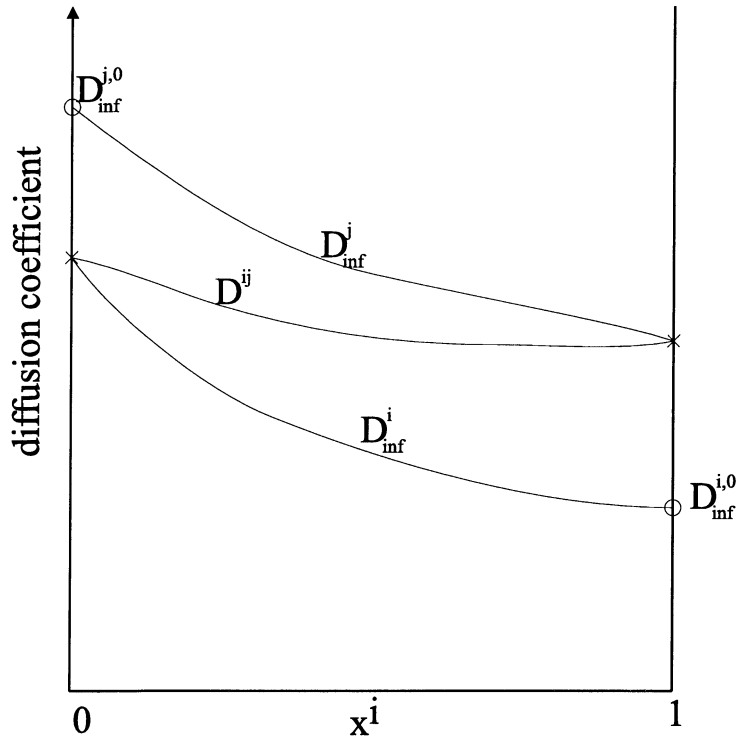

Figure 2.3: Mutual self and tracer diffusion coefficients in a binary mixture (after Reid and Prausnitz [17] and Dysthe [18])

2.4 Solid Structure of Wax

2.4.1 Solid Structure of Pure Components

A characteristic and well-known phenomenon of the *n*-alkanes in the range investigated in this work is the odd-even effect. The *n*-alkanes with an even

number of carbon atoms are better packed in the solid phase than the *n*-alkanes with an odd number of carbon atoms. According to Forsman and Andersson [19] this effect is due to the zig-zag configuration forcing the two methyl end groups in odd-numbered alkanes to be parallel.

The structures of odd-numbered alkanes, i.e: C_{17} and C_{19}, at temperatures just below the melting temperature are called rotator phases and are characterized, by Sirota [20], as lamellar crystals lacking long-range order in the rotational degree of freedom of the molecules about their long axes. When the temperature is lowered further, experimental investigations done by Zerbi et al. [21] have shown that the structure is changed into a orthorhombic structure. For C_{19}, both Zerbi et al [21] and Taylor et al [22] have found that this change occurs at 295.95 K. C_{17} change into an orthorhombic structure at 284.22 K [23].

The even-numbered alkanes, C_{16} and C_{18}, on the other hand, crystallize directly into a triclinic structure. This structure is denser and more orderly structured than the corresponding rotator phases of the odd numbered alkanes. No additional change of structure occurs as the temperature is lowered further.

2.4.2 Solid Structure of Mixtures

The solid structures of binary mixtures of *n*-alkanes have been studied by several investigators.

Maroncelli, Strauss and Snyder [24] have investigated the structure of the binary C_{19}-C_{21} system by infrared spectroscopy and calorimetry. They have shown that the structure of a solid mixture of odd numbered *n*-alkanes is not qualitatively different from the pure component structure.

Like the pure components, these mixtures solidify in rotator phase before settling into an orthorhombic structure on further cooling. Mazee's [25] work on the binary system C_{21}-C_{21} confirms this behavior.

Dirand et al [26] report solid phase diagrams for binary mixtures of *n*-alkanes with between 22 to 26 carbon atoms. All mixtures crystallize into rotator

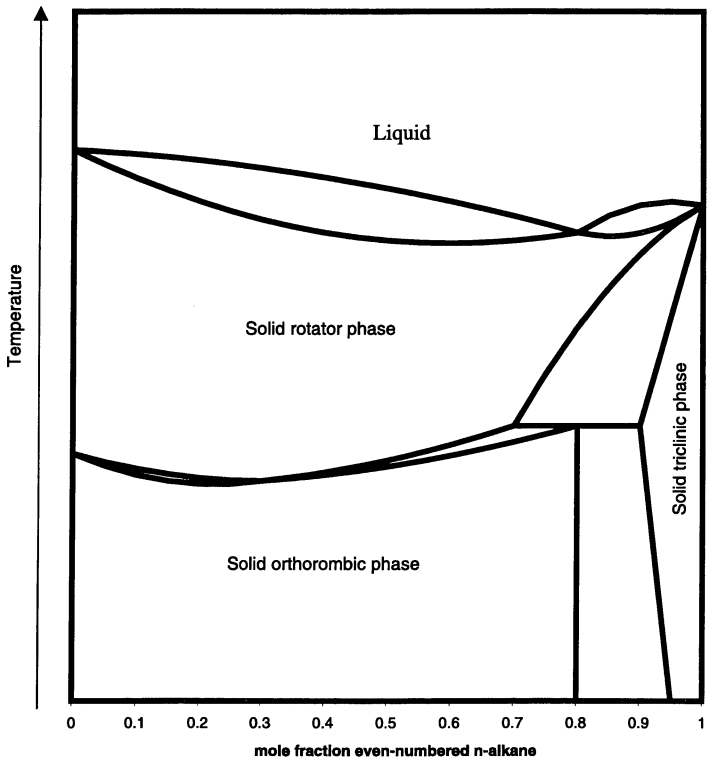

Figure 2.4: Schematical phase diagram for a binary system of even/odd *n*-alkanes. After Coutinho[28] and Mondieig et al [27].

phases, even though one or both *n*-alkanes have an even number of carbon atoms. At lower temperatures orthorhombic and to a small extent triclinic phases are stable.

An analogous observation was noted by Mondieig et al [27] while studying the solid structure of mixtures of C_{18}-C_{19} and C_{18}-C_{20}. Their phase diagrams show that only pure or almost pure C_{18} crystallizes into a triclinic phase. All other solidification processes yield a rotator phase.

A schematical phase diagram for a binary mixture of an even- and an odd-numbered *n*-alkanes can be found in Fig. (4.5). This diagram is drawn by combining diagrams made by Coutinho[28] and Mondieig et al [27].

As a gross generalization one can therefore conclude that all mixtures of n-

alkanes solidify into a rotator phase, and with further cooling rearrange into an orthorhombic phase.

Chapter 3

Thermal Conductivities of Pure Solid and Liquid *n*-Alkanes during Phase Transition

3.1 Introduction

Simulations of wax precipitation are helpful both prior to construction and during operation of pipelines. The quality of these simulations depends on the quality of the input data. The physical properties around the melting point are of particular interest. Since predicting wax formation is a question of solving the temperature field, values for the thermal conductivities at the temperatures around the melting point are instrumental in these simulations.

Results from measurements of liquid conductivities over a temperature range have been collected by Vargaftik [29].

Irby, Parsons and Keshock [30] have found discrepancies in the reported measurements of the thermal conductivity of solid octadecane, but they have resolved this disagreement by conducting additional measurements with various techniques.

Griggs and Yarbrough [6] report measurements of thermal conductivity of solid, unbranched C_{16}, C_{17}, C_{18} and C_{19}, while Yarbrough and Chih-Ning

Kuan [31] have measured the conductivities of solid C_{17} and C_{18}. Forsman and Andersson [19] have measured thermal conductivities at high pressure of solid odd-numbered *n*-alkanes ranging from C_9H_{20} to $C_{19}H_{40}$.

In this study data for the thermal conductivities for both the solid and liquid phases at the temperatures of phase transition are presented. This work has been presented at the Fourteenth Symposium on Thermophysical Properties in Boulder June 2000 [32].

The method employed is a minor modification of the method developed by Lamvik and Zhou [13].

3.2 Numerical Procedure

Eqs. (2.2), (2.3) and (2.4) are the working equations used in this work.

$$k_s^i = \rho_l^i \frac{\Delta h_{mp}^i}{M_r} \frac{dx_{mp}}{dt} \left(\frac{\partial T_s}{\partial x} \right)^{-1} \tag{3.1}$$

$$k_l^i = -\rho_s^i \frac{\Delta h_{mp}^i}{M_r} \frac{dx_{mp}}{dt} \left(\frac{\partial T_l}{\partial x} \right)^{-1} \tag{3.2}$$

$$\frac{k_l^i}{k_s^i} = \frac{\frac{\partial T_s}{\partial x}}{\frac{\partial T_l}{\partial x}} \tag{3.3}$$

To be able to use the results from experiments to calculate thermal conductivities from the working equations, approximations to the derivatives must be found.

Denoting the total height of the cell as H and assuming that the thermal gradients are linear, estimates of $\frac{\partial T}{\partial x}$ are :

$$\frac{\partial T_l}{\partial x} \approx \frac{T_H - T_{mp}^i}{H - x_{mp}} \tag{3.4}$$

and

$$\frac{\partial T_s}{\partial x} \approx \frac{T^i_{mp} - T_0}{x_{mp}} \tag{3.5}$$

Since the position of the interface is measured at heights at a predetermined interval denoted Δx, $\frac{dx_{mp}(t)}{dt}$ can be approximated:

$$\frac{dx_{mp}(t)}{dt} \approx \frac{2\Delta x}{t(x_{mp}+\Delta x) - t(x_{mp}-\Delta x)} \tag{3.6}$$

3.3 Experimental Procedure

The experimental procedure is a modification of the method presented by Lamvik [13]. The apparatus applied is described in Appendix B

3.3.1 Chemicals

All chemicals were delivered from Merck. According to Merck, hexadecane (C_{16}), heptadecane (C_{17}) and octadecane (C_{18}) were more than 99 % pure, while the purity of nonadecane (C_{19}) exceeded 98 %. No information was given regarding the nature of the impurities.

3.3.2 Procedure

Prior to all experiments the cell was washed with the appropriate wax and then filled with liquid wax through the liquid reservoirs.

To ensure that a minimum amount of gas was dissolved in the wax, the wax was repeatedly frozen and thawed until no bubbles appeared. The bubbles were removed by tilting the cell so that the they could escape through the liquid reservoirs.

Both the cell and the cathetometer were leveled using a carpenter's level.

To assure that the liquid in the cell could communicate with the liquid in the reservoirs, all freezing was done from the bottom and up.

To find the setpoints of the water baths closest to the melting point the wax was frozen and the temperature of the upper plate was gradually increased in steps of 0.1 K until melting started.

Before commencing with measurements, the wax in the cell was melted by increasing the temperature of the plates above melting point.

3.3.2.1 Solid Thermal Conductivity

The temperature of the plates was reduced to melting point. After more than one hour of thermal equilibrating, the temperature of the lower plate was reduced to the desired temperature. The cathetometer was raised at least 0.5 mm above the lower plate. When the interface reached the cathetometer, the time was recorded. The cathetometer was then raised in intervals, normally 0.2 mm. Time and position of the interface were recorded at each interval. Measurements were made at at least five levels. The temperatures of the plates were continuously monitored and recorded.

3.3.2.2 Liquid Thermal Conductivity

The wax in the cell was frozen by reducing the temperature of the lower plate under the melting temperature while the temperature of the upper plate was kept at melting point. When the wax was solid, the temperature of the lower plate was increased to the melting point. After more than one hour of thermal equilibrating, the temperature of the upper plate was increased to the desired temperature. The cathetometer was positioned at least 0.5 mm under the top plate. When the interface reached the cathetometer, time was recorded. The cathetometer was then lowered in intervals, normally 0.2 mm. Time and position of the interface were recorded at each interval. Measurements were made at at least five levels. The temperatures of the plates were continuously monitored and recorded.

3.3.2.3 Ratio of Solid and Liquid Conductivities

The wax in the cell was frozen by reducing the temperature of the lower plate to the desired temperature while the temperature of the upper plate was kept at melting point. The temperature of the upper plate was then raised to the desired level, and after equilibrating over night, the position of the interface and the temperatures of the plates were recorded.

3.4 Results

Experiments were preformed as described above.

Calculations of the thermal conductivities were done by utilizing Eqs. (2.2), (2.3) and (2.4).

Between five to seven experiments were performed for each component. For each experiment conducted to find liquid or solid conductivity, at least three values were calculated. The averaged results are given in Table 3.1

Table 3.1: Results from experiments

	Hexadecane	**Heptadecane**	**Octadecane**	**Nonadecane**
k_l $(\mathbf{Wm^{-1}K^{-1}})$	0.21	0.22	0.18	0.23
k_s $(\mathbf{Wm^{-1}K^{-1}})$	0.29	0.19	0.31	0.14
$\frac{k_l}{k_s}$	0.53	1.0	0.45	1.0

An example of how the calculations were preformed is presented in appendix C.

3.5 Discussion

3.5.1 Random Errors

3.5.1.1 Measurement of Temperature

The measurements of temperature were made by using thermocouples as described earlier. The error in the temperature measurements was estimated to $\sigma_T = 0.1$ K

3.5.1.2 Measurement of the Position of the interface

Measurements of the position of the interface were done as described by using a cathetometer. When measuring the position of a clear and steady object, it was possible to determine the position to the closest 0.01 mm. The border between the solid and the liquid phase was nor clear or steady, so this position could not be measured closer than to the nearest 0.05 mm, i.e.:

$\sigma_x = 0.025$ mm $= 2.5{*}10^{-5}$ m

3.5.1.3 Measurement of Time

Time was read off on an ordinary digital clock from Casio. There is no reason to anticipate an error more noticeable than the time required to move the eye from the measurement of position to the clock, i.e: $\sigma_t = 1$ s

3.5.2 Systematic Errors

3.5.2.1 Errors in Physical Constants

All physical constants are more or less burdened with errors.

The reported melting points in the literature differed up to 0.3 K. The maximum discrepancy was found for $T_{mp}^{C_{16}}$. Finke et al. [33] report $T_{mp}^{C_{16}} = 291.34$

K while Parks et al.[34] report $T_{mp}^{C_{16}} = 291.1$ K. Impurities in the chemicals used might answer for additional uncertainty. Assuming that the reported melting points found in [34], [23] and [35] are reliable to the closest 0.5 K, $\sigma_{T_{mp}}$ can be estimated to:

$\sigma_{T_{mp}} = 0.25$ K

The densities of the solid phase of C_{16}, C_{17} and C_{18} were calculated from liquid density. The shrinking during solidification was assumed to 10 % for all components, even though the density, as described in section 2.4.1, of the odd-numbered *n*-alkanes is higher than the densities of even-numbered. The shrinking of 10 % is equivalent to the shrinkage at solidification reported by Schaerer et al. [35] for other heavier n-paraffinic waxes. This assumption is very uncertain, and thus : $\sigma_\rho = 50$ kg m^{-3}

The enthalpies of melting in the literature ([33], [34], [35] and [23]) differed so much that $\frac{\Delta h_{mp}}{M_r}$ could not be determined more precisely than to the closest 10000 $J{\cdot}kg^{-1}$ i.e: $\sigma_{\frac{\Delta h_{mp}}{M_r}} = 5000$ J kg $^{-1}$

The values of the physical constants used in this work can be found in appendix A.

3.5.2.2 Dendritic Growth of Solid Phase

During measurements of the thermal conductivity of the solid phase, i.e. freezing, the solid phase grew in a dendritic manner making measurements of the location of the interface difficult. A strong lamp was placed in the back of the experimental cell and the position was read off at the point where no light came through. Since some precipitation did not contribute to this position, the measured speed of the interface was too low and consequently the calculated thermal conductivity was too low as well.

This is supported by the measurements of the ratio $\frac{k_l}{k_s}$ and the measurements of k_l (see table 3.1). The direct measurements of the thermal conductivity of the solid phase are therefore disregarded and k_s is instead calculated from measurements of the ratio $\frac{k_l}{k_s}$ and the measurements of k_l.

3.5.2.3 Solid-Solid equilibria

As described in section 2.4.1, C_{17} and C_{19}, but not C_{16} and C_{18}, change solid phase at a transition point below the melting temperature. All experiments were preformed above these transition points, i.e: t he solid conductivities are measured in the rotator phases of C_{17} and C_{19} while C_{18} and C_{20} are in an orthorhombic structure.

3.5.3 Total Assessment of Errors

3.5.3.1 Gauss's Equation for Propagation of Random Error

An assessment of the total error in the calculation of the liquid thermal conductivities was done using Gauss's equation for propagation of random error as described by Nesse [36] :

$$\sigma_{k_l^i} = \sqrt{\left(\sigma_{\rho_s^i}\frac{\partial k_l^i}{\partial \rho_s^i}\right)^2 + \left(\sigma_{\frac{\Delta h_{mp}}{M_r}}\frac{\partial k_l^i}{\partial \frac{\Delta h_{mp}}{M_r}}\right)^2 + \left(\sigma_{\frac{dx_{mp}}{dt}}\frac{\partial k_l^i}{\partial \frac{dx_{mp}}{dt}}\right)^2 + \left(\sigma_{\frac{\partial T_l}{\partial x}}\frac{\partial k_l^i}{\partial \frac{\partial T_l}{\partial x}}\right)^2} \tag{3.7}$$

The total error is found to be 15 % in a typical experiment.

An estimate for the error in the ratio $\frac{k_l^i}{k_s^i}$ is done analogously:

$$\sigma_{\frac{k_l^i}{k_s^i}} = \sqrt{\left(\sigma_{\frac{\partial T_l}{\partial x}}\frac{\partial \frac{k_l^i}{k_s^i}}{\partial \frac{\partial T_l}{\partial x}}\right)^2 + \left(\sigma_{\frac{\partial T_s}{\partial x}}\frac{\partial \frac{k_l^i}{k_s^i}}{\partial \frac{\partial T_s}{\partial x}}\right)^2} \tag{3.8}$$

This error is calculated to 11 % for a typical experiment.

Finally, the error in k_s^i is calculated as:

$$\sigma_{k_s^i} = \sqrt{\left(\sigma_{k_l^i}\frac{\partial k_s^i}{\partial k_l^i}\right)^2 + \left(\sigma_{\frac{k_l^i}{k_s^i}}\frac{\partial k_s^i}{\partial \frac{k_l^i}{k_s^i}}\right)^2} \tag{3.9}$$

$\sigma_{k_s^i} = 19\%$ of k_s^i in the calculated example.

The calculations of these errors are shown in detail in appendix D.

3.5.3.2 Standard Deviation

Standard deviation is calculated on the basis of the seven experiments carried out to find $k_l^{C_{18}}$. The estimate of the standard deviation is found to be, $\sigma_{k_l^{C_{18}}} = 0.028 W \cdot m^{-1} \cdot K^{-1}$, which is less than 16 % of $k_l^{C_{18}}$, and accordingly in agreement with the estimate based on Gauss's equation for propagation of random error.

This calculation is shown in appendix D.

3.5.3.3 Total Assessment

Assuming that the calculation of standard deviation and the estimate of the error found from using Gauss's equation for propagation of error are typical, an uncertainty of 20% in both k_l^i and k_s^i should be a reasonable estimate.

3.5.4 Theoretical Assumptions

3.5.4.1 Linear temperature gradients

The approximations of $\frac{\partial T}{\partial x}$, Eqs. (3.4) and (3.5), assume linear thermal gradients. According to Grigull and Sandner [37] the Stefan number is a measure of the error associated with this assumption. For the liquid phase, the Stefan number is :

$$Ph_l^i = \frac{\frac{\Delta h_{mp}^i}{M_r^i}}{C_{p,l}^i(T_l - T_{mp}^i)} \tag{3.10}$$

The expression for the solid phase is:

$$Ph_s^i = \frac{\frac{\Delta h_{mp}^i}{M_r^i}}{C_{p,s}^i(T_{mp}^i - T_s)} \tag{3.11}$$

Grigull and Sandner [37] show that with $Ph \geq 10$, the error in the approximative solution of Eq. (2.1) is less than 2 %.

$Ph \geq 10$ for all experiments reported here. The error is consequently disregarded.

3.5.4.2 Convection

Since the measured values for the thermal conductivity of the liquids are higher than previously published, one could suspect that convection has improved the heat transfer. But all experiments were conducted with the coldest part of the cell at the bottom and thus without a driving force for convection.

Using an almost indistinguishable experimental cell Zang et al [38],[39] have measured the Soret coefficient and diffusion coefficient of liquid mixtures assuming that there is no convection when the coldest part of the cell is at the bottom. They obtain an accuracy of 1-3 % for the Soret coefficient. This small error shows that the contribution from convection can be neglected when using this type of experimental setup.

The same conclusion is reached by Webb and Viskanta [40] when working with an analogous experimental cell. They even introduced fish scales into their apparatus, but they could not detect any fluid motion induced by buoyancy.

3.5.4.3 No Gradient in Unchanged Phase

The crucial step in the derivation of the equations for calculation of the thermal conductivities, Eqs. (2.2) and (2.3), is the assumption that there is no thermal gradient in the disappearing phase. This is virtually impossible

to achieve. That means that Eqs. (2.2) and (2.3) have to include an extra term, which in the liquid case is:

$$k_l^i = \left(k_s^i \frac{\partial T_s}{\partial x} - \rho_s^i \frac{\Delta h_{mp}^i}{M_r^i} \frac{dx_{mp}}{dt} \right) \left(\frac{\partial T_l}{\partial x} \right)^{-1} \tag{3.12}$$

The setpoints of the water baths closest to the melting points were found by gradually increasing the temperature of solid wax in steps of 0.1 K until melting started. There is therefore no reason to anticipate an error exceeding the uncertainty in T_{mp} which is estimated to be 0.25 K in section 3.5.2.1.

Numerically this has the greatest impact when the gradient in the growing phase is low. Calculation on such a case is done in appendix E and shows that the error is 2 %. This error will always give a too low liquid thermal conductivity, but compared with the random errors this error is nevertheless diminutive and is disregarded.

3.5.4.4 One Dimensional Heat Transfer

The assumption of a one dimensional method can be justified since the experimental cell was, as described in appendix B, thoroughly insulated. If the cell had not been sufficiently insulated, melting or crystallization would have occurred on the walls of the experimental cell. No melting or crystallization on the walls was observed.

3.5.5 Comparison with Previously Published Data

3.5.5.1 Thermal Conductivity of Liquid n-Paraffinic Waxes

Vargaftik [29] presents thermal conductivities over a large temperature range. For the components in question here, values are given for temperatures from around 590 K to 313 K. These values lie on a line and seem to stem from a linear interpolation. No uncertainties are reported.

If one extrapolates Vargaftik's [29] data to the melting point, liquid conduc-

tivities for all components considered are found to be 0.15 W m^{-1} K^{-1}.

A linear interpolation of Wada, Nagasaka and Nagashima's [41] measurements of the thermal conductivity of liquid C_{16} confirms the value of 0.15 W m^{-1} K^{-1}.

This is lower than the liquid conductivities presented in this work.

In absolute value, the measurements of Ziebland and Patient [42] are in the same range as the extrapolation of Vargaftik's [29] data, but nonlinear augmentation of thermal conductivities close to solidification is observed. They assign the increased conductivity with decreasing temperature to fractional crystallization.

A similar hypothesis is introduced by Earnshaw and Hughes [43]. They measured the surface tension of purified *n*-alkanes in the C_{15}-C_{18} range. At a temperature close to, but distinct from the melting point, they observed that the surface tension departs from the accepted steady increase to a monotonic decrease as the temperature is lowered. They assign this phenomenon to a marked reduction in the available degrees of freedom.

It is reasonable to believe that this reduction in the available degrees of freedom, i.e., entropy, becomes more and more significant the closer the temperature is to the melting point. A reduction in the entropy is normally connected to an increase in thermal conductivity. It is therefore quite possible that the discrepancy between this work and Vargaftik's [29] and Wada, Nagasaka and Nagashima's [41] measurements may be due to this phenomenon.

3.5.5.2 Thermal Conductivity of Solid n-Paraffinic Waxes

Griggs and Yarbrough [6] report measurements of thermal conductivity of solid C_{16}, C_{17}, C_{18} and C_{19}, while Yarbrough and Kuan [31] report $k_s^{C_{17}}$ and $k_s^{C_{18}}$. All measurements are made over a temperature range, but the variation with temperature is within their reported error and can therfore be neglected. Both papers disregard solid-solid equilibria even if the experiments are preformed well below the transition temperatures for C_{17} and C_{19}. Averaged results from these papers are presented in Table 3.2.

Table 3.2: k_s (W m^{-1} K^{-1}) as reported in the literature.

Reference	$\mathbf{C_{16}}$	$\mathbf{C_{17}}$	$\mathbf{C_{18}}$	$\mathbf{C_{19}}$
Griggs and Yarbrough [6]	0.35 ± 0.07	0.21 ± 0.06	0.3 ± 0.1	0.27 ± 0.05
Yarbrough and Kuan [31]	—	0.19 ± 0.02	0.32 ± 0.03	—
Forsman and Andersson [19]	—	0.2	—	0.2
Irby, Parsons and Keshock [30]	—	—	0.43 ± 0.03	—
This work	0.40 ± 0.08	0.22 ± 0.04	0.40 ± 0.08	0.23 ± 0.05

Irby, Parsons and Keshock [30] have found that the reported measurements of the thermal conductivity of solid octadecane ranged from 0.15 W m^{-1} K^{-1} to 0.56 W m^{-1} K^{-1}. They resolved this disagreement by making measurements with various techniques. Their recommended value is 0.43 W m^{-1} K^{-1}. They explain the lower value of Griggs and Yarbrough [6] with voids.

Forsman and Andersson [19] have measured thermal conductivities at high pressure of solid odd-numbered *n*-alkanes ranging from C_9 to C_{19}. Their measurements show that the thermal conductivities are 0.2 W m^{-1} K^{-1} for all investigated components at temperatures right below the melting point. They assign the low value to obstruction by orientational disorder in the rotator phase. This is discussed in section 2.4.1.

3.5.6 Recommendation for Future Works

The greatest weakness of the results of this chapter are the experimental uncertainties. This could be improved on by using better methods for determining the temperatures and the positions of the interface.

The method employed in this chapter is particularly suitable for determining the ratio between the solid and liquid conductivity. Since the solid conductivity is easier to measure than the liquid, one could use the method to determine the liquid conductivity when the solid conductivity is known.

Table 3.3: Thermal conductivity of solid and liquid C_{16} to C_{19} at their melting point

	Hexadecane	**Heptadecane**	**Octadecane**	**Nonadecane**
$k_l(\mathbf{Wm^{-1}K^{-1}})$	0.21 ± 0.04	0.22 ± 0.04	0.18 ± 0.04	0.23 ± 0.05
$k_s(\mathbf{Wm^{-1}K^{-1}})$	0.40 ± 0.08	0.22 ± 0.04	0.40 ± 0.08	0.23 ± 0.05

3.6 Conclusion

Thermal conductivities have been determined at the melting point for solid and liquid unbranched alkanes ranging from C_{16} to C_{19}. An assessment of the error of the method has been performed.

The measurements of solid conductivities are in accordance with measurements reported previously and confirm the applicability of the method. Liquid conductivities are higher than extrapolated values from the literature. This is believed to be caused by structural changes which occur close to the melting point temperature. The structural changes are not taken into account when extrapolating the values from the literature.

The results are presented in Table 3.3.

It is recommended to use the method employed to find liquid conductivity when the solid conductivity is known.

Chapter 4

Calculation of Solid-Liquid Equilibria

4.1 Introduction

In general, equilibrium is assumed when studying solid-liquid phase transitions. Even though the main topic of this thesis is transport processes which are not at equilibrium, models for the equilibria are required.

A major difference between the behavior of mixtures and pure components at solid-liquid transitions is that the melting point and freezing point of a mixture are at two separate temperatures opposed to being equal for pure components. The temperatures where the liquid mixtures start to freeze are called the liquidus, and the melting points of a solid mixture are on the solidus. The area between the lines connecting the melting and freezing temperatures is the phase envelope.

The main concern of investigators handling wax deposition problems has been the development of models of the solid-liquid equilibria of petroleum waxes. A review of such models can be found in Pauly, Dauphin and Daridon [8] or in Coutinho, Andersen and Stenby [9].

Since the phase envelopes for the mixtures studied here are not available, the solid-liquid equilibria must be calculated. Equations for the liquidus are

necessary in subsequent work and will also be presented in this chapter.

4.2 Procedure

4.2.1 Equations to be Solved

The sum of mole fractions must equal one:

$$\sum_i x^i = 1 \tag{4.1}$$

$$\sum_i s^i = 1 \tag{4.2}$$

$$\sum_i z^i = 1 \tag{4.3}$$

The equilibrium constant, K^i, can be calculated as shown in section 2.3, and is equal to the ratio of solid and liquid mole fraction.

$$K^i = \frac{s^i}{x^i} \tag{4.4}$$

The amount of feed must be equal to the amount of solid and liquid.

$$F = S + L \tag{4.5}$$

This must also be the case for all components:

$$z^i F = s^i S + x^i L \tag{4.6}$$

4.2.2 Overview

A flowchart showing the algorithm used to find the liquidus is presented in Fig. (4.1).

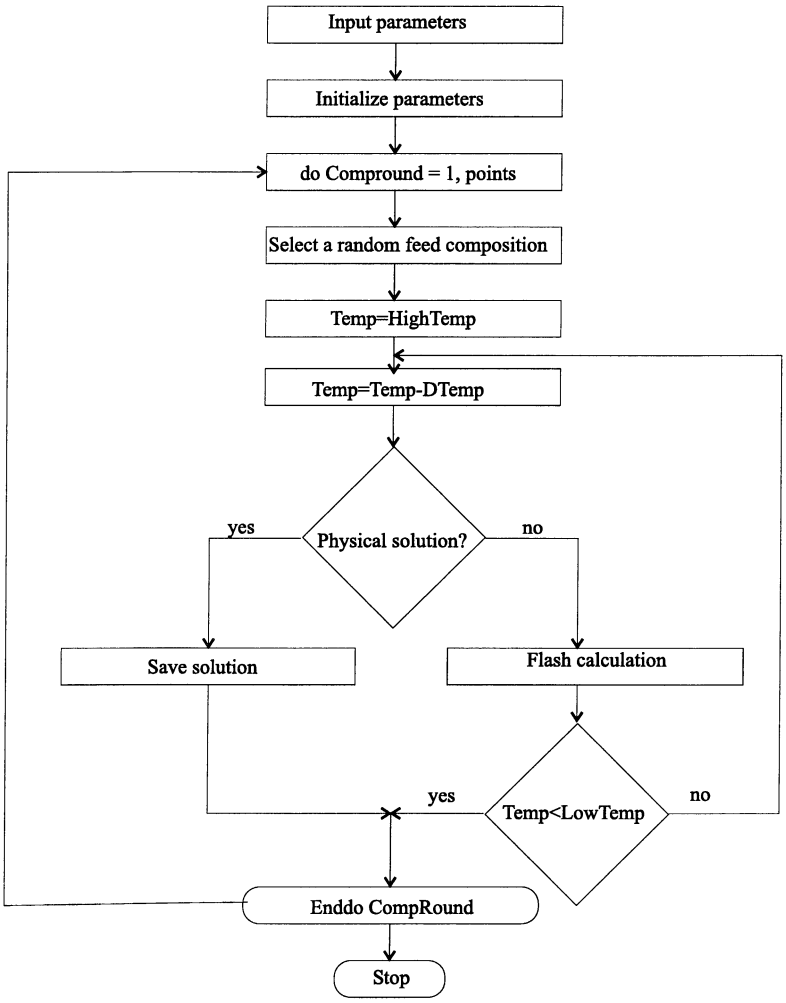

Figure 4.1: Algorithm applied to find the liquidus

The input to the program consists of the following parameters:
- components to be considered
- the number of points to be calculated

- name of file for storing the results in
- physical properties of the components

The initialization consists of statements which assign values to variables.

To ensure a good distribution of the points considered, a random composition is selected and used as composition of the feed (z^i). Thereafter the temperature is set to 5 K above the highest pure component melting point, this to ensure that the temperature is above the liquidus.

The temperature is then lowered in intervals until a solution is reached or the temperature is 5 K below the lowest pure component melting point, which should be below the solidus.

If a solution is reached and found to be physically sound, i.e: all mole fractions are between nil and one and the sum of all mole fractions are one, the solution is accepted and saved.

Next, a new random composition is selected and the procedure from that point on is repeated a prescribed number of times.

A transcript of the Fortran 77 program used in the calculations is given in appendix F.

The solidus was found equivalently, but initially the temperature was at a point lower than the solidus and raised in intervals of DTemp until a solution was found.

4.2.3 Flash Calculation

The method for solution of the isothermal flash calculation is a modification of the procedure given by Won [44].

A function, f is needed and is defined as:

$$f = \sum s^i - \sum x^i = 0 \tag{4.7}$$

f can also be expressed as:

$$f(S) = \sum \frac{z^i F(K^i - 1)}{S(K^i - 1) + F} \tag{4.8}$$

The derivative of $f(S)$ with respect to S is also needed in the procedure:

$$\frac{df(S)}{dS} = -\sum \frac{z^i F(K^i - 1)^2}{(S(K^i - 1) + F)^2} \tag{4.9}$$

The algorithm used in the flash calculations is shown in Fig. (4.2).

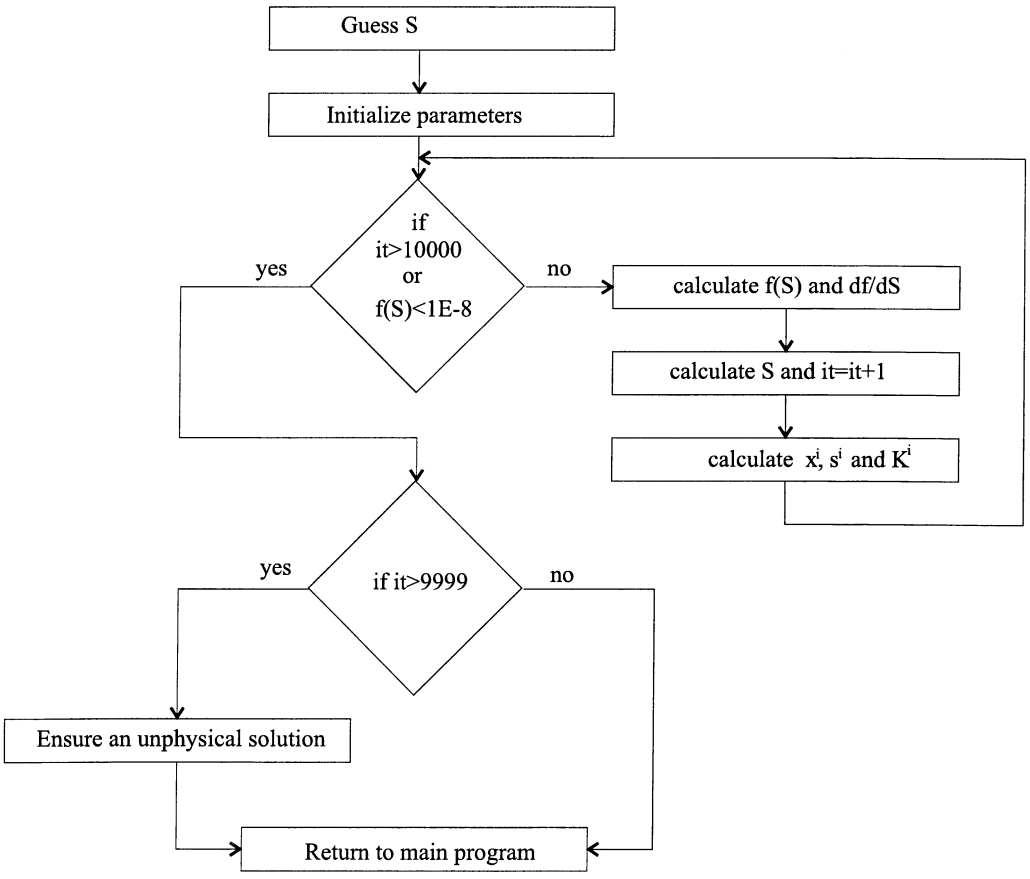

Figure 4.2: Algorithm used to perform flash calculation

Initially a solution for S, the amount of solid, is guessed and parameters are initialized before the iterations begin. The amount of feed F is set to 1 mole.

During each iteration, $f(S)$ and $\frac{df(S)}{dS}$ are calculated. The values are used to find a new approximation of S:

$$S = S + 0.1 * \frac{f(S)}{(\frac{df(S)}{dS})} \tag{4.10}$$

Once a solution for S is found, x^i and s^i can be calculated:

$$x^i = \frac{z^i F}{SK^i + F - S} \tag{4.11}$$

and:

$$s^i = x^i * K^i \tag{4.12}$$

The iterations continue until $f(S)$ is less than $1*10^{-8}$ or the maximum number of iterations, 10000, is reached. If the maximum number of iterations is reached, the solution is rendered unphysical just to ensure that it will not be stored.

4.3 Results

4.3.1 Phase diagrams

The results of the calculations on the binary systems investigated are presented in Figs. (4.3-4.5)

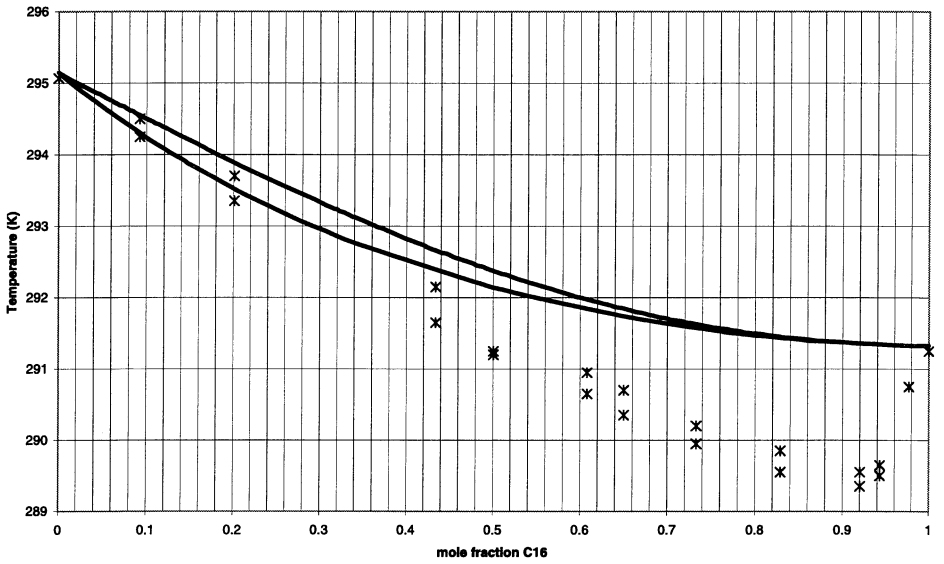

Figure 4.3: Calculated solid-liquid envelope of C_{16}-C_{17} shown as a solid line. Experimental data from Timmermanns [45] shown as points.

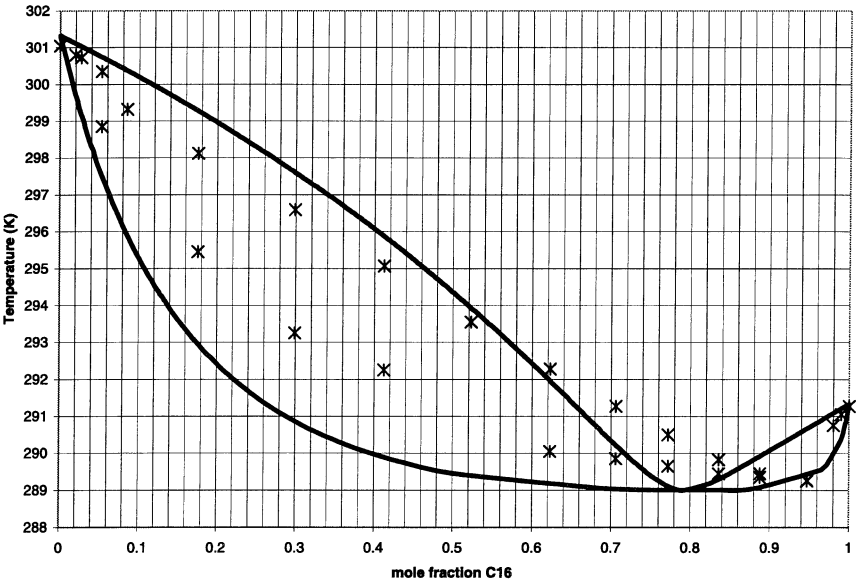

Figure 4.4: Calculated solid-liquid envelope of C_{16}-C_{18} shown as a solid line. Experimental data from Smith [46] shown as points.

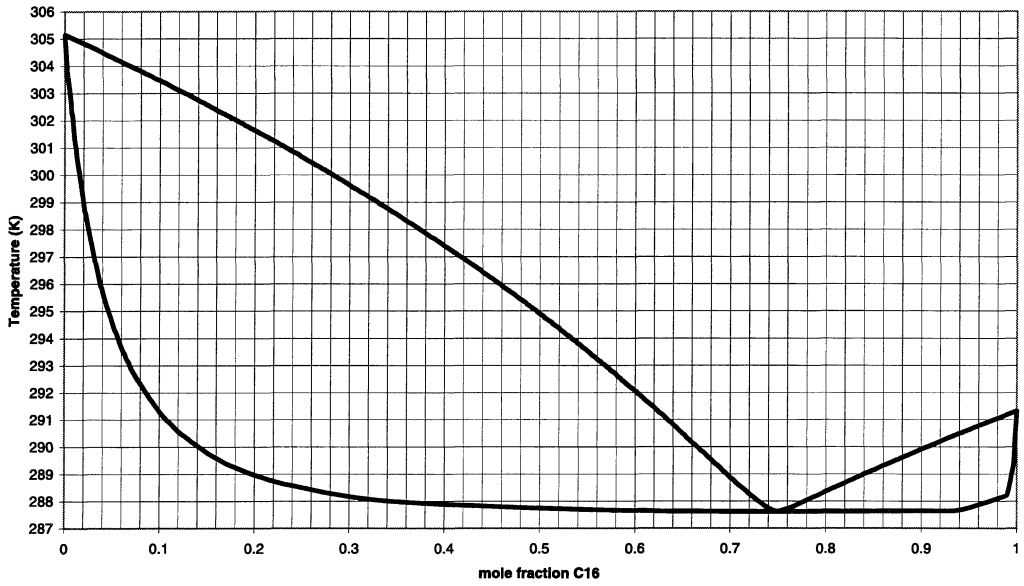

Figure 4.5: Calculated solid-liquid envelope of C_{16}-C_{19}

4.3.2 Numerical Models of the Liquids

In order to use the calculated models in subsequent simulations, it is necessary to represent the liquidus as an equation. Linear regressions have therefore been performed to find polynomial representations.

Binary mixtures are modeled as:

$$T_{liq}^{i-j} = \sum_{k=1}^{10} a^k (x^i)^k \tag{4.13}$$

where x^i is the mole fraction of the component with the fewest number of C-atoms.

The equation for the ternary mixture is:

$$\begin{aligned} T_{liq}^{C_{16}-C_{18}-C_{19}} &= a_0 + a_1 x^{C_{18}} + a_2 (x^{C_{18}})^2 + a_3 x^{C_{16}} + a_4 x^{C_{16}} x^{C_{18}} + a_5 x^{C_{16}} (x^{C_{18}})^2 \\ &\quad + a_6 (x^{C_{16}})^2 + a_7 (x^{C_{16}})^2 x^{C_{18}} + a_8 (x^{C_{16}})^2 (x^{C_{18}})^2 \end{aligned} \tag{4.14}$$

Table 4.1: Numerical models of the liquidus of binary mixtures

	C_{16}-C_{17}	C_{16}-C_{18}	C_{16}-C_{19}	C_{16}-C_{18}-C_{19}	C_{16}-C_{17}-C_{18}-C_{19}
a_0	295.1	301.4	305.2	307.3	302.6
a_1	-6.873	-21.20	20.98	-16.28	-12.28
a_2	9.303	324.4	183.9	10.98	-15.60
a_3	-84.41	-4230	-2916	-31.54	-9.164
a_4	498.2	28351	22626	53.85	3.832
a_5	-1728	-110900	-100344	-42.65	-9.164
a_6	3746	266006	268192	13.32	33.19
a_7	-5111	-395685	-438157	-73.94	-0.3832
a_8	4265	355048	426505	93.32	
a_9	-1987	-175598	-226412		
a_{10}	395.7	36693	50329		

For the four-component mixture:

$$T_{liq}^{C_{16}-C-17-C_{18}-C_{19}} = a_0 + a_1 x^{C_{18}} + a_2 x^{C_{17}} + a_3 x^{C_{17}} x^{C_{18}} + a_4 x^{C_{16}} + a_5 x^{C_{16}} x^{C_{18}} + a_6 x^{C_{16}} x^{C_{17}} + a_7 x^{C_{16}} x^{C_{17}} x^{C_{19}} \quad (4.15)$$

The results from these regressions can be found in Table 4.1.

4.4 Discussion

4.4.1 Choice of Activity Coefficient Models

Pauly, Dauphin and Daridon [8] have utilized six different models in calculation of the solid-liquid equilibria of C_{18}-C_{30} diluted in C_{10}.

Won [44] has simplified the expression for K^i and models the activity coefficients using regular solution theory.

Pedersen, Skovborg and Rønningsen's model [47] is also based on the regular solution theory, but the expression for K^i is less simplified and other

correlations for the physical properties are used.

The model used by Hansen et al [48] differs from Won's [44] concerning how the non-ideality is dealt with. The solid phase is assumed to be ideal. The liquid phase is modeled using Flory-Huggins [49] theory.

Ungerer et al [50] assume that each heavy component crystallizes as a pure component and they calculate the pure liquid fugacity from the Peng-Robinson equation of state.

The model developed by Coutinho et al [9],[16], described in this work, is also tested.

Finally, an ideal solution model is investigated.

When Pauly, Dauphin and Daridon [8] compared their experimental result with calculations, they found that the only model which represent the shortest components, i.e: C_{18}, reasonably is the model of Coutinho et al. which is adopted in this work.

This is not surprising since most of the other models are primarily developed to predict the onset of crystallization from crude oils, the wax appearance temperature, not to calculate the solid-liquid envelope of *n*- alkane mixtures.

Thus, Coutinho's model seems to be the best choice for the investigated equilibria. An additional advantage with the model in the form presented here is that it is deterministic. Most other models need to be tuned by changing the value of a parameter until the model represents experimental data.

4.4.2 Errors in Physical Properties

The model is very susceptible to errors in the physical properties. This sensitivity is actually so decisive that Erickson, Nilsen and Brown [51] suggested to use the dependency of Δh_{mp} instead of activity coefficients to model the non-ideality of the solid-liquid equilibria of wax deposition from crude oils.

All measurements are burdened with errors and the introduction of physical

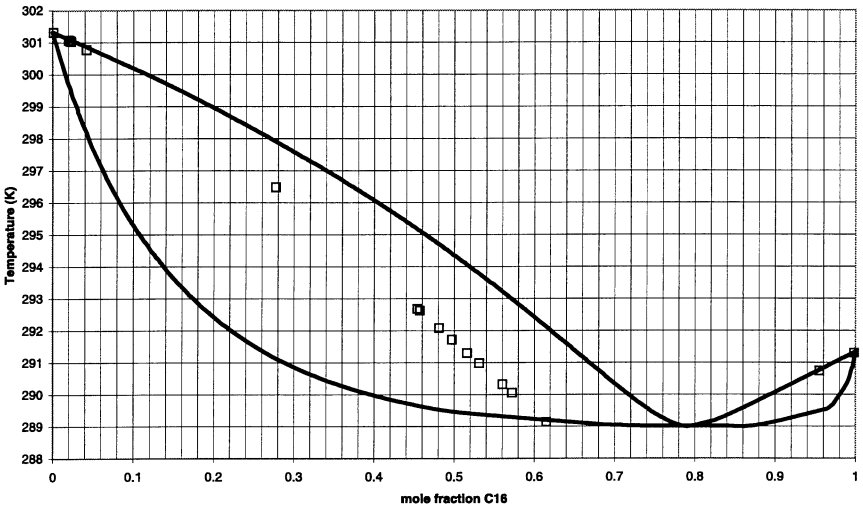

Figure 4.6: Solid line : calculated solid-liquid envelope of C_{16}-C_{18}, □ : $\Delta h_{sub}^{C_{16}}$ increased by 10 % and $\Delta h_{sub}^{C_{18}}$ decreased by 10 %

properties in the model is also an introduction of error.

Calculations, using different values for the physical properties have shown that the results from the calculations change the most when the physical properties used to calculate the activity coefficients are changed.

As an example, calculations with a 10 % change in Δh_{sub} are plotted in Fig. (4.6). This was one of the parameters with the greatest impact on the results.

When modeling the solid activity coefficient, one should, as noted in section 2.3.1.3, use the Δh_{sub} which refers to a transition from a orthorhombic solid phase to a vapor. This value is not accessible for C_{16} and C_{18} since these components solidify directly into a triclinic structure. As shown in Fig. (4.6), the error introduced may be substantial.

4.4.3 Uncertainty in Regression

For binary systems in particular, the uncertainty in regression is diminutive compared with the errors of the model. The maximum standard deviation of the regression is in the regression of the liquidus of the C_{16}-C_{19} system.

This error is 0.09 K which can be ignored compared with the other errors.

The multicomponent systems are not represented as well as the binary systems, but the standard deviations of the regressions do not exceed 0.4 K for the system with three components and 0.7 K for the system with four components.

4.4.4 Comparisons with Experimental Data

Experimental data collected by Timmermanns [45] are plotted in Fig. (4.3) while data from Smith [46] are plotted in Fig. (4.4). The calculated solid-liquid envelope of the C_{16}-C_{18} system seems to represent the experimental data quite well, but the deviation is more notable in the C_{16}-C_{17} system.

As discussed previously, in section 4.4.2, the values for $\Delta h_{sub}^{C_{16}}$ and $\Delta h_{sub}^{C_{18}}$ are uncertain. This means that there is reason to believe that the relative Δh_{sub} odd-even is even more uncertain. That may explain the difference between experimental and calculated values for the C_{16}-C_{17} system.

Close to the pure components the difference between model and experiment is, as should be expected, not substantial. Around the eutectic point the deviation is up to 2 K.

4.4.5 Total Assessment of Model

The deviation between the model and the experimental data is not only believed to be due to the model but also caused by uncertainties in the physical properties. The errors introduced by regression are presumed to be insignificant.

Although the Coutinho's model does not reproduce the experimental data exactly, the deviation from ideality is correct in both cases. I.e., the curvature of the curves are correct, and the model is therefore far superior to inferring ideality.

As a conservative estimate for the equations representing the liquidus, the

uncertainty is estimated at 4 K, i.e : $\sigma_{T_{liq}}$= 2 K for all calculations.

4.5 Conclusion

The solid-liquid envelopes of five different mixtures of *n*-alkanes in the C_{16}-C_{19} range have been calculated. The liquidus have been represented by polynomials.

The non-ideality is modeled as shown by Coutinho et al [9],[16]. The greatest asset of this model is that there is no parameter that needs to be tuned.

The results obtained in this chapter will be verified in the next chapters. The results will be used as input to models of both stationary and transient freezing of mixtures of *n*-alkanes.

Chapter 5

Experimental Investigation of Wax Deposition from Mixtures

5.1 Introduction

After having dealt with wax deposition from pure components without convection in chapter 3,the next natural step on the path toward a model for deposition of wax from crude oils is the introduction of mixtures.

In this chapter the experimental results will be reported. In chapter 6, numerical models of the same experiments are developed.

Webb and Viskanta [40] have investigated the mushy zone (i.e: a mixture of solid and liquid) of hexadecane and octadecane, and reported that during solidification, a mushy zone developed that compromised of small dendrites protuding vertically into the surrounding liquid.

Tan and Leong [7] report experiments inside a rectangular experimental cell using both pure *n*-alkanes and a mixture of hexadecane and octadecane. Except for one vertical wall, all the walls of their experimental cell were adiabatic. They report that the mixture solidified in the same manner as the pure components i.e., no mushy zone was observed. Their conclusion was that n-paraffinic materials are not suitable for studies of the mushy zone.

The experimental setup used here is the same as used in chapter 3. The apparatus is described in detail in appendix B.

The results from the experiments preformed will not only be used to verify numerical models of transient freezing, but also to determine which solid structure is formed when mixtures crystallize. This can be done by calculating the ratio between the solid and liquid conductivities.

5.2 Procedure

5.2.1 Experimental Procedure

The apparatus used is the one applied to find the thermal conductivities of pure components as described in chapter 3. A description of the apparatus can be found in appendix B.

The apparatus was placed in a cooled room with an ambient temperature between 274-276 K.

Prior to the experiments, the experimental cell was heated to a temperature above the liquidus and it was washed with the appropriate mixture. The cell was then filled with the same mixture through the liquid reservoirs. The composition of the mixtures can be found in Table 5.1.

To ensure that as little gas as possible was dissolved in the wax, the wax was repeatedly frozen and thawed until no bubbles appeared. The bubbles were removed by tilting the cell so that they could escape through the liquid reservoirs.

Both the cell and the cathetometer were leveled using a carpenter's level. The total height of the cell was measured using the cathetometer. The liquid mixture of the liquid reservoirs was sampled and set aside for analysis (see Table 5.1).

Before commencing with measurements, the wax in the cell was melted by increasing the temperature of both plates to a temperature (T_H in Table 5.1) above the liquidus. The cell was then left for thermal equilibration for at

Table 5.1: Experimental Conditions

Exp.#	Initial Composition	T_H (K)	T_0. (K)
1	x^{C16}=0.637, x^{C18}=0.363	301.1 K	287.8 K
2	x^{C16}=0.534, x^{C19}=0.466	302.2 K	285.8 K
3	x^{C16}=0.647, x^{C18}=0.353	300.4 K	285.9 K
4	x^{C16}=0.313, x^{C18}=0.396, x^{C19}=0.291	303.5 K	286.0 K
5	x^{C16}=0.259, x^{C18}=0.304, x^{C19}=0.437	308.3 K	288.8 K
6	x^{C16}=0.281, x^{C17}=0.296, x^{C18}=0.218, x^{C19}=0.205	308.4 K	288.8 K
7	x^{C16}=0.337, x^{C17}=0.231, x^{C18}=0.170, x^{C19}=0.262	308.3 K	289.6 K
8	x^{C16}=0.337, x^{C17}=0.663	304.5 K	286.8 K

least one hour.

The temperature of the lower plate was then reduced to a temperature below the solidus (T_0 in Table 5.1) and the measurement of time was started.

At various intervals, most frequent in the beginning of the experiment, time and position of the solid-liquid interface were recorded. The temperatures of the plates were continuously monitored and recorded.

The temperature on the interface was measured after equilibrium was established, i.e., right before completion of the experiment, by inserting a thermocouple through the liquid reservoirs.

After a minimum of 12 hours, the experiment was completed.

As much liquid as possible was then removed from the cell with a syringe. The temperature of the top plate was reduced to the temperature of the bottom plate. After the liquid remnants of the cell were frozen, the cell was dismantled and the solid wax was removed.

The solid wax was cut so that only a part of the solid which had frozen out during the experiment was analyzed.

All compositions were analyzed at Statoil's laboratory in Trondheim using a gas chromatograph.

The experimental conditions are presented in Table 5.1

5.2.2 Numerical Procedure

The working equation is the same as used to calculate the ratio of solid-liquid conductivity of pure components in chapter 3, Eq. (2.4):

$$\frac{k_l}{k_s} = \frac{\frac{\partial T_s}{\partial x}}{\frac{\partial T_l}{\partial x}} \tag{5.1}$$

In order to find a numerical value, one needs to find approximations of $\frac{\partial T_s}{\partial x}$ and $\frac{\partial T_l}{\partial x}$

This can be done like in chapter 3, but since the melting point of the mixture is not defined it must be replaced.

The temperature on a solid-liquid interface at equilibrium is always on the liquidus. If the liquid composition is known, one can calculate the temperature on the liquidus from the equations presented in chapter 4.

After equilibrium is established, the liquid composition of the experimental cell is homogeneous. Due to the volume of the liquid reservoirs, the composition of the experimental cell will be the same as the initial composition of the cell.

Alternatively T_{liq} can be found by measurements.

Thus T_{mp}=T_{liq}, where T_{liq} is either T_{liq}^{calc} or T_{liq}^{meas}. The thermal gradients can be approximated by:

$$\frac{\partial T_l}{\partial x} \approx \frac{T_H - T_{liq}}{H - x_{mp}} \tag{5.2}$$

and

$$\frac{\partial T_s}{\partial x} \approx \frac{T_{liq} - T_0}{x_{mp}} \tag{5.3}$$

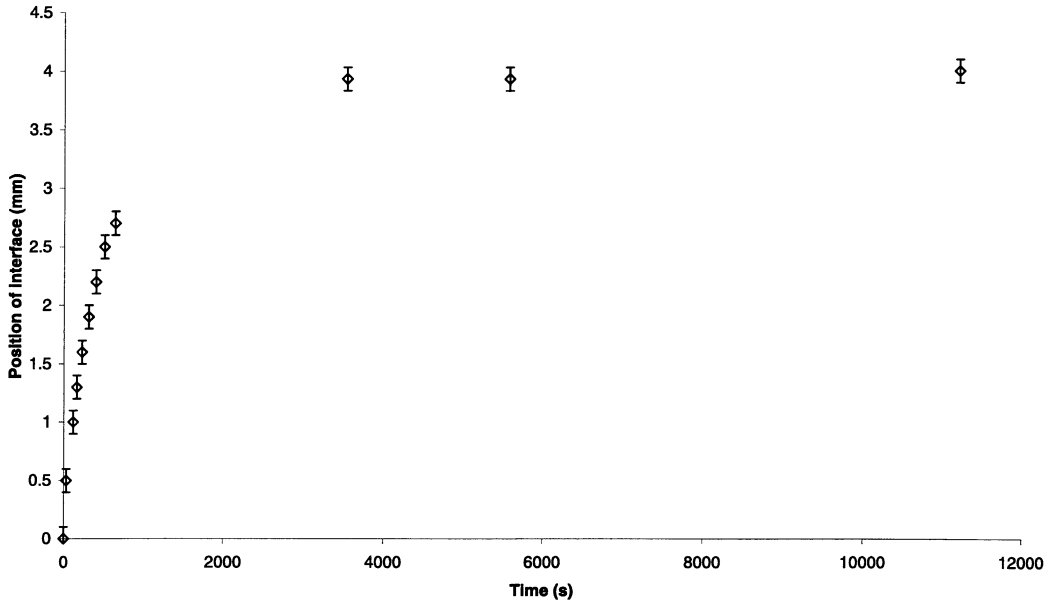

Figure 5.1: Position of solid-liquid interface during experiment # 1

5.3 Results

5.3.1 Position of Interface

As an example, the results from experiment # 1 are plotted in Fig. (5.1).

The results from the other experiments can be found in appendix G. In order to increase the readability of the charts, the positions of the interfaces at steady state are not included in the charts of appendix G.

The measurements at steady state are instead presented in Table 5.3. The total height of the experimental cell can also be found in the same table.

5.3.2 Temperatures on the Interface

The temperatures on the interfaces at steady state were measured as described in section 5.2.1. The results are presented in Table 5.2.

Table 5.2: Measured temperatures on the solid-liquid interface.

Exp.#	T_{liq}^{meas} (K)
1	293.2
2	295.6
3	291.7
4	296.4
5	298.1
6	296.9
7	295.7
8	292.0

Table 5.3: Measured values at steady state and calculated ratios of solid and liquid conductivities.

Exp.#	H (m)	x_{mp}(m)	$\frac{k_l}{k_s}$ (T_{liq}=T_{liq}^{calc})	$\frac{k_l}{k_s}$ (T_{liq}=T_{liq}^{meas})
1	$12.0*10^{-3}$	$4.0*10^{-3}$	0.82	1.38
2	$12.0*10^{-3}$	$7.5*10^{-3}$	0.53	0.77
3	$12.0*10^{-3}$	$5.6*10^{-3}$	0.72	0.78
4	$13.3*10^{-3}$	$9.3*10^{-3}$	0.77	0.64
5	$12.9*10^{-3}$	$7.1*10^{-3}$	0.78	0.73
6	$12.0*10^{-3}$	$4.5*10^{-3}$	0.71	1.19
7	$12.0*10^{-3}$	$4.1*10^{-3}$	0.91	0.90
8	$12.2*10^{-3}$	$3.7*10^{-3}$	1.35	1.01

5.3.3 Ratio of Conductivities

Table 5.3 presents measured values at equilibrium and calculated ratios of solid and liquid conductivities. The calculations are carried out as outlined in section 5.2.2.

5.4 Discussion

5.4.1 Position of Interface

5.4.1.1 Dendritic Growth of Solid Phase

As noted in section 3.5.2.2, when doing experiments to find the solid thermal conductivities of pure components, i.e., freezing, dendritic growth rendered it impossible to determine the position of the solid-liquid interphase.

No such problems were encountered when working with mixtures. This is most probably due to the fact that there are thermal gradients in the liquid phase. They were not present in the earlier measurements.

The thermal gradients hinder the growth of dendrites.

5.4.1.2 Mushy Zone

Webb and Viskanta [40] have observed the development of a mushy zone.

A mushy zone is a zone where solid and liquid coexist. In the mushy zone, the temperature is higher than the freezing point of the liquid and at the same time lower than the melting point of the solid. This is rendered possible by the compositions of the solid and liquid phase.

No mushy zone was observed at any time during the experiments reported here. In all experiments carried out, the solid-liquid interface was distinct and sharp.

There are two possible explanations for this phenomenon.

First, if the composition of the liquid is at the eutectic point, the mixture can be regarded as a pure component, i.e: the composition of the solid and liquid the same.

The other possibility is that the chemical diffusion goes faster than the diffusion of heat. If that is the case, both the liquid and solid will be homogeneous.

The compositions of the solid and liquid are not equal, but the melting point of the solid and the freezing point of the liquid will be the same temperature.

Since the compositions were not always close to the eutectic point, one must therefore assume that the latter hypothesis is correct, and that the chemical diffusion is faster than the diffusion of heat.

This is supported by the observations of Tan and Leong [7]. They did not observe a mushy zone during freezing of a 50 % mixture of octadecane and hexadecane. They concluded that mixtures of octadecane and hexadecane are not suitable for the study of a mushy zone in solidification experiments.

The observations of Webb and Viskanta [40] might have been caused by their experimental conditions. Their experimental cell was initially at a temperature between the melting points of octadecane and heptadecane. All of the walls in their cell were adiabatic, except for the bottom. This implies that there was only a small thermal gradient in the liquid phase, and it is therefore quite possible that dendrites, as reported in section 3.5.2.2, would form. These dendrites may be mistaken for a mushy zone.

Webb and Viskanta [40] write that they neglect species diffusion. They report that the Lewis number, Eq. (5.4), is typically of the order of 100 (see also section 6.4.6):

$$Le = \frac{k}{D\rho\left(\frac{C_p}{M_r}\right)} \tag{5.4}$$

The value of the Lewis number caused Webb and Viskanta [40] to conclude that the diffusion of heat occured much more rapidly than diffusion of the species. On the other hand, this conclusion is not consistent with their numerical model. Their numerical model is developed on the assumption of uniform concentration in both liquid and solid. This implies rapid chemical diffusion.

An additional difference between this work and the work of Webb and Viskanta [40] is that Webb and Viskanta [40] did not replenish the liquid as the solid formed. Consequently, the composition of their liquid phase will, as solidification occurs, change toward the eutectic point.

Table 5.4: Difference in calculated and measured interface temperature.

Exp.#	T_{liq}^{calc} (K)	T_{liq}^{calc}-T_{liq}^{meas} (K)
1	291.6	-1.6
2	294.0	-1.6
3	291.4	-0.3
4	297.1	0.7
5	298.4	0.3
6	294.6	-2.3
7	295.8	0.1
8	293.1	1.1

In the experimental cell used in this work, fresh liquid was continously replenished from the liquid reservoirs.

5.4.2 Temperature on the Interface

5.4.2.1 Comparison of Measurements with Calculations

The differences between calculated and measured interface temperature , Table 5.4, range from 2.3 K to 0.1 K.

For the binary mixtures C_{16}-C_{17} and C_{16}-C_{18} the differences can be explained by looking at the calculated binary phase envelopes in chapter 4. (Figs. (4.3 and 4.4)) The discrepancies between the measured values and the calculated values are of the same order and sign as the differences between the experimental values of Smith [46] and the calculated liquidus. This observation supports the view that the measured values are more correct than the calculated.

5.4.2.2 Measurements during Experiment

When carrying out the first three experiments, a measurement of the temperature on the interface as freezing occurred was carried out. The decision was made to abandon these measurements since the value did not differ signifi-

cantly from the value at steady state. The measurements were also difficult to accomplish in practice.

These small differences observed in the first three experiments nevertheless support the view that the chemical diffusion is more rapid than the diffusion of heat. Otherwise, the temperature on the interface would have changed if the composition of the liquid changed.

5.4.2.3 Total Assessment of Error in Temperature on the Interface

The temperature was measured by inserting a thermal element through the liquid reservoirs. The most difficult part of the measurement was to find the right position. The solid was soft and gave way if the thermocouple was pressed down too hard, but the temperature did not deviate more than 1 K. A conservative estimate for the error in temperature is :

$\sigma_{T_{liq}^{meas}} = 1$ K.

This is consistent with the fact that the greatest difference between the calculated and the measured interface temperature, 2.3 K in experiment # 6, is less than $\sigma_{T_{liq}^{meas}} + \sigma_{T_{liq}^{calc}} = 3$ K.

5.4.3 Ratio of Conductivities

5.4.3.1 Solid Structure

The average value of the ratio of conductivities is 0.93. This is close to the values for the rotator phases of heptadecane and octadecane. It is therefore reasonable to conclude that the structure of the solid is rotator.

As discussed in section 2.4.2, this conclusion is supported by spectroscopic and calorimetric studies. But as the temperature is lowered, one should expect that the solid transforms into an orthorhombic structure.

Since the orthorhombic phase is less entropic than the rotator, the thermal conductivity is expected be higher, and the ratio $\frac{k_l}{k_s}$ lower. If the solid

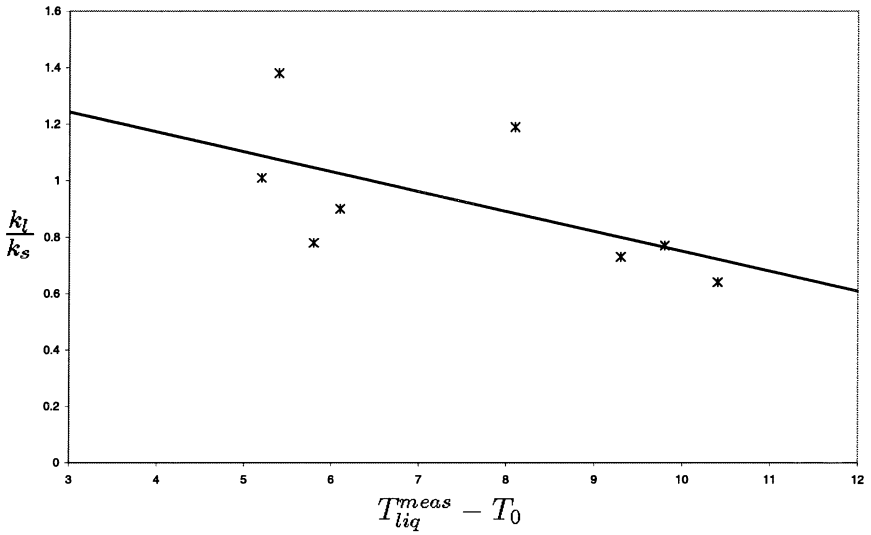

Figure 5.2: Points : $\frac{k_l}{k_s}$ against $T_{liq}^{meas} - T_0$, solid line: linear regression

rearrange into an orthorhombic structure on cooling, one should therefore observe a tendency to a lower ratio as the difference $T_{liq}^{meas} - T_0$ is increased. In Fig. (5.2) $\frac{k_l}{k_s}$ is plotted against $T_{liq}^{meas} - T_0$.

As one can see, there is a slight tendency toward a lower ratio as the difference $T_{liq}^{meas} - T_0$ is increased. This indicates that the conductivity of the solid is higher as the temperature is lowered. This may be caused by a change of solid structure into an orthorhombic phase.

5.4.3.2 Total Assessment of Error in Ratio of Conductivities

An assessment of the error is done analogously to the assessment of error in the pure component conductivities, see section 3.5.3.

As shown in section 5.2.2 the thermal gradients are calculated using the temperature on the liquidus instead of the melting temperature. Since $\sigma_{T_{liq}^{calc}}$ = 2 K (section 4.4.5) and $\sigma_{T_{liq}^{meas}} = 1$ K compared to $\sigma_{T_{mp}}$= 0.25 K the errors in the thermal gradients are more notable than in the pure component case.

The values for the experiment # 1 on the mixture of C_{16}-C_{18} are used as an

example.

Using $\sigma_{T_{liq}^{meas}} = 1$ K instead, one finds that the error is 25 % of the reported value, using $\sigma_{T_{liq}^{calc}} = 2$ K, the uncertainty is calculated to 50 % of the reported value.

5.4.4 Recommendation for Future Work

It would have been a major improvement if one could continously monitor the temperature on the solid-liquid interface. This ought to be implemented in future experiments. One possibility is to introduce several thermoelements inside the cell and log these temperatures as solidification occurs.

As a further complication, one should introduce crude oils in the cell. This has already been tested with some success. But since the position of the solid-liquid interface was difficult to measure adequately accurate, the results from these experiments are not reported in this work.

However, it is possible to imagine other and better methods for measuring the position of the interface. An obvious approach to the problem is to use a stronger lamp at the back of the cell. Another possibility is to remove the asphaltenes of the crude oil. This will make the oil more transparent.

It might also be an idea to devote more attention to the deposited solid. The deposited solid could carefully be sliced into thin pieces. These pieces should subsequently be analyzed in order to decide whether or not the composition of the solid changes as freezing occurs. This may help to resolve the question of limiting mechanism.

5.5 Conclusion

Experiments have been performed for the purpose of investigating the freezing of mixtures of *n*-alkanes in the C_{16}-C_{19} range. The positions of the solid-liquid interfaces have been measured as freezing occurred.

Calculations of the ratio of liquid and solid conductivities show that the

solid structure is predominantly in a rotator structure at the temperatures investigated. There are indications of a transformation into an orthorhombic structure at lower temperatures.

The temperatures on the solid-liquid interface have been measured, and compared with calculated values from chapter 4. The temperature of the interface is represented better by the measured interfacial temperatures than by the calculated interfacial temperatures.

The experimental results support the hypothesis that the diffusion of heat is the limiting mechanism and the chemical diffusion is more rapid. This result in a homogeneous liquid composition.

Chapter 6

Numerical Modeling

6.1 Introduction

The final aim of this thesis is to simulate freezing of mixtures of *n*-alkanes in the C_{16}-C_{19} range. The initial and boundary conditions will be chosen as to imitate the conditions of the experiments reported in chapter 5.

The basis of the numerical procedure is described by Versteeg and Malalasekera [11] and Patankar[12].

Webb and Viskanta [40] report modeling of mixtures of C_{16}-C_{18}. Their focus is primarily on the mushy zone and they do not model diffusion.

Voller's [52] approach to the problem is based on casting of metals and is also concerned with the mushy zone. The solid, but not the liquid, is assumed to be a eutectic mixture .

The simulations will be used to test different hypothesis regarding physical properties and mechanisms.

Parts of this work was presented at the seventh international conference on heat transfer, in Halkidiki April 2002 [53].

6.2 Procedure

6.2.1 Overview

The method which is applied is based on the numerical solution of heat and mass transfer outlined by Versteeg and Malalasekera [11] and Patankar[12].

The method can be termed quasi-implicit. The temperature field and the liquid composition are solved implicitly, but the position of the solid-liquid interface is found explicitly.

6.2.1.1 Equations to Be Solved

The equation solved to find the position of the interface is Eq.(2.1):

$$-k_s\frac{\partial T_s}{\partial x} + k_l\frac{\partial T_l}{\partial x} + \rho\frac{\Delta h_{mp}}{M_r}\frac{dx_{mp}}{dt} = 0 \tag{6.1}$$

The temperature fields are calculated from Eq.(2.6):

$$\rho\frac{C_p}{M_r}\frac{\partial T}{\partial t} = \frac{\partial}{\partial x}k\frac{\partial T}{\partial x} \tag{6.2}$$

Finally, the liquid composition is determined from the solution of Eq. (6.3), which is found in Laidler and Meiser [54]:

$$\frac{\partial C^i}{\partial t} = -\frac{\partial}{\partial x}J^i \tag{6.3}$$

6.2.1.2 General Simplifying Assumptions

- Only freezing is considered.
- All heat and mass transfer is one-dimensional.

- There is local equilibrium at the solid-liquid interface.
- There is no convection, i.e., buoyancy induced mass flow in the liquid.

6.2.1.3 Grid

The calculation domain is divided into calculation volumes as shown in Fig. (6.1). Inside each calculation volume, all properties are constant.

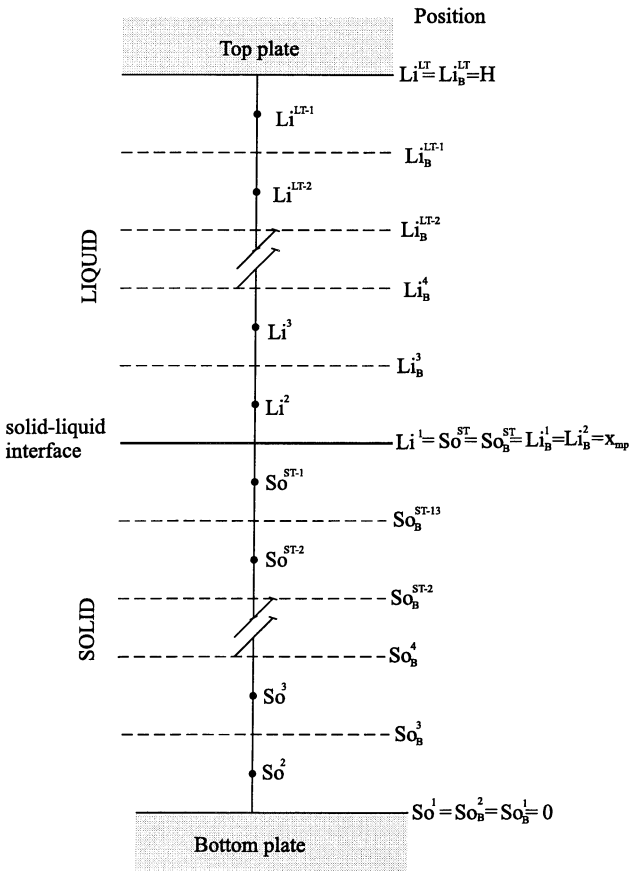

Figure 6.1: Division of the calculation domain into calculation volumes

In this chapter, superscripts may refer to the calculation volume the property refers to. For instance $T_l^{p,2}$ is the temperature in the liquid calculation

volume # 2 at the previous time step, ρ_s^{ST-1} is the density of the solid calculation volume which borders on the interface and $k_{B,l}^3$ denotes the thermal conductivity at the border between liquid calculation volumes 3 and 2.

Note that the superscript ^{n} or numbers in superscript solely refer to calculation volume, while ^{i} and ^{j} refer to component.

6.2.1.4 Overview of Algorithm

The algorithm used is outlined in Fig. (6.2).

6.2.2 Determination of the Position of the Solid-Liquid Interface

6.2.2.1 Initial Conditions of the Position of the Solid-Liquid Interface

- Initially there is no solid in the cell, x_{mp}=0.
- $x_{mp} = Li^2$ once the temperature of liquid cell 2 is lower than T_{liq}.

6.2.2.2 Numerical Solution of the Position of the Solid-Liquid Interface

The liquid and solid calculation domains are divided by the solid-liquid interface. The position of the solid-liquid interface is found from the solution of Eq. (6.1). Considering only freezing, the equation is written as Eq.(6.4):

$$-k_s\frac{\partial T_s}{\partial x} + k_l\frac{\partial T_l}{\partial x} + \rho_l\frac{\Delta h_{mp}}{M_r}\frac{dx_{mp}}{dt} = 0 \tag{6.4}$$

Eq (6.4) is discretized in order to calculate the position explicitly:

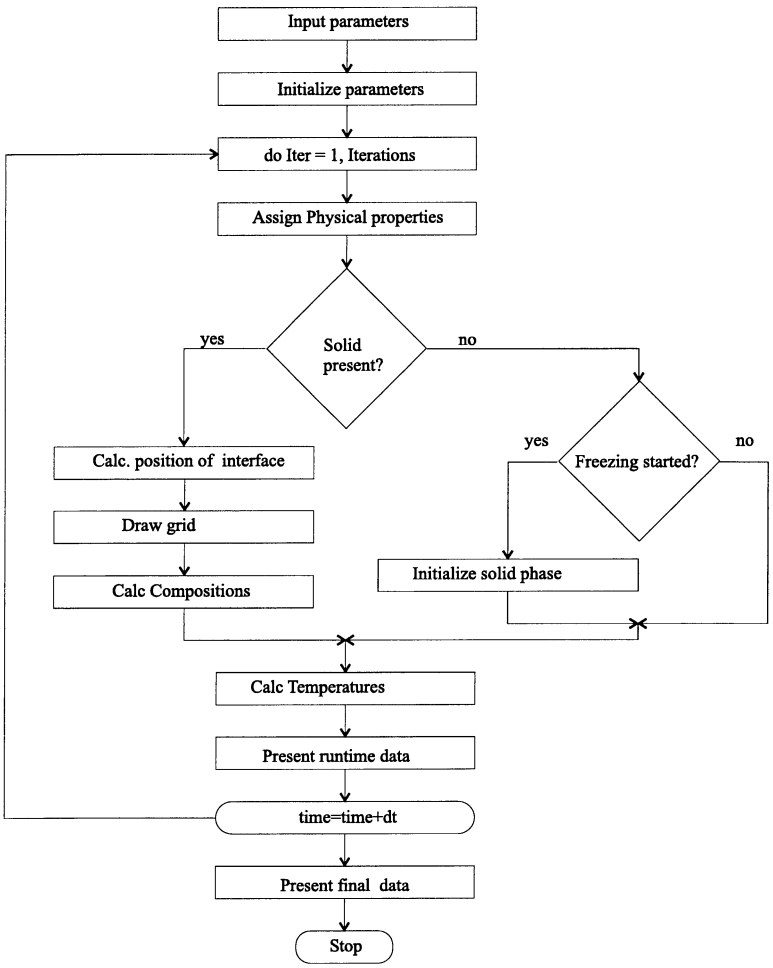

Figure 6.2: Overview of algorithm used for determination of the position of the solid-liquid interface.

$$x_{mp} = x^p_{mp} + \frac{dtM^1_{r,l}}{\rho^1_l \Delta h_{mp}} \left(k^{ST}_s \frac{T_{liq} - T^{ST-1}_s}{So^{ST} - So^{ST-1}} - k^1_l \frac{T^2_l - T_{liq}}{Li^2 - Li^1} \right) \tag{6.5}$$

The temperature on the liquidus is found either from the measured values of chapter 5 or from utilizing the liquid compositions in calculation volume 2 as input to the appropriate correlations. (see section 4.3.2)

6.2.3 Determination of the Temperature Fields

6.2.3.1 Initial Conditions for the Temperature Fields

- The temperature of the experimental cell is uniform.
- When a solid forms, the temperature field is linear.

6.2.3.2 Boundary Conditions for the Temperature Fields

- The temperatures at the top and bottom of the calculation domain are constant.
- The temperature of the solid-liquid interface is determined from measurements or correlations. (see section 6.2.2.2)

6.2.3.3 Numerical Solution of the Temperature Fields

The temperature fields of the respective phases are found by the solution of Eq. (6.2) :

$$\rho \frac{C_p}{M_r} \frac{\partial T}{\partial t} = \frac{\partial}{\partial x} k \frac{\partial T}{\partial x} \tag{6.6}$$

These equations are discretized implicitly. The results can be presented as:

$$a^n T^n = a^{n-1} T^{n-1} + a^{n+1} T^{n+1} + a^{p,n} T^{p,n} \tag{6.7}$$

The coefficients of the matrices for the liquid and solid phases are found in Table 6.1.

The solutions for the top and bottom calculation volumes are found by implementing the boundary conditions. At the top of the liquid T^{LT}=T_H. At the bottom of the liquid, T_l^1=T_{liq} when there is solid phase present, but before

Table 6.1: Coefficients of temperature matrices

Calc. vol.	a^n	a^{n-1}	a^{n+1}	$a^{p,n}$
Liquid cell #n	$a^{p,n} + a^{n-1} + a^{n+1}$	$\frac{k^n_{B,l}}{Li^n - Li^{n-1}}$	$\frac{k^{n+1}_{B,l}}{Li^{n+1} - Li^n}$	$\frac{C^n_{p,l}}{M^n_{r,l}} \rho^n_l \frac{Li^{n+1}_B - Li^n_B}{dt}$
Solid cell #n	$a^{p,n} + a^{n-1} + a^{n+1}$	$\frac{k^n_{B,s}}{So^n - So^{n-1}}$	$\frac{k^{n+1}_{B,s}}{So^{n+1} - Li^n}$	$\frac{C^n_{p,s}}{M^n_{r,s}} \rho^n_s \frac{So^{n+1}_B - So^n_B}{dt}$

freezing has started T^1_l=T_0. The boundary conditions for the solid phase are T^{ST}_s=T_{liq} and T^1_s=T_0

These matrices are solved using TDMA as described by Versteeg and Malalasekera [11].

6.2.4 Determination of the Compositions

6.2.4.1 Simplifying Assumptions for the Compositions

- No diffusion in the solid phase.

6.2.4.2 Initial Conditions for the Compositions

- The content of the experimental cell is liquid.
- The composition of the experimental cell is equal to the composition of the liquid reservoirs.
- When a solid is formed, the composition is uniform.

6.2.4.3 Boundary Conditions for the Compositions

- No diffusion through the bottom.
- The liquid composition at the top plate is equal to the composition of the liquid reservoirs.
- The compositions on the interface are at equilibrium.

6.2.4.4 Determination of the Liquid Composition

The calculation of the liquid composition is done on a molar concentration basis. Since mole fractions are used elsewhere, a conversion is required:

$$C_l^{n,j} = \frac{\rho_l^n x^{n,j}}{M_{r,l}^n} \tag{6.8}$$

Laidler and Meiser [54] show that the rate of change in concentration due to diffusion can be expressed:

$$\frac{\partial C_l^i}{\partial t} = -\frac{\partial}{\partial x} J_l^i \tag{6.9}$$

This equation forms the basis of the solution of the liquid composition. Before the equation can be discreticized, one has to find appropriate expressions for the flux, J_l^i.

For the inner calculation volumes the flux is found from Eq. (2.32) on a mole fraction basis:

$$J_l^i = -D_l \frac{\rho_l}{M_{r,l}} \frac{\partial}{\partial x} \frac{C_l^i M_{r,l}^i}{\rho_l} \tag{6.10}$$

It is necessary to give special attention to the flux out of the bottom calculation volume.

Denoting the properties of the newly formed solid (dark colored area in Fig. (6.3)) during a timestep with a subscript $_{new}$, the composition of the solid phase formed during a timestep is:

$$s_{new}^j = x^{2,j} K^j \tag{6.11}$$

K^j is the solid-liquid equilibrium constant calculated at the interface. On a molar concentration basis the solid concentration can be expressed as:

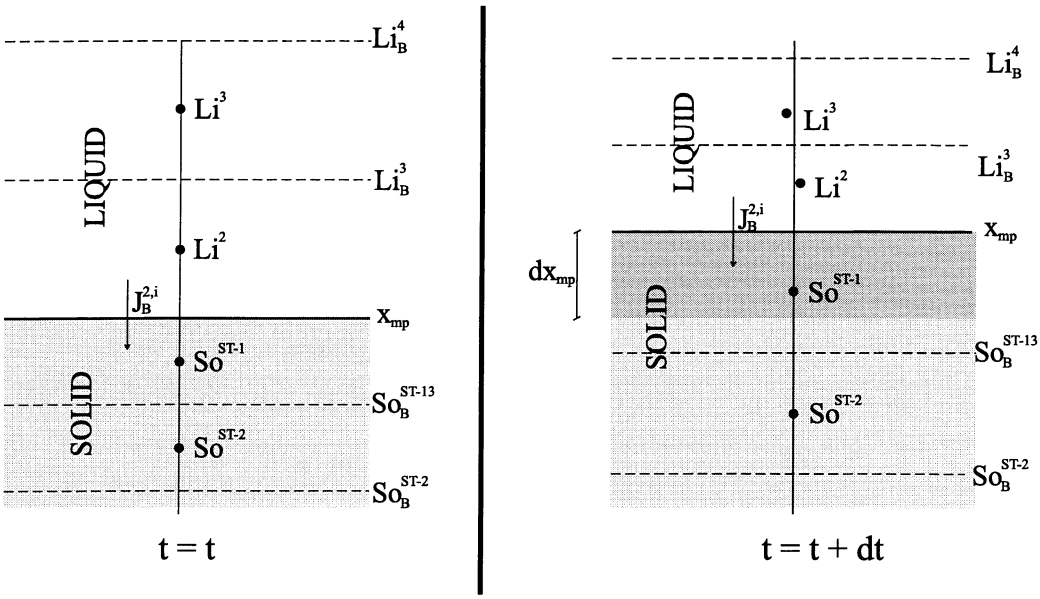

Figure 6.3: Schematic growth of solid phase

$$C^j_{s,new} = \frac{\rho^j_{s,new}}{M_{r,s,new}} \frac{K^j C^{2,j}_l M^2_{r,l}}{\rho^2_l} \tag{6.12}$$

The number of moles that enters the new solid phase during a timestep is:

$$dn^j_{s,new} = C^j_{s,new} dx_{mp} A = \frac{\rho^j_{s,new}}{M_{r,s,new}} \frac{K^j C^{2,j}_l M^2_{r,l}}{\rho^2_l} dx_{mp} A \tag{6.13}$$

A is here the area of the interface.

Finally, the flux from the liquid into the solid is expressed as:

$$J^{2,j}_{B,l} = \frac{dn^j_{s,new}}{dt} \frac{1}{A} = \frac{dx_{mp}}{dt} \frac{\rho^j_{s,new}}{M_{r,s,new}} \frac{K^j C^{2,j}_l M^2_{r,l}}{\rho^2_l} \tag{6.14}$$

The concentration of the top calculation volume can easily be determined by remembering the boundary condition. Since the content of the experimental cell shrinks during freezing, the concentration of the top calculation volume is

Table 6.2: Coefficients of liquid composition matrix

cal.vol.	Inner	Bottom	Top
a^n	$a^{n,p} + \frac{A_B^{n+1} M_r^{n,i}}{(Li^{n+1} - Li^n)\rho^n} + \frac{A_B^n M_r^{n,i}}{(Li^n - Li^{n-1})\rho^n}$	$a^{2,p} + \frac{A_B^3 M_r^{2,i}}{(Li^3 - Li^2)\rho^2} + \frac{dx_{mp}\rho_s^{new} K^i M_r^2}{dt M_{r,s}^{new} \rho_l^2}$	0
a^{n+1}	$\frac{A_B^{n+1} M_r^{n+1,i}}{(Li^{n+1} - Li^n)\rho^{n+1}}$	$\frac{A_B^3 M_r^{3,i}}{(Li^3 - Li^2)\rho^3}$	0
a^{n-1}	$\frac{A_B^n M_r^{n-1,i}}{(Li^n - Li^{n-1})\rho^{n-1}}$	0	0
$a^{n,p}$	$\frac{Li_B^{n+1} - Li_B^n}{dt}$	$\frac{Li_B^3 - Li_B^2}{dt}$	1

simply given by the composition of the liquid reservoirs. The concentration of the liquid reservoirs is the same as the initial concentration of the cell, thus:

$$C_l^{LT,j} = C_l^{LT,j,p} \tag{6.15}$$

The expressions for $J_{B,l}^j$, Eqs. (6.10 and 6.14),are implemented in Eq.(6.3) and discretized. The results are presented on the same form applied in section 6.2.3.3, i.e.:

$$a^n C^n = a^{n-1} C^{n-1} + a^{n+1} C^{n+1} + a^{n,p} C^{p,n} \tag{6.16}$$

The coefficients are presented in Table 6.2. A_B^i is defined as:

$$A_B^i = \frac{D_B^{n,i} \rho_{B,l}}{M_{r,l,B}} \tag{6.17}$$

The resulting matrix is solved using TDMA, as described in Versteeg and Malalasekera [11].

6.2.4.5 Determination of the Solid Composition

The growth of the solid phase is schematically shown in Fig. (6.3).

Assuming that there is no diffusion in the solid phase, the solid composition does not change once formed. The new solid composition is found by a

reconfiguration of the grid.

6.2.5 Determination of the Thermophysical Properties

The thermophysical properties for the pure components used in the calculations are given i Appendix A.

6.2.5.1 Simplifying Assumptions

- The physical properties are only functions of composition and phase, not of temperature.
- The liquid mixture is ideal.

6.2.5.2 Determination of Liquid Properties

Since ideal mixing is assumed, i.e. no volume or heat change, the molar volume of the mixture can be calculated as:

$$v_l = \sum x^j v_l^j \tag{6.18}$$

The molar mass of the mixture is found equivalently,

$$M_{r,l} = \sum x^j M_r^j \tag{6.19}$$

Using the above expressions, the density of the liquid mixture is estimated as:

$$\rho_l = \frac{M_{r,l}}{v_l} \tag{6.20}$$

Both the enthalpy and heat capacity are found by molar fraction weighted averages. For example, the heat capacity is calculated as:

$$C_{p,l} = \sum x^j C_p^j \tag{6.21}$$

In order to find the diffusion coefficient, the tracer diffusion coefficients are approximated from correlations presented by Wong and Hayduk [55]:

$$D_{inf}^i = \frac{1}{10000}\left(0.317 M_{r,l}(1000 M r_{r,l}^i)^{-0.569} \exp\left(\frac{-487.7 - 8570 M_{r,l} + 9000 M_{r,l}^2}{T}\right)\right) \tag{6.22}$$

The Darken relation as presented in Dysthe [18] is applied to find the mutual diffusion coefficients:

$$D^{ij} = \sum_i x^i D_{inf}^i \tag{6.23}$$

When this diffusion coefficient is used without any alteration, the diffusion is termed to be slow.

Quick diffusion is simply modeled by multiplying the diffusion coefficient with 100,000.

6.2.5.3 Determination of Solid Properties

One of two methods is used to determine the solid properties.

The first method is to calculate the solid properties in the same way as the liquid properties, i.e: to use molar averages.

The other method is to determine the molar mass using the solid equivalent of Eq. (6.19) and otherwise use the molar properties of solid C_{17}.

Table 6.3: Input Conditions for Numerical Simulations

Sim.#	Exp.#	Solid Prop.	T_{liq}	Diffusion	dt	ST/LT
1	1	C_{17}	meas.	quick	0.01	100/100
2	2	C_{17}	meas.	quick	0.01	100/100
3	3	C_{17}	meas.	quick	0.01	100/100
4	4	C_{17}	meas.	quick	0.01	100/100
5	5	C_{17}	meas.	quick	0.01	100/100
6	6	C_{17}	meas.	quick	0.01	100/100
7	7	C_{17}	meas.	quick	0.01	100/100
8	8	C_{17}	meas.	quick	0.01	100/100
9	1	C_{17}	meas.	quick	0.1	100/100
10	1	C_{17}	meas.	quick	0.001	100/100
11	1	C_{17}	meas.	quick	0.01	50/50
12	1	C_{17}	meas.	quick	0.01	200/200
13	1	molar avg.	meas.	quick	0.01	100/100
14	1	C_{17}	calc.	slow	0.01	100/100
15	1	C_{17}	calc.	quick	0.01	100/100

6.3 Results

6.3.1 Simulation Performed

Table 6.3 presents the input data to the simulations performed. Experiment # refers to experiment # in Table 5.1.

The boundary conditions of the simulations, like T_H and T_O, can be found in Table 5.1.

6.3.2 Position of Interface

As an example, only the results from a calculation performed to simulate experiment # 1, done with the C_{16}-C_{18} mixture, will be presented here, see Fig. (6.4).

The results of simulations # 1 to # 8 can be found in appendix G.

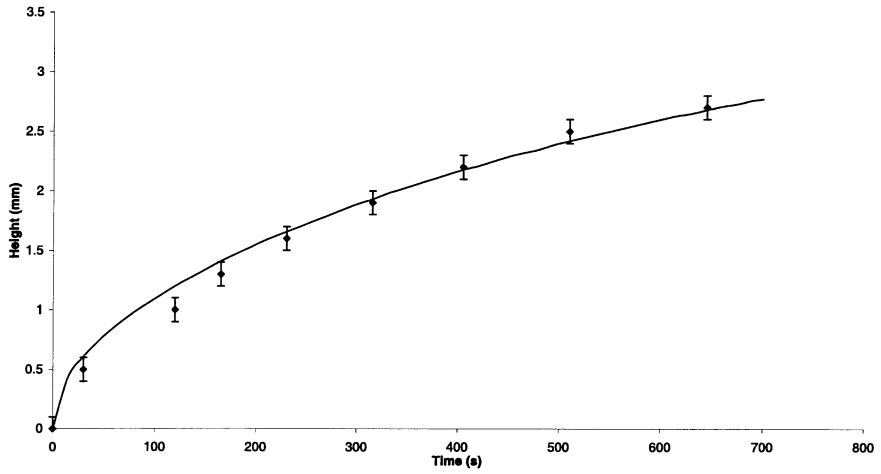

Figure 6.4: Calculated and experimental position of solid-liquid interface during experiment and simulation # 1, Points: experimental value, solid line: result from numerical simulation

6.4 Discussion

6.4.1 Overview

6.4.1.1 Simplifying Assumptions

Obviously only freezing is considered since the experiments simulated were all freezing experiments.

Using a one dimensional method can be justified since the experimental cell was, as described in appendix B, thoroughly insulated. If the cell had not been sufficiently insulated, crystallization would have occurred on the walls of the experimental cell. No such crystallization was observed.

The assumption of local equilibrium is a prerequisite for the theory of irreversible thermodynamics as formulated by Onsager and is discussed by Førland, Førland and Ratkje [56].

In section 3.5.4.2 it is discussed why there is no buoyancy induced flow in the experimental cell.

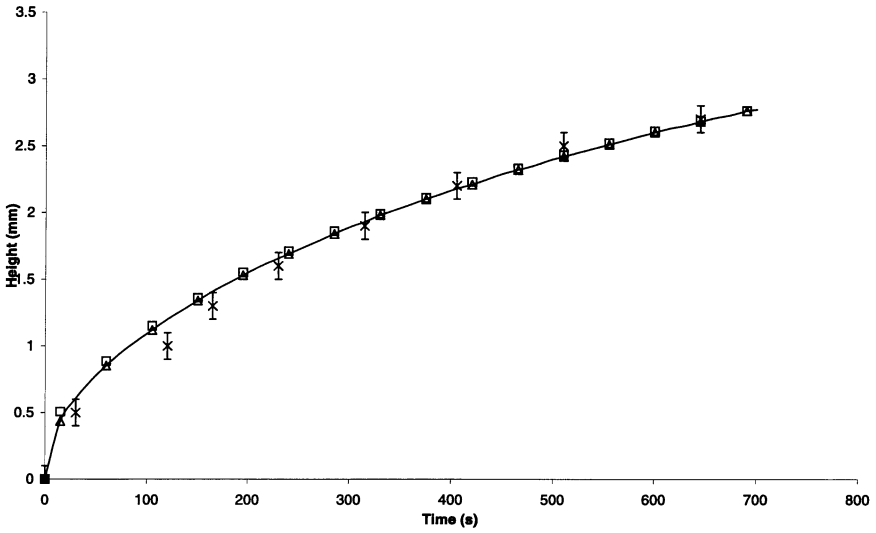

Figure 6.5: Calculated and experimental position of solid-liquid interface during experiment and simulation # 1. △: LT=ST=50, solid line: LT=ST=100, □: LT=ST=200, ∗: experimental points

6.4.1.2 Dependency of Grid

The simulations were normally executed with 100 calculation volumes in both the liquid and solid grids. In Fig.(6.5) simulations with 50 and 200 calculation volumes are presented. There is a slight deviation between the simulation performed with the coarsest grid and the two other calculations only in the first 100 seconds. The difference is caused by the initialization of the solid phase.

The minor dependency implicates that the discretization is good. The approximation of grid independency in the solution of the liquid composition and the temperature fields is also warranted by the small differences.

6.4.1.3 Dependency of Time step

In Fig.(6.6) results from simulation preformed with dt=0.1 s and dt=0.001 s are plotted along with results from an ordinary simulation where dt=0.01 s. There is some discrepancy, particularly in the beginning of the simu-

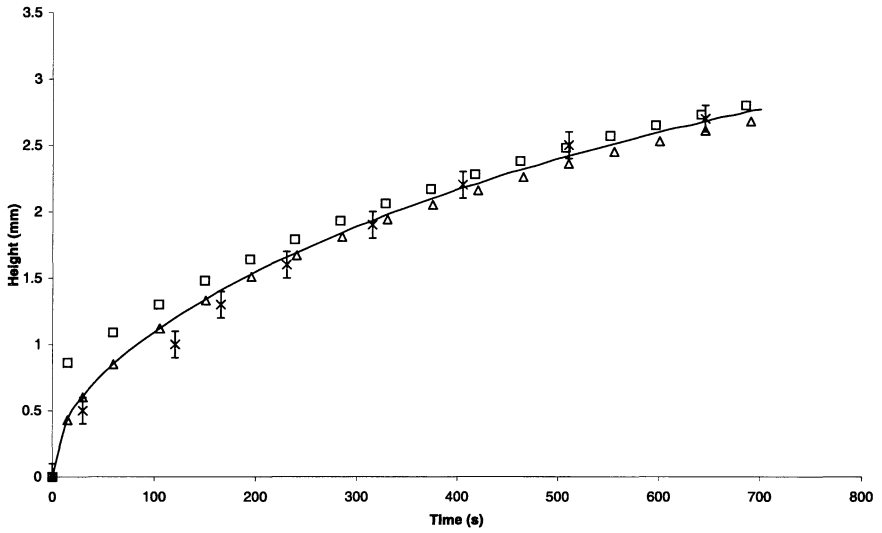

Figure 6.6: Calculated and experimental position of solid-liquid interface during experiment and simulation # 1. △: dt=0.1, solid line: dt=0.01, □: dt=0.001, ∗: experimental points

lations. The difference between the simulation carried out with dt=0.01 s and dt=0.001 is, as will be shown in the following, too small to be of any importance.

Like in the case of grid dependency, the early differences can be explained by the initialization of the solid phase.

A prerequisite for a valid solution is that the solid grows less than the length of a liquid calculation volume during a timestep. The freezing process went fastest in the beginning of the experiments. But the solid grew always less than 1 mm during the first 50 s or 5000 timesteps. Thus, the solid grew less than $2*10^{-7}$ m during each timestep. Assuming that the liquid covers half of the experimental cell, the liquid calculation volumes are $\frac{6*10^{-3}mm}{100}$=$6*10^{-5}$ m. Thus, the solid phase grew always much less than the length of a liquid calculation cell.

6.4.2 Determination of the Position of the Solid-Liquid Interface

6.4.2.1 Initial Conditions for the Position of the Solid-Liquid Interface

Since the solid initially was very thin, $x_{mp} = Li^2$, the initial conditions do not influence the solution substantially.

6.4.2.2 Numerical Solution of the Position of the Solid-Liquid Interface

Linear gradients seem to be acceptable approximations. Otherwise, the numerical solutions should have changed considerably when the grid was changed. As seen in Fig.(6.5), the solutions are adequately stable as the grid is changed.

6.4.3 Determination of the Temperature Fields

6.4.3.1 Initial Conditions for the Temperature Fields

It should be a natural assumption that the temperature field of the liquid is initially uniform. On the other hand, it is not evident that the temperature field of the newly formed solid is linear. As discussed previously the solid is extremely thin when formed and the initial conditions are therefore not significant.

6.4.3.2 Boundary Conditions for the Temperature Fields

Since the top and bottom plates were thermostated, constant temperature on the top and bottom plate are necessary conditions.

The temperature on the solid-liquid interface is more difficult to determine. In chapter 5 there was a discussion on whether calculated or measured values

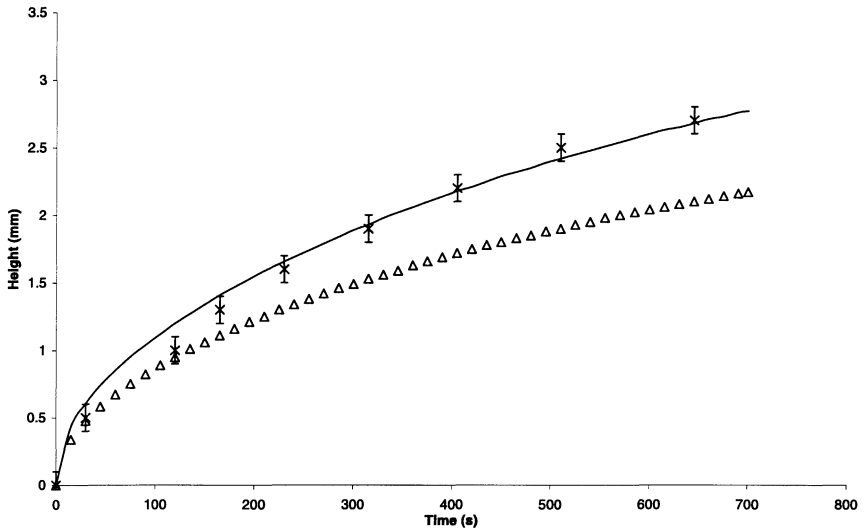

Figure 6.7: Calculated and experimental position of solid-liquid interface during experiment and simulation # 1. △: calculated T_{liq}, solid line: measured T_{liq} ,∗: experimental points

should be used. In Fig. (6.7) results from both measured value and calculated value are presented. As one can see, the deviation is considerable. The difference between calculated and measured value is 1.6 K. In chapter 5 it was argued for the use of the measured value, and the practice is continued in this chapter.

The uncertainty of the measured interfacial temperature, T_{liq}^{meas}, is assessed in section 5.4.2.3 to $\sigma_{T_{liq}^{meas}} = 1$ K. This uncertainty is one of the major weaknesses of the simulations.

6.4.3.3 Numerical Solution of the Temperature Fields

Patankar [12] shows that all coefficients must have the same sign if the solution should be stable. As one can see in Table 6.1 all coefficients are positive.

The solution is also independent of both timestep and grid. This should infer a stable and convergent solution.

6.4.4 Determination of the Compositions

6.4.4.1 Simplifying Assumptions for the Compositions

Even if there is diffusion in the solid phase it ought to be neglected in the simulations. Solid diffusion processes are far too slow to be of any significance in the context of this work.

6.4.4.2 Initial Conditions for the Compositions

It is obvious that the content of the experimental cell is initially a homogeneous liquid. Since, as discussed above, the solid initially is extremely thin, the approximation of the composition of the newly formed solid as the equilibrium composition is inferior to other, more notable errors.

6.4.4.3 Boundary Conditions for the Compositions

The condition of no mass flow through the bottom plate is evident since the bottom plate was solid.

At the top plate, the composition of the liquid must be equal to the liquid reservoirs. This is due to the shrinking during solidification which forces the liquid to be replenished from the liquid reservoirs.

As mentioned, the numerical procedure is based on local equilibrium at the solid liquid interface. This implies that the compositions of the solid and liquid should be calculated from the expression for equilibrium.

6.4.4.4 Numerical Solution of Liquid Composition

As shown in Table 6.2, the condition of Patankar [12] regarding positive coefficients is satisfied.

The solution is also independent of time step and grid, see Figs. (6.6 and 6.5), implying a stable and convergent solution.

6.4.5 Thermophysical Properties

6.4.5.1 Simplifying Assumptions for the Thermophysical Properties

As will be shown in the following, constant thermophysical properties are a minor approximation compared to other uncertainties.

The assumption of an ideal liquid phase is supported by the measurements of Ghogomu et al [57]. They have found that liquid mixtures of long-chain *n*-alkanes of similar chain length can be regarded as ideal, i.e., excess enthalpies, volumes and entropies are negligible.

6.4.5.2 Properties of the Liquid Phase

Wada, Nagasaka and Nagashima [41] measured and correlated the thermal conductivities of liquid mixtures of some *n*-alkanes in the C_7-C_{16} range. A linear mixing rule does not show any significant deviation from their measurements.

The magnitude of the chemical diffusion coefficient will be discussed in section 6.4.6.

6.4.5.3 Properties of the Solid Phase

As discussed in section 5.4.3.1, it is reasonable to believe that the solid crystallizes in a rotator phase. since C_{17} has a rotator structure, the molar properties of solid C_{17} were normally used to represent the solid phase.

In Fig.(6.8) results from a simulation carried out with the solid properties estimated as a molar average are plotted along with an ordinary simulation. The results indicate that the properties of C_{17} represent the solid phase better than the molar average.

When the temperature of the solid phase is lowered further, one should as discussed in 5.4.3.1, expect that the solid changes structure. No model for

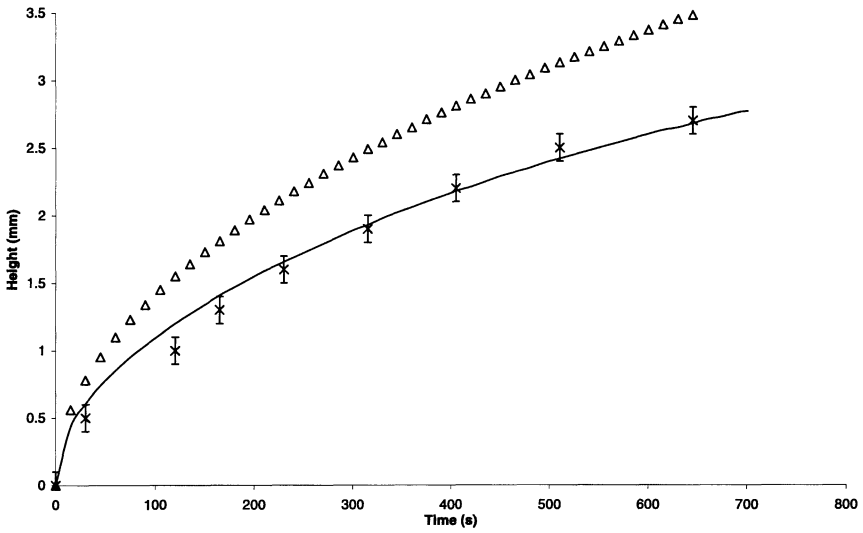

Figure 6.8: Calculated and experimental position of solid-liquid interface during experiment and simulation # 1. △: solid properties found as a molar average, solid line: solid properties as C_{17},∗: experimental points

such a solid-solid equilibrium is implemented in the current simulations.

As one can see from the graphs in appendix G, not all experiments are simulated as well as experiment # 1. This is particularly true of the simulations of experiments # 2,3,4 and 5. These deviations are believed to stem from a combination of erroneous solid properties and interfacial temperatures.

6.4.5.4 Total Assessment of Error in Physical Properties

The uncertainty of the properties of the solid is, together with the uncertain interfacial temperature, the greatest contributor to erroneous simulations.

6.4.6 Limiting Mechanism

The Lewis number is defined in Eq. (5.4) as the ratio between the thermal diffusion and the chemical diffusion:

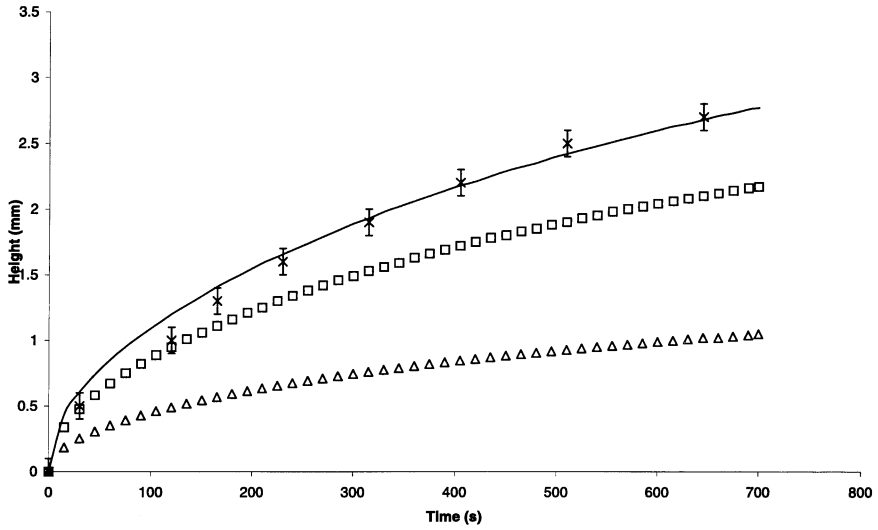

Figure 6.9: Calculated and experimental position of solid-liquid interface during experiment and simulation # 1. Solid line: measured T_{liq} and quick diffusion ,$*$: experimental points, □: calculated T_{liq} and quick diffusion, △: calculated T_{liq} and slow diffusion

$$Le = \frac{k}{D\rho\left(\frac{C_p}{M_r}\right)} \tag{6.24}$$

Inserting typical values, i.e., D=5*10^{-10} ms^{-1}, k_l=0.20 $WK^{-1}m^{-1}$, ρ=750 kgm^3 and $\frac{C_p}{M_r}$=2200 $Jkg^{-1}K^{-1}$, one finds that Le=240 which should imply that the chemical diffusion is slow compared to the thermal diffusion.

In Fig. (6.9) the results from three simulations are plotted. It is interesting to compare the □ (calculated T_{liq} and quick diffusion) with △ (calculated T_{liq} and slow diffusion). The results from the simulation with slow diffusion are significantly below the experimental points.

It is worth noting that none of the results from the simulations where the thermal diffusivity was the limiting step (see appendix G) indicate that the chemical diffusion should be the limiting step. If the chemical diffusion was limiting, the simulated results using the thermal diffusion as limiting would have been well above the experimental results.

But if thermal diffusion were the limiting mechanism, the estimated chemical diffusion coefficients must be far too low. Wong and Hayduk [55] acknowledge that measurements of chemical diffusion coefficients are potentially associated with significant errors, and admit that their correlations subsequently have even more major errors. One should therefore not give too much attention to the calculated Lewis number.

6.4.7 Total Assessment of the Numerical Model

The model represents the experiments within the uncertainties of the physical properties and the interfacial temperature.

6.4.8 Suggestions for Future Work

The results indicate that future work ought to emphasize the importance of more accurate properties of the solid phase instead of calculations of the solid-liquid equilibria.

A final goal should be to implement a wax deposition model in flow simulation code. In order to do that, one must extend the model to two or three dimensions, and the code must be optimized regarding computational speed.

6.5 Conclusion

A numerical model has been developed in order to simulate the experimental freezing of mixtures. The model represents the experiments within the limit of the uncertainties of the physical properties and the interfacial temperature.

The model suggests that the solid structure is predominantly in a rotator structure at the temperatures investigated. The properties of the rotator phase are represented better by the physical properties of solid C_{17} than by molar averages. At lower temperatures there are indications of a transformation into an orthorhombic structure.

The results from the simulations support the hypothesis that the limiting mechanism of deposition is the thermal diffusion. This implies that further work should focus on the determination of the thermophysical properties of solid wax instead of further development of models for the solid-liquid equilibrium.

Chapter 7

Conclusion

In this work thermal conductivities have been determined at the melting point for solid and liquid unbranched alkanes ranging from C_{16} to C_{19}. An assessment of the error of the method has been performed.

The measurements of solid conductivities are in accordance with measurements reported previously and confirm the applicability of the method. Liquid conductivities are higher than extrapolated values from the literature. This is believed to be caused by structural changes close to the melting point. The structural changes are not taken into account when extrapolating the values from the literature.

Experiments have been performed for the purpose of investigating the freezing of mixtures of *n*-alkanes in the C_{16}-C_{19} range. The positions of the solid-liquid interfaces have been measured as freezing occured.

Calculations of the ratio of liquid and solid conductivities show that the solid structure is predominantly in a rotator structure at the temperatures investigated. There are indications of a transformation into an orthorhombic structure at lower temperatures.

The temperatures on the solid-liquid interface have been measured, and compared with calculated values from chapter 4. The temperature of the interface is represented better by the measured interfacial temperatures than by the calculated interfacial temperatures.

The experimental results indicate that the diffusion of heat is the limiting mechanism and the chemical diffusion is more rapid. This results in a homogeneous liquid composition.

A numerical model has been developed in order to simulate the experimental freezing of mixtures. The model represents the experiments within the limit of the uncertainties of the physical properties and the interfacial temperature.

Also the numerical model suggests that the solid structure is predominantly in a rotator structure at the temperatures investigated. The properties of the rotator phase are represented better by the physical properties of solid C_{17} than by molar averages.

The results from the simulations support the hypothesis that the limiting mechanism of deposition is the thermal diffusion. This implies that further work should focus on the determination of the thermophysical properties of solid wax instead of further development of models for the solid-liquid equilibrium.

Bibliography

[1] B. Vos and K. van den Haak. Wax Interaction Modifiers for Waxy Crude Oils. May 1980. Ninth Annual Convention.

[2] R. J. Russel and E. D. Chapman. The Pumping of 85 °F Pour Point Assam (Nahorkatiya) Crude Oil at 65 °F. *Journal of the Institute of Petroleum*, 57(554):117–128, March 1971.

[3] H.P. Rønningsen, B. Bjørndal, A.B. Hansen, and W.B. Pedersen. Wax Precipation from North Sea Crude Oils. 1. Crystalliazation and dissolution Temperatures, and Newtonian and Non-Newtonian Flow Properties. *Energy & Fuels*, 5, 1991.

[4] J.F. Branthaver, K.P. Thomas, S.M. Dorrence, and R.A. Heppner. An Investigation of Waxes Isolated from Heavy Oils Pruduced from Northwest Asphalt Ridge Tar Sands. *Liquid Fuels Technology*, 1(2):127–146, 1983.

[5] Schoeller Switzerland. Comfortemp textiles. *http://www.schoeller-textiles.com/*.

[6] E. I. Griggs. and D. W. Yarbrough. Thermal Conductivity of Solid Unbranched Alkanes from n-Hexadecane to n-Eicosane. In *Proceedings of the Southeastern Seminar on Thermal Sciences*, pages 256–267, Raleigh, NC., USA, april 1978. North Carolina University.

[7] F.L Tan and K.C. Leong. Effect of Wall Temperature and Aspect Ration on the Solid-Liquid Interface During Freezing Inside a Rectangular Enclosure. *International Communications in Heat and Mass Transfer*, 21(5):641–650, 1994.

[8] J. Pauly, C. Dauphin, and J. L. Daridon. Liquid-solid equlibria in a decane + multi paraffins system. *Fluid Phase Equlibria*, 149:191–207, 1998.

[9] J. Coutinho, S. I. Andersen, and E. H. Stenby. Evaluation of activity coefficient models in prediction of alkane solid-liquid equilibria. *Fluid Phase Equlibria*, 103:23–39, 1995.

[10] H. Hart. *Organic Chemistry.* Houghton Mifflin Company, Boston, 1983.

[11] H. K. Versteeg and W. Malalasekera. *An Introduction to Computational Fluid Dynamics.* Longman, Harlow, England, 1995.

[12] S. V. Patankar. *Numerical Heat Transfer and Fluid Flow.* Taylor and Francis, 1980.

[13] M. Lamvik and J. M. Zhou. Experimental study of Thermal Conductivity of Solid and Liquid Phases at the Phase Transition. *International Journal of Thermophysics*, 16(2):567–576, March 1995.

[14] F. M. White. *Viscous Fluid Flow*, chapter 2, page 73. McGraw-Hill, New York, 1991.

[15] Prausnitz. *Molecular Thermodynamics of Fluid Phase Equilibria*, chapter 9. Prentice Hall, 1986.

[16] J. Coutinho, K. Knudsen, S. I. Andersen, and E. H. Stenby. A Local Composition Model for Paraffinic Solid Solutions. *Chemical Engineering Science*, 51:3237–3282, 1996.

[17] R. C. Reid, J. M. Prausnitz, and B. E. Poling. *The Properties of Gases and Liquids.* McGraw-Hill Book Company, New York, 4 edition, 1987.

[18] D. K. Dysthe. *Diffusion in dense binary fluid mixtures of dissimilar molecules.* PhD thesis, The Norwegian Institute of Technology, University of Trondheim, July 1995.

[19] H. Forsman and P. Andersson. Thermal conductivity at high pressure of solid odd-numbered *n*-alkanes ranging from C_9H_{20} to $C_{19}H_{40}$. *Journal of Chemical Physics*, 80(6):2804–2807, March 1984.

[20] E. B. Sirota. Supercoling and transient phase induced nucleation *n*-alkane solutions. *Journal of Chemical Physics*, 112(1):492–500, January 2000.

[21] G. Zerbi, R. Magni, M. Gussoni, K. H. Moritz, A. Bigotto, and S. Dirlikov. Molecular mechanics for phase transition and melting og *n*-alkanes: A spectroscopic study of molecular mobility of solid *n*-nonadecane. *Journal of Chemical Physics*, 75(7):3175–3194, 1981.

[22] M. G. Taylor, E. C. Kelusky, I. C. P. Smith, H. L. Casal, and D. G. Cameron. A ^{2}H NMR study of the solid-phase behavior of nonadecane. *Journal of Chemical Physics*, 78(8):5108–5112, April 1983.

[23] J. F. Messerly, G. B. Guthrie, S. S. Todd, and H. L. Finke. Low Temperature Data for n-Pentane, n-Heptadecane, and n-Octadecane. *Journal of Chemical and Engineering Data*, 12:338–347, July 1967.

[24] M. Maroncelli, H. L. Strauss, and R. G. Snyder. Structure of the *n*-Alkane Binary Solid *n*-$C_{19}H_{40}$/*n*-$C_{21}H_{44}$ by Infrared Spectroscopy and Calorimetry. *The Journal of Physical Chemistry*, 89:5260–5267, 1985.

[25] W.M. Mazee. Physical and Chemical Properties of Petroleum Waxes. *Journal of the institute of petroleum*, 44(419):401–405, November 1958.

[26] M. Dirand, Z. Achour, B. Jouti, A. Sabour, and J. C. Gachon. Binary Mixtures of *n*-Alkanes. Phase Diagram Generalization: Intermediate Solid Solutions, Rotator Phases. *Mol. Cryst. Liq. Cryst.*, 275:293–304, 1996.

[27] D. Mondieg, P. Espeau, L. Robles, Y. Haget, H. A. J. Oonk, and M. A. Cuevas-Diarte. Mixed crystals of *n*-alkane pairs. *J. Chem Soc Faraday Trans.*, 93(18):3343–3346, 1997.

[28] J.A.P. Coutinho, S. I. Andersen, and E. Stenby. Solid-liquid equilibrium of n-alkanes using the chain delta lattice parameter model. *Fluid Phase Equilibria*, 117:138–145, 1996.

[29] N. B. Vargafitk. *Tables on the Thermophysical Properties of Liquids and Gases.* John Wiley & Sons, Washington-London, 2 edition, 1975.

[30] R. G. Irby, J. R. Parsons, and E. G. Keshok. An investigation of the thermal transport properties of octadecane, a material used in thermal energy storage systems. *Therm. Conduct.*, 19:121–143, 1988.

[31] D. W. Yarbrough and Chih-Ning Kuan. The Thermal Conductivity of Solid n-Eicosane, n-Octadecane, n-Heptadecane, n-Pentadecane and n-Tetradecane. In *Proceedings of the 17th International Thermal Conductivity Conference*, pages 265–274, New York, 1983. Plenum Press.

[32] R. Holmen, M. Lamvik, and O. Melhus. Measurements of the Thermal Conductivities of Solid and Liquid Unbranched Alkanes in the C_{16} to C_{19} Range During Phase Transition . *International Journal of Thermophysics*, 23(1):27–39, 2002.

[33] H.L. Finke, M.E. Gross, G. Waddington, and H.M. Huffman. Low-temperature Thermal Data for the Nine Normal Paraffin Hydrocarbons from Octane to Hexadecane. *J. Am. Chem. Soc.*, 76:333–341, 1954.

[34] G.S. Parks, G.E. Moore, M.L. Renquist, B.F. Naylor, L. A. McClaine, P.S. Fujii, and J.A. Hatton. Thermal Data on Organic Compounds. XXV. Some Heat Capacity, Entropy and Free Energy Data for Nine Hydrocarbons of High Molecular Weight. *J. Am. Chem. Soc.*, 71:3386–3389, 1949.

[35] A. A. Scaerer, C. J. Busco, A. E. Smith, and L. B. Skinner. Properties of pure Normal Alkanes in the C_{17} to C_{36} Range. *J. Am. Chem Soc.*, 77:2017–2019, April 1955.

[36] N. Nesse. *Beregning av usikkerheten ved målinger.* Institutt for Kjemiteknikk, NTH, Trondheim, Mai 1968.

[37] U. Grigull and H. Sandner. *Wärmeleitung.* Springer-Verlag, Berlin, 1979.

[38] K. J. Zang, M. E. Briggs, R. W. Gammon, and J. V. Sengers. Thermal and mass diffusion in a semidilute good solvent-ploymer solution. *Journal of Chemical Physics*, 111(5):2270–2282, 1999.

[39] K. J. Zang, M. E. Briggs, R. W. Gammon, and J. V. Sengers. Optical measurement of the Soret coefficient of liquid mixtures. *Journal of Chemical Physics*, 104(17):6881–6892, May 1996.

[40] B. W. Webb and R. Viskanta. An Experimental and Analytical Study of Solidification of a Binary Mixture. In *Proceedings of the 8th International Heat Transfer Conference*, pages 1739–1744, 1989.

[41] Y. Wada, Y. Nagasaka, and A. Nagashima. Measurements and Correlation of the Thermal Conductivity of Liquid *n*-Parafiin Hydrocarbons and Their Binary and Ternary Mixtures. *International Journal of Thermophysics*, 6(3):251–265, 1985.

[42] H. Ziebland and J. E. Patient. New Measurements and a Critical Appraisal of the Article by Sutherland, Davis and Seyer. *Journal of Chemical and Engineering Data*, 7(4):530–531, October 1962.

[43] J. C. Earnshaw and C. J. Hughes. Surface-induced phase transition in normal alkane fluids. *Physical Review A*, 46(8):4494–4496, 1992.

[44] K. W. Won. Thermodynamics for solid solution-liquid-vapor equilibria: Wax phase formation from heavy hydrocarbon mixtures. *Fluid Phase Equilibria*, 30:265–279, 1986.

[45] J. Timmermanns. *The Pysico-chemical Constants of Binary Systems in Concentrated Solutions*, volume 1. Interscience Publishers Inc., New York, 1959.

[46] J. C. Smith. Higher Aliphatic Compounds. Part II,. the Systems Hexadecyl Iodide-Octadecyl Iodide and Hexadecane-Octadecane. *J. Chem. Society*, pages 737–741, 1932.

[47] W.B. Pedersen and P. Skovborg H.P. Rønningsen. *Energy & Fuels*, 5:924, 1991.

[48] J.H. Hansen, A. Fredenslund, K.S. Pedersen, and H.P. Rønningsen. *AIChE J.*, 34:1937, 1988.

[49] P.J. Flory. *Principles of Polymer Chemistry.* Cornell Univ. Press, Ithaca, NY, 1953.

[50] P. Ungerer, B. Faissat, C. Leibovici, H. Zhou, and E. Behar. *Fluid Phase Equilibria*, 111:287, 1995.

[51] D. D. Erickson, V. G. Niesen, and T.S. Brown. Thermodynamic Measurement and Prediction of Paraffin Precipitation in Crude Oil. *SPE 26604*, pages 993–948, 1993.

[52] V. R. Voller. A numerical scheme for solidification of an alloy. *Canadian Metallurgical Quarterly*, 37(3-4):169–177, 1998.

[53] R. Holmen. Numerical simulation of heat and mass transfer during solidification of binary mixtures of *n*-alkanes. In B. Sunden and C. A. Brebbia, editors, *Heat Transfer VII*, Advanced Computational Methods. WIT Press, May 2002.

[54] K. J. Laidler and J. H. Meiser. *Physical Chemistry*, chapter 18, page 821. Benjamin/Cummins, Menlo Park, Califorina, 1982.

[55] C. F. Wong and W. Hayduk. Correlations for Prediction of Molecular Diffusivities in Liquids at Infinite Dilution. *The Canadian Journal of Chemical Engineering*, 68:849–859, 1990.

[56] K. S. Førland, T. Førland, and S. K. Ratkje. *Irreversible Thermodynamics.* John Wiley & Sons, Chichester, 1988.

[57] P. M. Ghogomu, M. Bouroukba, J. Dellacherie, D. Balesdent, and M. Dirand. On the ideality of liquid mixtures of long-chain *n* -alkanes. *Thermochimica Acta*, 306:69–71, 1997.

[58] G: Aylward and T. Findlay. *SI Chemical Data.* John Wiley & Sons, Brisbane, 3 edition, 1994.

[59] Grigor'ev and Andolenko. Investigation of the isobaric heat capacity of n-paraffinic hydrocarbons at atmospheric pressure. *Neft i Gaz*, 2:60–62, 1984.

[60] NIST. Standard reference database number 69 - february 2000 release. *http://webbook.nist.gov/cgi/cbook.cgi?Name=nonadecane&Units=SI.*

[61] T. E. Daubert and R. P. Danner. *Physical and Thermodynamical Properties of Pure Chemicals: Data Compilation.* Hemisphere Publishing Corporation, Washington, 1989.

[62] R. L. Powell, W. J. Hall, Jr. C . H. Hyink, L. L. Sparks, G. W. Burns, M. G. Scroger, and H. H. Plumb. *Thermocouple Reference Tables Based on the IPTS-68.* U.S. Department of Commerce, National Bureau of Standards, Washington-Boulder, march 1974.

[63] A. Høyland. *Statistisk metodelære.* Tapir, Trondheim, 4 edition, 1989.

Appendix A

Physical and Thermodynamic Properties of Pure Components

Property	Unit	C_{16}	C_{17}	C_{18}	C_{19}
M_r	kg mol^{-1}	0.22645 [1)]	0.24047 [1)]	0.2545 [1)]	0.26853 [1)]
ρ_l	kg m^{-3}	775 [2)]	777 [2)]	777 [2)]	778 [2)]
ρ_s	kg m^{-3}	853 [4)]	854 [4)]	855 [4)]	859 [3)]
Δh_{mp}	J mol^{-1}	5.16*10^4 [5)]	4.02*10^4 [6)]	6.13*10^4 [3)]	4.59*10^4 [3)]
$C_{p,l}$	J mol^{-1} K^{-1}	501 [7)]	534 [7)]	559 [5)]	590 [8)]
$C_{p,s}$	J mol^{-1} K^{-1}	425 [6)]	888 [6)]	496 [6)]	972 [10)]
T_{mp}	K	291.33 [6)]	295.14 [6)]	301.33 [6)]	305.15 [3)]
v_l	m^3 mol^{-1}	2.94*10^{-4} [9)]	3.11*10^{-4} [9)]	3.29*10^{-4} [9)]	3.46*10^{-4} [9)]
v_w	m^3 mol^{-1}	1.71*10^{-4} [9)]	1.81*10^{-4} [9)]	1.91*10^{-4} [9)]	2.01*10^{-4} [9)]
param1 [11)]		9.752*10^7 [9)]	1.02*10^8 [9)]	1.0695*10^8 [9)]	1.467*10^8 [9)]
param2 [11)]		4.122*10^{-1} [9)]	4.33*10^{-1} [9)]	4.51*10^{-1} [9)]	4.476*10^{-1} [9)]
T_c	K	720.60 [9)]	733.37 [9)]	745.26 [9)]	755.93 [9)]
Δh_{ss}	J mol^{-1}	0 [6)]	1.09*10^4 [6)]	0 [3)]	1.38*10^4 [3)]

Sources:

All data are converted to SI-units where necessary.

1) Calculated from atomic weights found in SI Chemical Data [58].
2) Extrapolated to the melting point, values from Vargaftik [29].

3) Schaerer et al [35].
4) Calculated assuming 10 % contraction at freezing.
5) Parks [34]
6) Messerly et al [23]
7) Finke et al [33]
8) Reference to Grigor'ev and Andolenko [59] in NIST chemistry webbook [60].
9) Daubert and Danner [61]
10) Calculated assuming same value on a mass basis as heptadecane in Messerly et al [23].
11) Parameters used to calculate heats of vaporization :
$\Delta h^i_{vap} = param1^i(1 - T^i_r)^{param2^i}$

Appendix B

Apparatus

The apparatus was the same as used by Lamvik [13]. The only exception was the thermostated liquid reservoirs, see Fig. B.1.

The experimental cell was made up of two circular plates with a cylindrical glass ring between. A cylindrical cavity with diameter 60 mm was formed between the plates. The height of the cavity, H, was 12- 12.8 mm. The plates were channeled and connected via a system of valves to two thermostated water baths. The system of valves rendered it possible to connect the plates either to the same bath or to separate baths.

A ring of expanded polyester was used as insulation outside the glass ring. A hole in the insulation made it possible to use a cathetometer to measure the level of the interface.

The liquid reservoirs were also channeled, and thermostated water was pumped through. The temperatures of the reservoirs were always kept as close as possible to the temperature of the upper plate.

Measurements of temperature were done by inserting temperature elements into pockets in the plates. The elements were of type K. The reference junctions were kept at 0 °C and the voltage was read off from a Fluke 45 Voltmeter. The voltage was correlated to temperature using data from Powell et al. [62].

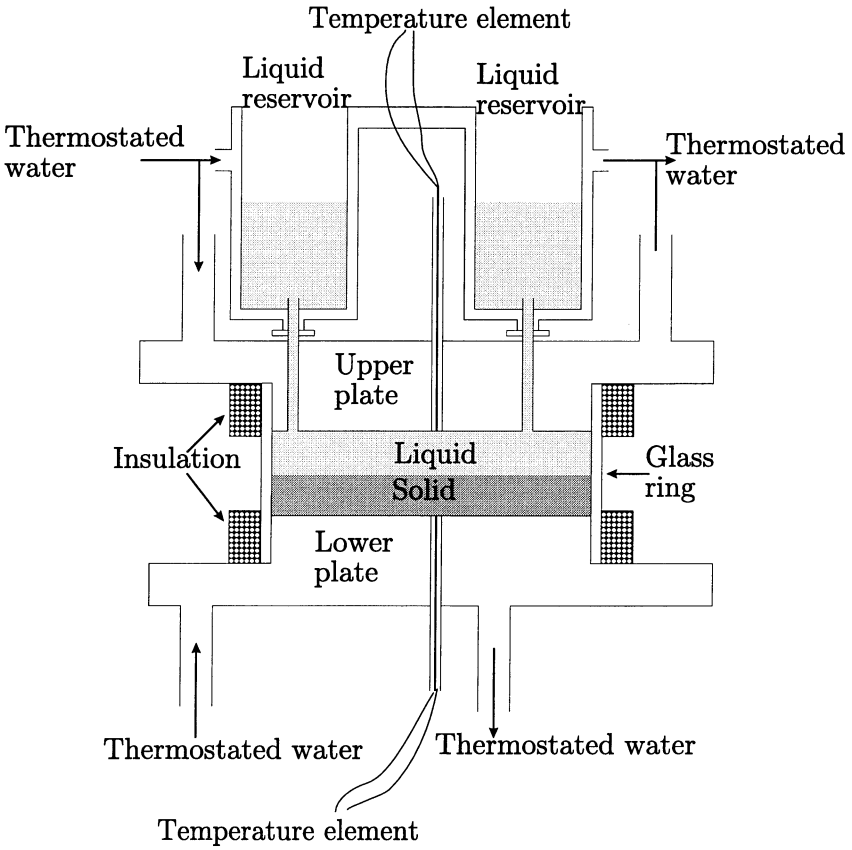

Figure B.1: Experimental cell

Time was measured by reading the time from a Casio Travel & Clock TC-1000.

A cathetometer, model LS 701 from Heidehain, was used to measure the position of the interface.

Appendix C

Calculation of Pure Component Thermal Conductivity

C.1 Calculation of Liquid Thermal Conductivity

Experiments were preformed to measure the liquid thermal conductivity as described in section 3.3.2. Data from an experiment preformed on octadecane 22 February 2000 is given in Table C.1

Table C.1: Data from experiment preformed on octadecane 22 February 2000

t (s)	x_{mp} (m)	$\frac{\partial T_l}{\partial x}$ (K m^{-1})	$\frac{dx_{mp}(t)}{dt}$ (m s^{-1})	k_l (W K^{-1} m-1)
0	0.0112	—	—	—
90	0.0110	1843	-1.67*10^{-6}	0.186
240	0.0108	1536	-1.48*10^{-6}	0.199
360	0.0106	1316	-1.21*10^{-6}	0.190
570	0.0104	1152	-0.86*10^{-6}	0.154
825	0.0102	1024	-1.06*10^{-6}	0.215
945	0.0100	—	—	—

The total height of the cell was $H = 12 * 10^{-3}$ m and $T_H = 303.17$ K.

The gradients in liquid temperature were calculated from Eq. (3.4):

$$\frac{\partial T_l}{\partial x} \approx \frac{T_H - T^i_{mp}}{H - x_{mp}} \tag{C.1}$$

As one can see from Table C.1, Δx_{mp} = - 0.0002 m. This value was used to calculate $\frac{dx_{mp}(t)}{dt}$ from Eq. (3.6):

$$\frac{dx_{mp}(t)}{dt} \approx \frac{2\Delta x}{t(x_{mp}+\Delta x) - t(x_{mp}-\Delta x)} \tag{C.2}$$

Finally, the calculated gradients and physical properties from appendix A are inserted in equation 2.3:

$$k_l = -\frac{\rho_s \Delta h_{mp}}{M_r} \frac{dx_{mp}}{dt} \left(\frac{\partial T_l}{\partial x}\right)^{-1} \tag{C.3}$$

The values for $k_l^{C_{18}}$ are given in Table C.1. The average value $k_l^{C_{18}}$ = 0.189 W K^{-1} m$-$1 is used in subsequent calculations.

C.2 Calculation of Ratio of Solid and Liquid Conductivities

As an example, measurements from an experiment preformed 21 February 2000 are given. The temperatures of the top and bottom plates were T_H = 305.16 K and T_0 = 298.17 K. The position of the interface was x_{mp} = 7.8*10^{-3} m and the height of the cell, H = 12*10^{-3} m. These values are used to calculate the gradients Eq.(3.4):

$$\frac{\partial T_l}{\partial x} \approx \frac{T_H - T^i_{mp}}{H - x_{mp}} = 912 K m^{-1} \tag{C.4}$$

and Eq.(3.5):

$$\frac{\partial T_s}{\partial x} \approx \frac{T^i_{mp} - T_0}{x_{mp}} = 405 K m^{-1} \tag{C.5}$$

Using Eq(2.4:

$$\frac{k^i_l}{k^i_s} = \frac{\frac{\partial T_s}{\partial x}}{\frac{\partial T_l}{\partial x}} = 0.444 \tag{C.6}$$

C.3 Calculation of Solid Thermal Conductivity

The average of all experiments preformed to find the liquid thermal conductivity is $k_l^{C_{18}} = 0.179$ W K^{-1} m^{-1}. The average of the ratios is, $\frac{k^i_l}{k^i_s} = 0.450$.

The solid thermal conductivity is simply calculated by :

$$k_s^{C_{18}} = \left(\frac{k^i_l}{k^i_s}\right)^{-1} k^i_l = 0.398 W K^{-1} m^{-1} \tag{C.7}$$

Appendix D

Calculation of Uncertainties in Pure Component Thermal Conductivities

D.1 Gauss' Equation for Propagation of Random Error

As an example, the values are taken from the experiments preformed on octadecane refereed to in Appendix C. The values from the experiments with assigned errors as described in section 3.5.1 are used.

D.1.1 Error in Liquid Thermal Conductivities

The values used in the calculation are given in Table D.1.

In order to calculate the error in the liquid thermal conductivity, it is necessary to make an assessment of the error in the liquid temperature gradient:

$$\sigma_{\frac{\partial T_l}{\partial x}} = \sqrt{\left(\sigma_{T_H}\frac{\partial\frac{\partial T_l}{\partial x}}{\partial T_H}\right)^2 + \left(\sigma_{x_{mp}}\frac{\partial\frac{\partial T_l}{\partial x}}{\partial x_{mp}}\right)^2 + \left(\sigma_{T_{mp}}\frac{\partial\frac{\partial T_l}{\partial x}}{\partial T_{mp}}\right)^2} \tag{D.1}$$

Table D.1: Data used in the calculation of error in liquid thermal conductivity

Property	Value	σ	Unit	Note
T_{mp}	301.33	0.25	K	from appendix A
ρ_s	855	50	kg m^{-3}	from appendix A
$\frac{\Delta h_{mp}}{M_r}$	2.41*10^5	5*10^3	J K^{-1}	from appendix A
T_H	303.15	0.25	K	from section C.1
H	1.2*10^{-2}	—	m	from section C.1
x_{mp}	1.06*10^{-2}	2.5*10^{-5}	m	from section C.1
Δx	- 2*10^{-4}	2.5*10^{-5}	m	from section C.1
$t(x-\Delta x)$	240	1	s	from section C.1
$t(x+\Delta x)$	570	1	s	from section C.1
$\frac{dx_{mp}}{dt}$	- 1.21*10^{-6}	—	m s^{-1}	from section C.1
$\frac{\partial T_l}{\partial x}$	1316	—	K m^{-1}	from section C.1
k_l	0.190	—	W m^{-1} K^{-1}	from section C.1

Where:

$$\sigma_{T_H}\frac{\partial\frac{\partial T_l}{\partial x}}{\partial T_H} = \frac{\sigma_{T_H}}{H - x_{mp}} = 71Km^{-1} \tag{D.2}$$

$$\sigma_{x_{mp}}\frac{\partial\frac{\partial T_l}{\partial x}}{\partial x_{mp}} = \frac{\sigma_{x_{mp}}(T_H - T_{mp})}{(H - x_{mp})^2} = 23Km^{-1} \tag{D.3}$$

$$\sigma_{T_{mp}}\frac{\partial\frac{\partial T_l}{\partial x}}{\partial T_{mp}} = -\frac{\sigma_{T_{mp}}}{H - x_{mp}} = -179Km^{-1} \tag{D.4}$$

Inserting these values in Eq. (D.1), $\sigma_{\frac{\partial T_l}{\partial x}} = 194$ K m^{-1}.

One also needs to calculate $\sigma_{\frac{dx_{mp}}{dt}}$:

$$\sigma_{\frac{\partial x_{mp}}{\partial t}} = \sqrt{\left(\sigma_{\Delta x}\frac{\partial\frac{\partial x_{mp}}{\partial t}}{\partial\Delta x}\right)^2 + \left(\sigma_{t(x+\Delta x)}\frac{\partial\frac{\partial x_{mp}}{\partial t}}{\partial t(x+\Delta x)}\right)^2 + \left(\sigma_{t(x-\Delta x)}\frac{\partial\frac{\partial x_{mp}}{\partial t}}{\partial t(x-\Delta x)}\right)^2} \tag{D.5}$$

Where :

$$\sigma_{\Delta x}\frac{\partial\frac{\partial x_{mp}}{\partial t}}{\partial \Delta x} = \frac{2\sigma_{\Delta x}}{t(x+\Delta x) - t(x-\Delta x)} = 1.52 * 10^{-7} m s^{-1} \tag{D.6}$$

,

$$\sigma_{t(x+\Delta x)}\frac{\partial\frac{\partial x_{mp}}{\partial t}}{\partial t(x+\Delta x)} = -\frac{2\Delta x\sigma_{t(x+\Delta x)}}{(t(x+\Delta x) - t(x-\Delta x))^2} = 3.67 * 10^{-9} m s^{-1} \tag{D.7}$$

and

$$\sigma_{t(x-\Delta x)}\frac{2\Delta x\partial\frac{\partial x_{mp}}{\partial t}}{\partial t(x-\Delta x)} = \frac{2\Delta x\sigma_{t(x-\Delta x)}}{(t(x+\Delta x) - t(x-\Delta x))^2} = -3.67 * 10^{-9} m s^{-1} \tag{D.8}$$

Which give $\sigma_{\frac{\partial x_{mp}}{\partial t}} = 1.52{*}10^{-7}$ m s^{-7} in Eq. (D.5).

In order to calculate the total error in the liquid thermal conductivity, the following values are necessary :

$$\sigma_{\rho_s^i}\frac{\partial k_l^i}{\partial \rho_s^i} = \sigma_{\rho_s^i}\frac{k_l^i}{\rho_s^i} = 0.011 W K^{-1} m^{-1} \tag{D.9}$$

$$\sigma_{\frac{\Delta h_{mp}}{M_r}}\frac{\partial k_l^i}{\partial\frac{\Delta h_{mp}}{M_r}} = -\sigma_{\frac{\Delta h_{mp}}{M_r}}\frac{k_l^i}{\frac{\Delta h_{mp}}{M_r}} = -3.94 * 10^{-3} W K^{-1} m^{-1} \tag{D.10}$$

$$\sigma_{\frac{dx_{mp}}{dt}}\frac{\partial k_l^i}{\partial\frac{dx_{mp}}{dt}} = \sigma_{\frac{dx_{mp}}{dt}}\frac{k_l^i}{\frac{dx_{mp}}{dt}} = -0.017 W K^{-1} m^{-1} \tag{D.11}$$

$$\sigma_{\frac{\partial T_l(x_{mp})}{\partial x}}\frac{\partial k_l^i}{\partial\frac{\partial T_l(x_{mp})}{\partial x}} = -\sigma_{\frac{\partial T_l(x_{mp})}{\partial x}}\frac{k_l^i}{\left(\frac{\partial T_l(x_{mp})}{\partial x}\right)^2} = -0.020 W K^{-1} m^{-1} \tag{D.12}$$

Finally Eq. (3.7):

$$\sigma_{k_l^i} = \sqrt{\left(\sigma_{\rho_s^i}\frac{\partial k_l^i}{\partial \rho_s^i}\right)^2 + \left(\sigma_{\frac{\Delta_{mph}}{Mr}}\frac{\partial k_l^i}{\partial \frac{\Delta_{mph}}{Mr}}\right)^2 + \left(\sigma_{\frac{dx_{mp}}{dt}}\frac{\partial k_l^i}{\partial \frac{dx_{mp}}{dt}}\right)^2 + \left(\sigma_{\frac{\partial T_l(x_{mp})}{\partial x}}\frac{\partial k_l^i}{\partial \frac{\partial T_l(x_{mp})}{\partial x}}\right)^2} \tag{D.13}$$

$$= 0.029 W m^{-1} K^{-1} \tag{D.14}$$

which is 15 % of the calculated value.

D.1.2 Error in Ratio of Solid and Liquid Conductivities

The values used in the calculations are presented in Table D.2

The errors in the thermal gradients are found equivalently to the error of the thermal gradient in the previous section, giving $\sigma_{\frac{\partial T_l}{\partial x}} = 64$ K m^{-1} and $\sigma_{\frac{\partial T_s}{\partial x}} = 35$ K m^{-1}.

Table D.2: Data used in the calculation of error in ratio of conductivities.

Property	Value	σ	Unit	Note
$\frac{\partial T_l}{\partial x}$	913	64	K m^{-1}	from section C.2
$\frac{\partial T_s}{\partial x}$	405	35	K m^{-1}	from section C.2
$\frac{k_l}{k_s}$	0.444	—	—	from section C.2

$$\sigma_{\frac{\partial T_l}{\partial x}}\frac{\partial \frac{k_l^i}{k_s^i}}{\partial \frac{\partial T_l}{\partial x}} = -\sigma_{\frac{\partial T_l}{\partial x}}\frac{\frac{k_l^i}{k_s^i}}{\frac{\partial T_l}{\partial x}} = -0.031 \tag{D.15}$$

$$\sigma_{\frac{\partial T_s}{\partial x}}\frac{\partial \frac{k_l^i}{k_s^i}}{\partial \frac{\partial T_s}{\partial x}} = \sigma_{\frac{\partial T_s}{\partial x}}\frac{\frac{k_l^i}{k_s^i}}{\frac{\partial T_s}{\partial x}} = 0.038 \tag{D.16}$$

In Eq.(3.8) these values give:

$$\sigma_{\frac{k_l^i}{k_s^i}} = \sqrt{\left(\sigma_{\frac{\partial T_l}{\partial x}} \frac{\partial \frac{k_l^i}{k_s^i}}{\partial \frac{\partial T_l}{\partial x}}\right)^2 + \left(\sigma_{\frac{\partial T_s}{\partial x}} \frac{\partial \frac{k_l^i}{k_s^i}}{\partial \frac{\partial T_s}{\partial x}}\right)^2} = 0.049 \tag{D.17}$$

Since $\frac{k_l^i}{k_s^i}$= 0.444 , the error is 11 %.

D.1.3 Error in Solid Thermal Conductivities

The values used can be found in Table D.3. The errors in the ratio of conductivities and in the liquid conductivity are found by assuming that the errors in the previous sections, 15 % and 11 %, can be used.

Table D.3: Data used in the calculation of error in the liquid thermal conductivity.

Property	Value	σ	Unit	Note
k_s	0.179	0.027	W m^{-1} K^{-1}	from section C.3
$\frac{k_l}{k_s}$	0.450	0.050	W m^{-1} K^{-1}	from section C.3
k_s	0.398	—	W m^{-1} K^{-1}	from section C.3

$$\sigma_{k_l^i} \frac{\partial k_s^i}{\partial k_l^i} = \sigma_{k_l^i} \frac{k_s^i}{k_l^i} = 0.059 W m^{-1} K^{-1} \tag{D.18}$$

$$\sigma_{\frac{k_l^i}{k_s^i}} \frac{\partial k_s^i}{\partial \frac{k_l^i}{k_s^i}} = -\sigma_{\frac{k_l^i}{k_s^i}} \frac{k_s^i}{\frac{k_l^i}{k_s^i}} = 0.043 W m^{-1} K^{-1} \tag{D.19}$$

Finally Eq.3.9:

$$\sigma_{k_s^i} = \sqrt{\left(\sigma_{k_l^i} \frac{\partial k_s^i}{\partial k_l^i}\right)^2 + \left(\sigma_{\frac{k_l^i}{k_s^i}} \frac{\partial k_s^i}{\partial \frac{k_l^i}{k_s^i}}\right)^2} = 0.073 W m^{-1} K^{-1} \tag{D.20}$$

Which is 19 % of the calculated value.

D.2 Standard Deviation

Seven experiments were performed on octadecane to find $k_l^{C_{18}}$. Since this is the largest number of repeated experiments, it will give the best basis for calculation of standard deviation. The results from the experiments were found as described in chapter 3 and are given in table D.4.

Table D.4: Calculated Values of $k_l^{C_{18}}$ from Experiments on Octadecane

Exp. #	$k_l^{C_{18}}$**(W K^{-1} m^{-1})**
1	0.160
2	0.215
3	0.189
4	0.134
5	0.183
6	0.165
7	0.208

Assuming normal distributed values, the standard deviation can be estimated as [63]:

$$\sigma_{k_l^{C_{18}}} = \sqrt{\frac{1}{1-n}\sum_{j=1}^{n}(k_l^{C_{18}}(j) - \bar{k}_l^{C_{18}})^2} \tag{D.21}$$

Where n is the total number of experiments and an overbar denotes average value.

Introducing the values in table D.4 into equation D.21 :

$$\sigma_{k_l^{C_{18}}} = 0.028 W K^{-1} m^{-1} \tag{D.22}$$

Since the average value of $k_l^{C_{18}}$= 0.179 W K^{-1} m^{-1}, the estimated standard deviation is less than 16 % .

Appendix E

Effect of Thermal Gradient in Disappearing Phase

Values from an experiment performed 22 February to find the thermal conductivity of C_{18} are shown in Table E.1

Table E.1: Measured and Calculated Values from Experiment on Octadecane 22 February 2000

Property	**Value**	**Unit**	**Note**
T_{mp}	301.33	K	from appendix A
ρ_s	855	kg m^{-3}	from appendix A
$\frac{\Delta h_{mp}}{M_r}$	2.41*10^5	J K^{-1}	from appendix A
T_H	303.15	K	from section C.1
H	12*10^{-3}	m	from section C.1
x_{mp}	11*10^{-3}	m	from section C.1
Δx	- 0.2*10^{-3}	m	from section C.1
$t(x-\Delta x)$	0	s	from section C.1
$t(x+\Delta x)$	240	s	from section C.1
$\frac{dx_{mp}}{dt}$	- 1.667*10^{-6}	m s^{-1}	from section C.1
$\frac{\partial T_l}{\partial x}$	1820	K m^{-1}	from section C.1

$\frac{dx_{mp}}{dt}$ and $\frac{\partial T_l}{\partial x}$ were calculated as described in section 3.3.2.

Assuming that the bottom plate is 0.25 K colder than the melting point, the

thermal gradient in the solid phase is:

$$\frac{\partial T_s}{\partial x} = \frac{0.25}{x_{mp}} = 22.73 K m^{-1} \tag{E.1}$$

The solid conductivity of octadecane is measured to $k_s = 0.40$. Using these values in table E.1 in Eq. (3.12):

$$k_l^i = \left(k_s^i \frac{\partial T_s}{\partial x} - \rho_s^i \frac{\Delta h_{mp}}{M_r^i} \frac{dx_{mp}}{dt} \right) \left(\frac{\partial T_l}{\partial x} \right)^{-1} = 0.193 W m^{-1} K^{-1} \tag{E.2}$$

Compared to the value of 0.189 W K^{-1} m^{-1} found previously, the new value is 2 % higher.

Appendix F

Fortran 77 Code Used to Calculate Phase Envelope

The code consists of two files. The main code can be found in F.1, while the global variables are presented in F.2.

F.1 Transcript of Program

```
CCCCCCCCCCCCCCCCCCCCCCCCCCCCCCCCCCCCCCCCCCCCCCCCCCCCCCCCCCCCCCCCCCCCCCCCCCCCCCC
      program Liquidus
C     Calculates the Liquidus
CCCCCCCCCCCCCCCCCCCCCCCCCCCCCCCCCCCCCCCCCCCCCCCCCCCCCCCCCCCCCCCCCCCCCCCCCCCCCCC
      implicit none
      integer j,i
      include 'PEData.for'
      call Input
      call init
      call TempInit
      do CompRound=1,Points
         call ConsInit
         write (*,*) 'Point no: ',CompRound,' of ',Points
         Temp=Hightemp
         Es(1,Epts)=10
         Epts=Epts+1
         do TempRound=1,TempPoints
            Temp=Temp-Dtemp

C     check if a physically viable solution is reached
            call ViableCheck

c     if not a viable solution is reached, make a flash calculation
            if (.not.viable) then
               call flash
            else
               call gamma
               write(*,*)
               write(*,*) 'Solution no:',epts,'reached at temp',Temp
               write(*,*) 'Ex(1)=',Ex(1,epts),'Ex(2)=',Ex(2,epts)
               write(*,*) 'sg(1)', sgamma(1),'sg(2)', sgamma(2)
               write(*,*) 'Lg(1)', Lgamma(1),'Lg(2)', Lgamma(2)
               call EnvelopePres
               goto 200
```

```
            endif

c     if there is no solution at this point, go to the next temp.
            if(TempRound.eq.(TempPoints)) then
               Write(*,*) 'No solution reached for z(1)=',Ez(1)
               epts=epts-1
            endif
 100     enddo                    ! TempRound
 200  enddo                       ! CompRound
      close(10)
      end

CCCCCCCCCCCCCCCCCCCCCCCCCCCCCCCCCCCCCCCCCCCCCCCCCCCCCCCCCCCCCCCCCCCCCCCCCCCCCCC
      subroutine input
C     provides input to the calculation, i.e: case data
C     all data given in basic SI-units, i.e: m, kg, mol, K etc..
CCCCCCCCCCCCCCCCCCCCCCCCCCCCCCCCCCCCCCCCCCCCCCCCCCCCCCCCCCCCCCCCCCCCCCCCCCCCCCC
      implicit none
      include 'PEData.for'
      integer nc16,nc17,nc18,nc19
      character*1 tab
      tab=char(9)

c     Points to be considered
      Points=1000

c     TempPoints
      TempPoints=1000

c     Filenames
      liqfilename='liquidus.dat'
      open(10,file=liqfilename,status='unknown')
      write(10,100) 'Tl',tab,'x1',tab,'x2',tab,'x3',tab,'x4'
 100  format (A2,A1,A2,A1,A2,A1,A2,A1,A2)

c     # of components
      comp=2
```

```
c     NB!!!!!! Remember to number in same order as the number of
c     carbon atoms
      nc16=1
      nc17=3
      nc18=2
      nc19=4

c     Thermophysical properties of the components :

C     Hexadecane:
      LCompCp(nC16)=501.0      ! (J/molK)
      SCompCp(nC16)=425.00      ! (J/molK)
      CompTransTemp(nC16)=291.33
      CompEntMelt(nC16)=5.16E4   !(J/mol)
      LiqmolVol(nC16)=2.94E-4 ! (m^3/mol)
      WaalsVol(nC16)=1.71E-4 ! (m^3/mol)
      Cno(nC16)=16
      CritTemp(nC16)=720.60
      VapHeatPar(nC16,1)=9.752E7
      VapHeatPar(nC16,2)=4.122E-1
      CompSSEnt(nC16)=0

c     Heptadecane:
      LCompCp(nC17)=534.00    ! (J/molK)
      SCompCp(nC17)=888.000     ! (J/molK)
      CompTransTemp(nC17)=295.14
      CompEntMelt(nC17)=4.02E4  !(J/mol)
      LiqmolVol(nC17)= 3.11E-4! (m^3/mol)
      WaalsVol(nC17)=1.81E-4 ! (m^3/mol)
      Cno(nC17)=17
      CritTemp(nC17)=733.37
      VapHeatPar(nC17,1)=1.02E8
      VapHeatPar(nC17,2)=4.33E-1
      CompSSEnt(nC17)= 1.09E4   ! (J/mol)

c     OCTADECANE:
```

```
      LCompCp(nC18)=559.00         ! (J/molK)
      SCompCp(nC18)=496.00       ! (J/molK)
      CompTransTemp(nC18)=301.33
      CompEntMelt(nC18)=61300   !(J/mol)
      LiqmolVol(nC18)=3.29E-4 ! (m^3/mol)
      WaalsVol(nC18)=1.91E-4 ! (m^3/mol)
      Cno(nC18)=18
      CritTemp(nC18)=745.26
      VapHeatPar(nC18,1)=1.0695E8
      VapHeatPar(nC18,2)=4.51E-1
      CompSSEnt(nC18)=0

c     NONADECANE:
      LCompCp(nC19)=590.00       ! (J/molK)
      SCompCp(nC19)=972.00       ! (J/molK)
      CompTransTemp(nC19)=305.15
      CompEntMelt(nC19)=45900   !(J/mol)
      LiqmolVol(nC19)=3.46E-4 ! (m^3/mol)
      WaalsVol(nC19)=2.01E-4 ! (m^3/mol)
      Cno(nC19)=19
      CritTemp(nC19)=755.93
      VapHeatPar(nC19,1)=1.1467E8
      VapHeatPar(nC19,2)=4.476E-1
      CompSSEnt(nC19)=1.38E4    ! (J/mol)

      return
      end

CCCCCCCCCCCCCCCCCCCCCCCCCCCCCCCCCCCCCCCCCCCCCCCCCCCCCCCCCCCCCCCCCCCCCCCC
      subroutine KValue
C     Calculate the Kvalue for each component
CCCCCCCCCCCCCCCCCCCCCCCCCCCCCCCCCCCCCCCCCCCCCCCCCCCCCCCCCCCCCCCCCCCCCCCC
      implicit none
      include 'PEData.for'
      integer j
      real DeltaCp,Tt,Hmp
```

```
      call gamma

C     Expression for K:
      do j=1,comp
         DeltaCp=LCompCp(j)-SCompCp(j)
         Tt=CompTransTemp(j)
         Hmp=CompEntMelt(j)
         K(j)=(Lgamma(j)/SGamma(j))*exp(
     &        Hmp/(R*Tt)*(Tt/Temp-1)+DeltaCp/R*
     &        (1-Tt/Temp+log(Tt/Temp)))

      enddo

      return
      end

CCCCCCCCCCCCCCCCCCCCCCCCCCCCCCCCCCCCCCCCCCCCCCCCCCCCCCCCCCCCCCCCCCCCCCCCCCCCCC
      subroutine Flash
C     makes a flash calculation at T=Temp
CCCCCCCCCCCCCCCCCCCCCCCCCCCCCCCCCCCCCCCCCCCCCCCCCCCCCCCCCCCCCCCCCCCCCCCCCCCCCC
      implicit none
      include 'PEData.for'
      logical pure
      integer j,i,it
      Real So,fsl,Fe,dfslds

C     Checks if composition corresponds to a pure substance, if so,
C     no need to make flash calculation
      pure=.false.
      do j=1,comp
         if (Ez(j).eq.1) then
            pure=.true.
            ETemp(Epts)=Temp
            do i=1,comp
               Ex(i,EPts)=0
               Es(i,EPts)=0
            enddo
```

```
            Es(j,EPts)=1
            Ex(j,Epts)=1
         endif
      enddo

      if (.not.pure) then
C     Flash calculation, modified Ratchford-Rice as describe by Won:86

C     initial guesses:
         Fe=1
         So=0.9
         fsl=0
         do j=1,comp
            Ex(j,Epts)=Ez(j)*0.5
            Es(j,Epts)=Ez(j)*0.5
         Enddo
         call Kvalue
         do j=1,comp
            fsl=fsl+(Ez(j)*Fe*(k(j)-1))/(So*(k(j)-1)+Fe)
         enddo
         it=0

 100     if ((ABS(fsl).gt.0.00000001).and.(it.lt.10000))then
            dfslds=0
            fsl=0
            call Kvalue
            do j=1,comp
               fsl=fsl+(Ez(j)*Fe*(k(j)-1))/(So*(k(j)-1)+Fe)
               dfslds=dfslds-((k(j)-1)**2*Ez(j)*Fe)/
     &              ((So*(k(j)-1)+Fe)**2)
            enddo
            So=So-0.01*fsl/dfslds
            it=it+1
            do j=1,comp
               Ex(j,EPts)=(Ez(j)*Fe)/(So*K(j)+Fe-So)
               Es(j,EPts)=Ex(j,EPts)*k(j)
            enddo
```

```
            goto 100
         endif
         if (it.gt.9999) then

C     ensure a new try
            Ex(1,EPTS)=5
         endif
         ETemp(EPts)=Temp
      endif
      return
      end

CCCCCCCCCCCCCCCCCCCCCCCCCCCCCCCCCCCCCCCCCCCCCCCCCCCCCCCCCCCCCCCCCCCCCCC
      subroutine EnvelopePres
C     Presents the phase-envelope in a suitable format
CCCCCCCCCCCCCCCCCCCCCCCCCCCCCCCCCCCCCCCCCCCCCCCCCCCCCCCCCCCCCCCCCCCCCCC
      implicit none
      include 'PEData.for'
      integer i,j
      character*1 tab
      tab=char(9)
      write(10,100) ETemp(epts),tab,Ex(1,epts),tab,Ex(2,epts),tab
     &     ,Ex(3,epts),tab,Ex(4,epts)

 100  format (F6.2,A1,F5.3,A1,F5.3,A1,F5.3,A1,F5.3)

      return
      end

CCCCCCCCCCCCCCCCCCCCCCCCCCCCCCCCCCCCCCCCCCCCCCCCCCCCCCCCCCCCCCCCCCCCCCC
      subroutine TempInit
C     Calculates initial temperature parameters
CCCCCCCCCCCCCCCCCCCCCCCCCCCCCCCCCCCCCCCCCCCCCCCCCCCCCCCCCCCCCCCCCCCCCCC
      implicit none
      include 'PEdata.for'
      integer j
```

```
      hightemp=0
      lowtemp=1000000
      do j=1,comp
         if (CompTransTemp(j).gt.HighTemp) HighTemp=CompTransTemp(j)
         if (CompTransTemp(j).lt.LowTemp) LowTemp=CompTransTemp(j)
      enddo
      HighTemp=HighTemp+5
      LowTemp=LowTemp-5
                                ! xxx
      DTemp=(hightemp-lowtemp)/(TempPoints)*1.00

      return
      end

CCCCCCCCCCCCCCCCCCCCCCCCCCCCCCCCCCCCCCCCCCCCCCCCCCCCCCCCCCCCCCCCCCCCCCCCCCCCCCC
      subroutine gamma
C     Calculates activity coefficients
CCCCCCCCCCCCCCCCCCCCCCCCCCCCCCCCCCCCCCCCCCCCCCCCCCCCCCCCCCCCCCCCCCCCCCCCCCCCCCC
      implicit none
      include 'PEdata.for'
      integer j,i,kl,ks
      real top(comp),bottom,fi(comp),lngamma(comp)
      real term(2),lambda(comp,comp),l(comp)
      real alfa(Comp,Comp),VapHeat(comp),inter(comp,comp)
      real topklsum,bunnklsum

c     LIQUID:
      do j=1,comp
         top(j)=Ex(j,Epts)*(LiqMolVol(j)**(1.0/3.0)
     &        -WaalsVol(j)**(1.0/3.0))**(3.3)
      enddo
      bottom=0

      do j=1,comp
         bottom=bottom+top(j)
      enddo
```

```
      do j=1,comp
         fi(j)=top(j)/bottom
         lngamma(j)=log(fi(j)/Ex(j,Epts))+1-fi(j)/Ex(j,Epts)
         lgamma(j)=exp(lngamma(j))
      enddo

C     SOLID:

C     Heat of vaporization
      do j=1,comp
         VapHeat(j)=0.001*VapHeatPar(j,1)*(1-Temp/CritTemp(j))
     &        **(VapHeatPar(j,2))
      enddo

C     l
      do j=1,comp
         l(j)=1.270*Cno(j)+1.98
      enddo

c     alfa
      do j=1,comp-1
         do i=j+1,comp
            alfa(i,j)=0.01501-73.98*(l(i)-l(j))**2/(l(j)**3)
         enddo
      enddo

c     lambda
      do j=1,comp
         lambda(j,j)=-2.0/6.0*((CompEntMelt(j)+VapHeat(j)+CompSSEnt(j))
     &        -R*Temp)
      enddo

      do j=1,comp-1
         do i=j+1,comp
            lambda(i,j)=lambda(j,j)*(1+alfa(i,j))
         enddo
      enddo
```

```
c     inter
      do i=1,comp
         inter(i,i)=1
      enddo

      do j=1,comp
         do i=1,comp
            if (i.lt.j) then
               ks=i
               kl=j
            else
               ks=j
               kl=i
            endif
            inter(i,j)=exp(-(lambda(kl,ks)-lambda(i,i))/(R*Temp))
         enddo
      enddo

c     sgamma
      do i=1,comp

c     term1
         term(1)=0
         do j=1,comp
            term(1)=term(1)+(Es(j,Epts)*inter(i,j))
         enddo
         term(1)=log(term(1))

c     term2
         term(2)=0
         do j=1,comp
            topklsum=0
            bunnklsum=0
            do kl=1,comp
               topklsum=topklsum+Es(kl,Epts)*Inter(j,kl)
               bunnklsum=bunnklsum+Es(kl,epts)*Inter(j,kl)
```

```
            enddo              ! kl
            term(2)=term(2)+Es(j,Epts)*(Inter(j,i)-topklsum)/bunnklsum
         enddo                  ! j

         lngamma(i)=-term(1)-term(2)
         sgamma(i)=exp(lngamma(i))

      enddo                     !i
      return
      end

CCCCCCCCCCCCCCCCCCCCCCCCCCCCCCCCCCCCCCCCCCCCCCCCCCCCCCCCCCCCCCCCCCCCCCCCCCCCCCC
      subroutine Init
C     Initiate variables
CCCCCCCCCCCCCCCCCCCCCCCCCCCCCCCCCCCCCCCCCCCCCCCCCCCCCCCCCCCCCCCCCCCCCCCCCCCCCCC
      implicit none
      include 'PEdata.for'
      integer j,i

      do j=1,maxcomp
         do i=1,MaxEIter
            Ex(j,i)=0
            Es(j,i)=0
         enddo
      enddo
      epts=0
      return
      end

CCCCCCCCCCCCCCCCCCCCCCCCCCCCCCCCCCCCCCCCCCCCCCCCCCCCCCCCCCCCCCCCCCCCCCCCCCCCCCC
      subroutine ConsInit
C     Calculates initial consentration parameters
CCCCCCCCCCCCCCCCCCCCCCCCCCCCCCCCCCCCCCCCCCCCCCCCCCCCCCCCCCCCCCCCCCCCCCCCCCCCCCC
      implicit none
      include 'PEdata.for'
      integer j
      real sum
```

```
      sum=0
      do j=1,comp
         Ez(j)=10.0*rand()
         sum=sum+Ez(j)
      enddo

      do j=1,comp
         Ez(j)=Ez(j)/sum
      enddo

      return
      end

CCCCCCCCCCCCCCCCCCCCCCCCCCCCCCCCCCCCCCCCCCCCCCCCCCCCCCCCCCCCCCCCCCCCCCCCCCCCCCC
      subroutine ViableCheck
C     Tests if calculated solution is physically possible
CCCCCCCCCCCCCCCCCCCCCCCCCCCCCCCCCCCCCCCCCCCCCCCCCCCCCCCCCCCCCCCCCCCCCCCCCCCCCCC
      implicit none
      include 'PEdata.for'
      integer j,i
      real xsum,ssum

      viable=.true.
      ssum=0
      xsum=0
      do j=1,comp
         ssum=es(j,epts)+ssum
         xsum=ex(j,epts)+xsum
         if (.not.((Es(j,Epts).gt.0).and.(Es(j,Epts).lt.1)))
     &        viable=.false.
         if (.not.((Ex(j,Epts).gt.0).and.(Ex(j,Epts).lt.1)))
     &        viable=.false.
      enddo

      if(.not.(ssum.lt.1.001).and.(ssum.gt.0.999))
     &     viable=.false.
```

```
 if(.not.(xsum.lt.1.001).and.(xsum.gt.0.999))
&     viable=.false.

 return
 end
```

F.2 Global Variables

```
C*****************************************************************
C   GLOBAL VARIABLES
C*****************************************************************
      integer Maxcomp,Maxpoints
      parameter (maxcomp=6,MaxPoints=1001)
c     maxcomp; maximum # of components
c     MaxPoints; Maximum # of points considered

      integer MaxEIter
      parameter(MaxEiter=MaxPoints)
C     MaxEIter; maximum # of iter during determ. og phaseenvel.

      integer Points,EPts,CompRound,TempRound,TempPoints
      common/counters/Points,Epts,CompRound,TempRound,TempPoints
C     Points; Total # of points to be considered each round
C     EPts;Total # of points where enevlopedata is calculated
c     TempRound; current temperature loop, upwards or down
c     CompRound; which component which is to be changed

      integer comp
      common/geoint/comp
c     comp; total # of components

      real LCompCp(maxcomp),SCompCp(maxcomp)
      Common/Cpvar/LCompCp,SCompCp
C     LCompCp(j);Heat capacity of pure liquid component j
C     SCompCp(j);Heat capacity of pure solid component j

      real CompTransTemp(maxcomp)
      Common/MeltPtvar/CompTransTemp
c     CompTransTemp(j); temperature of solid-liquid transition of comp.(j) (me

      real CompEntMelt(maxcomp),EntMelt,CompSSEnt(maxcomp)
      Common/EntMeltVar/CompEntMelt,EntMelt,CompSSEnt
```

```
c     CompEntMelt(j); Entalphy of melting of component j
c     CompSSEnt(maxcomp), Solid-Solid Entalphy

      real Temp, HighTemp, LowTemp,CritTemp(MaxComp)
      common/EnvelopeTemp/Temp, HighTemp, LowTemp,CritTemp
c     Temp; Temperature which is considered  in phase calc.
c     HighTemp; the highest temp. which is to be considered
c     LowTemp; the lowest temp. which is to be considered
c     CritTemp;Critical temperature

      real K(MaxComp),Ez(MaxComp),VapHeatPar(MaxComp,2)
      common/equlibria/K,Ez,VapHeatPar
c     K(j); ratio between solid and liquid molfraction of component j
c     Ez(j); feed to flashcomposition
C     VapHeatPar; Parameters needed to calc. heat of vaporization

      real ETemp(MaxEIter),Ex(MaxComp,MaxEIter),Es(MaxComp,MaxEIter)
      common/EComp/ETemp,Ex,Es
C     ETemp; Temperature
c     Ex; liquid molar fraction
c     Es; solid molar fration

      real R
      parameter(R=8.314510)
C     R;Gas Constant, Jmol^-1K^-1

      real Waalsvol(MaxComp),LiqMolVol(Maxcomp),Cno(MaxComp)
      common/activitcoeff/WaalsVol,LiqMolVol,Cno
c     WaalsVol; van der Waals volume from Daubert:89
c     LiqMolVol; Liq. molar volume from daubert:89
c     Cno; Number of C-atoms

      real lgamma(MaxComp),sgamma(MaxComp)
      common/gammavalue/lgamma,sgamma
c     lgamma(j); liquid activity coefficient of component j
c     sgamma(j); solid activity coefficient of component j
```

```
      character*12 liqfilename
      common/file/liqfilename
c     liqfilename; file where results are stored

      real dTemp
      common/diff/dTemp
c     dTemp; change in temperature

      logical viable
      common/logical/viable
c     viable; true if physically possible solution
```

Appendix G

Calculated and Experimental Position of Solid-Liquid Interface during Freezing

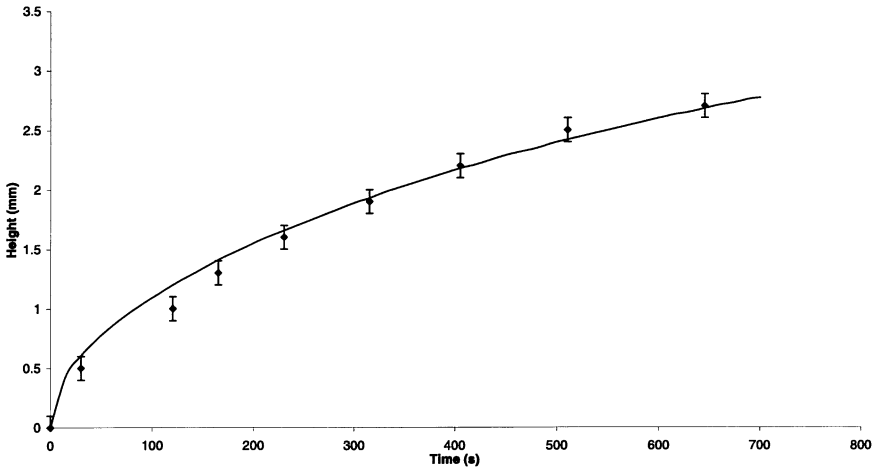

Figure G.1: Calculated and experimental position of solid-liquid interface during experiment and simulation # 1, Points: experimental value, solid line: result from numerical simulation

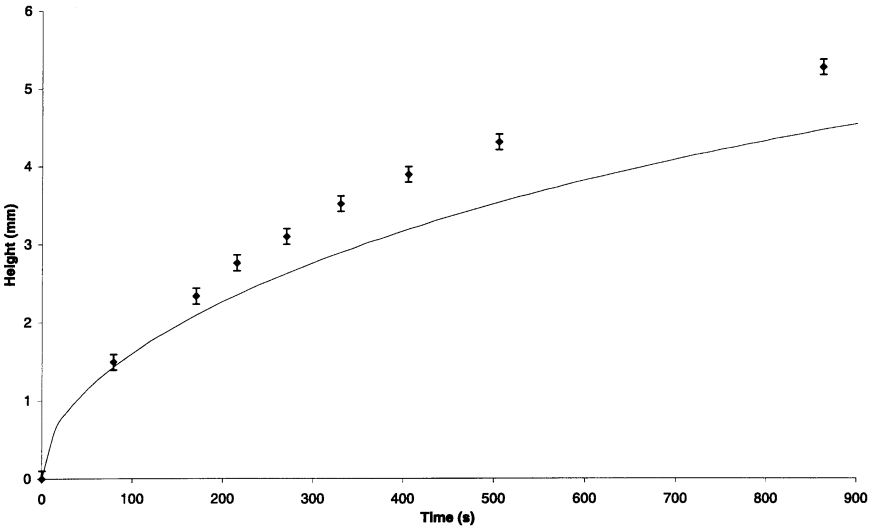

Figure G.2: Calculated and experimental position of solid-liquid interface during experiment and simulation # 2, Points: experimental value, solid line: result from numerical simulation

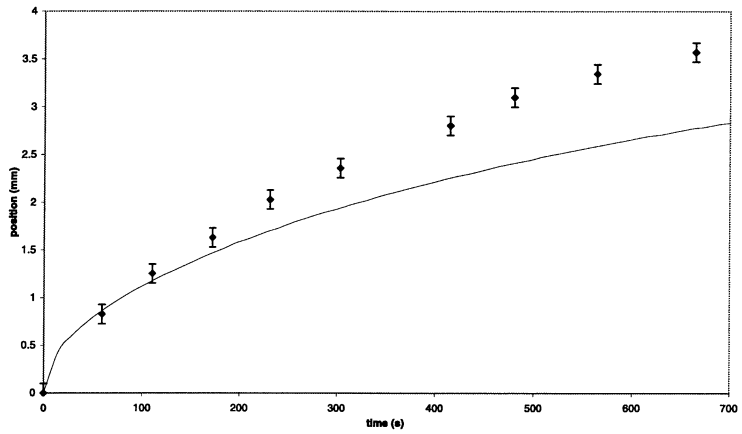

Figure G.3: Calculated and experimental position of solid-liquid interface during experiment and simulation # 3, Points: experimental value, solid line: result from numerical simulation

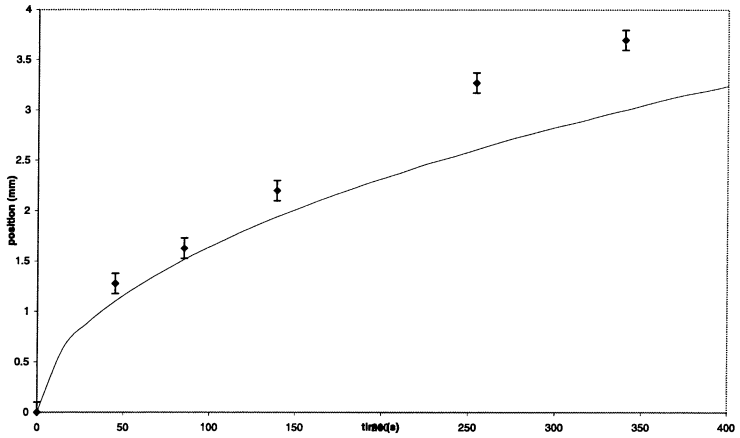

Figure G.4: Calculated and experimental position of solid-liquid interface during experiment and simulation # 4, Points: experimental value, solid line: result from numerical simulation

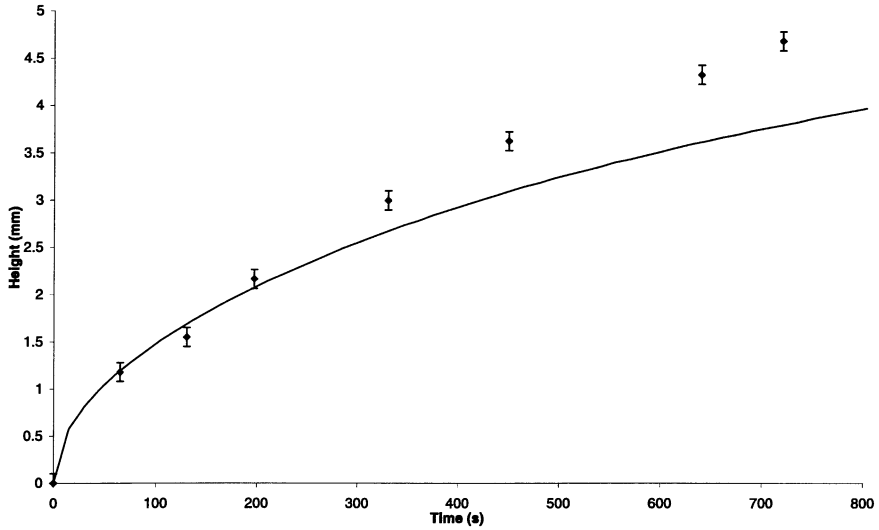

Figure G.5: Calculated and experimental position of solid-liquid interface during experiment and simulation # 5, Points: experimental value, solid line: result from numerical simulation

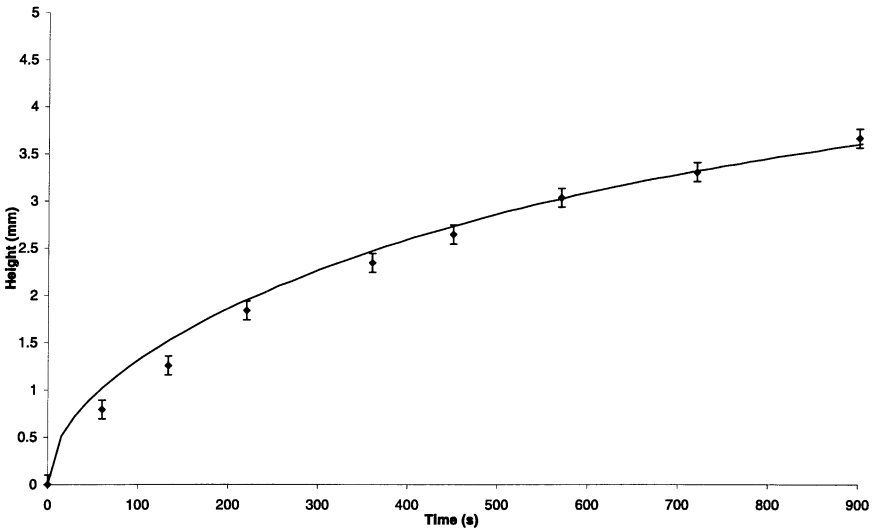

Figure G.6: Calculated and experimental position of solid-liquid interface during experiment and simulation # 6, Points: experimental value, solid line: result from numerical simulation

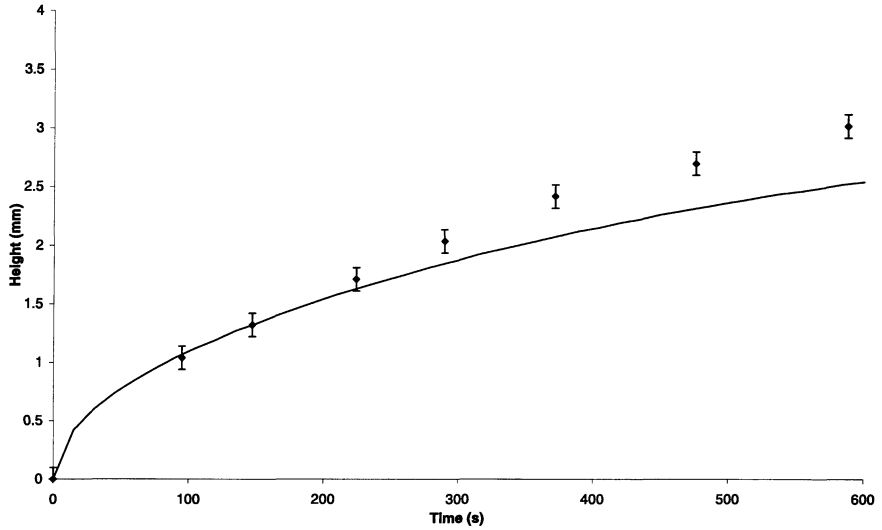

Figure G.7: Calculated and experimental position of solid-liquid interface during experiment and simulation # 7, Points: experimental value, solid line: result from numerical simulation

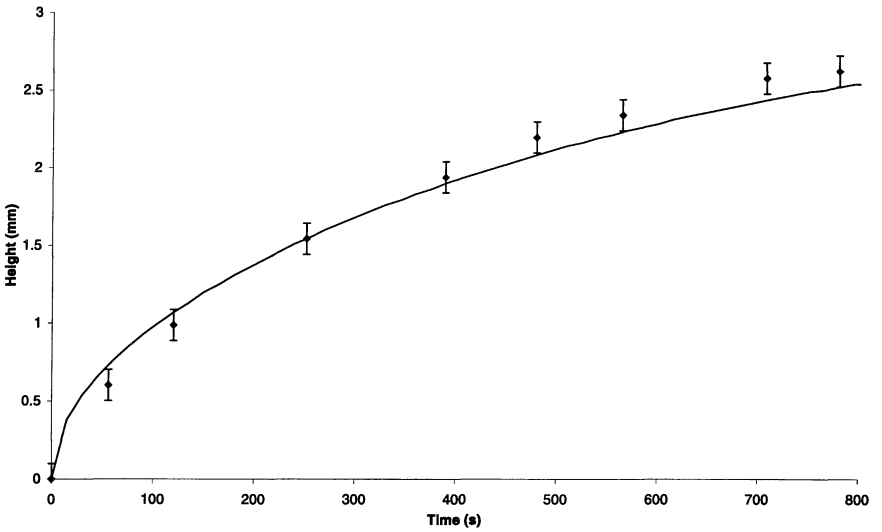

Figure G.8: Calculated and experimental position of solid-liquid interface during experiment and simulation # 8, Points: experimental value, solid line: result from numerical simulation

Appendix H

Fortran 77 Code Used to Calculate Heat and Mass Transfer during Phase Transition

The code consists of two files. The main code can be found in H.1, while the gobal variables are presented in H.2.

H.1 Transcript of Program

```
CCCCCCCCCCCCCCCCCCCCCCCCCCCCCCCCCCCCCCCCCCCCCCCCCCCCCCCCCCCCCCCCCCCC
      program neumann
CCCCCCCCCCCCCCCCCCCCCCCCCCCCCCCCCCCCCCCCCCCCCCCCCCCCCCCCCCCCCCCCCCCC
C     Calculates composition, temperature and position of
c     a  solid-liquid interface during
C     solidification and melting from  mixtures of alkanes
CCCCCCCCCCCCCCCCCCCCCCCCCCCCCCCCCCCCCCCCCCCCCCCCCCCCCCCCCCCCCCCCCCCC

      implicit none
      integer j
      include 'neumanndata.for'

      call input
      call init
      do iter=1,iterations
         call Thermodata
         if (solid) then
            call Position
            call grid
         endif
         call temperature
         if (solid) then
            call Thermodata
            call Composition
         else
            call TwoPhaseCheck
         endif
         call TempPres
         time=time+dt
      enddo
      close (20)
      call onscreenpres
      call FilePres
      end
```

```
CCCCCCCCCCCCCCCCCCCCCCCCCCCCCCCCCCCCCCCCCCCCCCCCCCCCCCCCCCCCCCCCCCCCCCCCCCCCCCC
      subroutine input
C     provides input to the calculation, i.e: case data
C     all data given in basic SI-units, i.e: m, kg, mol, K etc..
CCCCCCCCCCCCCCCCCCCCCCCCCCCCCCCCCCCCCCCCCCCCCCCCCCCCCCCCCCCCCCCCCCCCCCCCCCCCCCC
      implicit none
      include 'neumanndata.for'
      integer i,nc16,nc17,nc18,nc19

C     Timestep
      dt=0.01

C     # of iterations
      iterations=700/dt

C     Iterations between dumping of runtime data
      RunTime=15/dt
      if (runtime.eq.0)      runtime=1

C     Total lenght of cell
      H=12/1000.0

C     Total # of calc cells in liquid
      LT=100

C     Total # of calc cells in solid
      ST=100

c     Condition on top plate
      TopTemp=301.1

C     Condition on lower plate
      BottomTemp=287.8

c     # of components
      comp=2
```

```
c     Feed composition, assuming same initial composition of solid and liquid
      z(1)=0.637
      z(2)=1-Z(1)
      z(3)=0
      z(4)=0

c     Liquidus
      Liquidus(1,1)=301.3732
      Liquidus(1,2)=-21.1994
      Liquidus(1,3)=+324.3712
      Liquidus(1,4)=-4229.5181
      Liquidus(1,5)=+28351.14
      Liquidus(1,6)=-110899.6828
      Liquidus(1,7)=+266006.2178
      Liquidus(1,8)=-395684.5131
      Liquidus(1,9)=+355048.4817
      Liquidus(1,10)=-175598.3857
      Liquidus(1,11)=+36693.0656ss
c     Order of components, must be the same as number of carbonatoms
      nc16=1
      nc17=3
      nc18=2
      nc19=4

c     Thermophysical properties of the components

C     Hexadecane:
      LCompCp(nC16)=490.00       ! (J/molK)
      SCompCp(nC16)=430.00       ! (J/molK)
      CompTransTemp(nC16)=291.1
      CompEntMelt(nC16)=51600    !(J/mol)
      CompMr(nC16)=0.22645       !(kg/mol)
      LCompRho(nC16)=775
      SCompRho(nC16)=853
      SCompCond(nC16)=0.40
      LCompCond(nC16)=0.20
```

```
      LiqmolVol(nC16)=0.294064/1000  ! (m^3/mol)
      WaalsVol(nC16)=.17056/1000     ! (m^3/mol)
      Cno(nC16)=16
      CritTemp(nC16)=720.60
      VapHeatPar(nC16,1)=9.7520E7
      VapHeatPar(nC16,2)=4.122E-1
      CompSSEnt(nC16)=0

c     Heptadecane:
      LCompCp(nC17)=530.00    ! (J/molK)
      SCompCp(nC17)=890.000     ! (J/molK)
      CompTransTemp(nC17)=295.14
      CompEntMelt(nC17)=40200   !(J/mol)
      CompMr(nC17)=0.240470     !(kg/mol)
      LCompRho(nC17)=777
      SCompRho(nC17)=854
      SCompCond(nC17)=0.20
      LCompCond(nC17)=0.20
      LiqmolVol(nC17)=0.311120/1000  ! (m^3/mol)
      WaalsVol(nC17)=.18079/1000     ! (m^3/mol))
      Cno(nC17)=17
      CritTemp(nC17)=733.37
      VapHeatPar(nC17,1)=1.02E8
      VapHeatPar(nC17,2)=4.33E-1
      CompSSEnt(nC17)= 1.09E4   ! (J/mol)

c     OCTADECANE:
      LCompCp(nC18)=560.00        ! (J/molK)
      SCompCp(nC18)=480.00      ! (J/molK)
      CompTransTemp(nC18)=301.4
      CompEntMelt(nC18)=61300   !(J/mol)
      CompMr(nC18)=0.25450      !(kg/mol)
      LCompRho(nC18)=777
      SCompRho(nC18)=855
      SCompCond(nC18)=0.40
      LCompCond(nC18)=0.20
      LiqmolVol(nC18)=0.329141/1000  ! (m^3/mol)
```

```
      WaalsVol(nC18)=.19102/1000     ! (m^3/mol)
      Cno(nC18)=18
      CritTemp(nC18)=745.26
      VapHeatPar(nC18,1)=1.0695E8
      VapHeatPar(nC18,2)=4.51E-1
      CompSSEnt(nC18)=0

c     NONADECANE:
      LCompCp(nC19)=590.00       ! (J/molK)
      SCompCp(nC19)=860.00       ! (J/molK)
      CompTransTemp(nC19)=305.15
      CompEntMelt(nC19)=45900    !(J/mol)
      CompMr(nC19)=0.26850       !(kg/mol)
      LCompRho(nC19)=778
      SCompRho(nC19)=859
      SCompCond(nC19)=0.20
      LCompCond(nC19)=0.20
      LiqmolVol(nC19)=0.346128/1000  ! (m^3/mol)
      WaalsVol(nC19)=.20125/1000     ! (m^3/mol)
      Cno(nC19)=19
      CritTemp(nC19)=755.93
      VapHeatPar(nC19,1)=1.1467E8
      VapHeatPar(nC19,2)=4.476E-1
      CompSSEnt(nC19)=1.38E4     ! (J/mol)

      return
      end

CCCCCCCCCCCCCCCCCCCCCCCCCCCCCCCCCCCCCCCCCCCCCCCCCCCCCCCCCCCCCCCCCCCCCCCCCCCCCCC
      subroutine grid
C     Defines the grid
CCCCCCCCCCCCCCCCCCCCCCCCCCCCCCCCCCCCCCCCCCCCCCCCCCCCCCCCCCCCCCCCCCCCCCCCCCCCCCC
      implicit none
      integer i
      real dl,ds
      include 'neumanndata.for'
```

```
C     Assumes that the change in coordinates is small
C     as an initial assumption, the properties as temperature etc.
C     moves along with the grid.

C     Liquid
      dl=(H-interface)/(float(LT-2))
      L(1)=interface
      L(2)=L(1)+0.5*dl
      L_B(1)=interface
      L_B(2)=interface
      do i=3,LT-1
         L(i)=L(i-1)+dl
         L_B(i)=L_B(i-1)+dl
      enddo
      L(LT)=L(LT-1)+0.5*dl
      L_B(LT)=L_B(LT-1)+dl

C     Solid
      if (solid) then
         ds=(interface)/(float(ST-2))
         S(1)=0
         S(2)=S(1)+0.5*ds
         S_B(1)=0
         S_B(2)=0
         do i=3,ST-1
            S(i)=S(i-1)+ds
            S_B(i)=S_B(i-1)+ds
         enddo
         S(ST)=S(ST-1)+0.5*ds
         S_B(ST)=S_B(ST-1)+ds
      endif

      return
      end

CCCCCCCCCCCCCCCCCCCCCCCCCCCCCCCCCCCCCCCCCCCCCCCCCCCCCCCCCCCCCCCCCCCCCCC
      subroutine init
```

```
C     initialization of the variables, first approximations
CCCCCCCCCCCCCCCCCCCCCCCCCCCCCCCCCCCCCCCCCCCCCCCCCCCCCCCCCCCCCCCCCCCCCCCCCCC
      implicit none
      include 'neumanndata.for'
      integer i,j
      real dl,ds

      open(20,file='position.dat',status='unknown')
      write (20,100) 'time (s)',char(9), 'x_mp (m)'
 100  format(A10,A1,a10)

      PresNo=0

c     No solid has formed:
      solid=.false.
      interface=0

C     LIQUID GRID AND TEMPERATURE

c     temperature
      do i=1,LT-1
         LTemp(i)=Toptemp
      enddo
      LTemp(LT)=TopTemp
      do i=1,LT
         do j=1,comp
            Lx(j,i)=z(j)
         enddo
      enddo

c     grid
      dl=(H-interface)/(float(LT-2))
      L(1)=interface
      L(2)=L(1)+0.5*dl
      L_B(1)=interface
      L_B(2)=interface
      do i=3,LT-1
```

```
         L(i)=L(i-1)+dl
         L_B(i)=L_B(i-1)+dl
      enddo
      L(LT)=L(LT-1)+0.5*dl
      L_B(LT)=L_B(LT-1)+dl

      return
      end

CCCCCCCCCCCCCCCCCCCCCCCCCCCCCCCCCCCCCCCCCCCCCCCCCCCCCCCCCCCCCCCCCCCCCCC
      subroutine position
C     Calculates the position of the interface
CCCCCCCCCCCCCCCCCCCCCCCCCCCCCCCCCCCCCCCCCCCCCCCCCCCCCCCCCCCCCCCCCCCCCCC
      implicit none
      include 'neumanndata.for'
      real NewInterface

      NewInterface=Interface+dt/(Rho*(EntMelt/Mr))*
     &        (SCond(ST)*(TransTemp-STemp(ST-1))/(S(ST)-S(ST-1))-
     &        LCond(1)*(LTemp(2)-TransTemp)/(L(2)-L(1)))

      dxmp=NewInterface-Interface
      if (dxmp.gt.0) then
         Interface=NewInterface
      endif

      If (interface.gt.H) then
         interface=H-0.00001
      endif

      return
      end

CCCCCCCCCCCCCCCCCCCCCCCCCCCCCCCCCCCCCCCCCCCCCCCCCCCCCCCCCCCCCCCCCCCCCCC
      subroutine Thermodata
c     assigns thermophysical data
CCCCCCCCCCCCCCCCCCCCCCCCCCCCCCCCCCCCCCCCCCCCCCCCCCCCCCCCCCCCCCCCCCCCCCC
```

```
      implicit none
      include 'neumanndata.for'
      integer i,j
      real MolVol,Ix(comp),D0(Comp,LT),Di(LT),A(LT),B(3)

C     PROPERTIES OF THE INTERFACE

C     Composition used for calculating the properties at the
C     interface belongs to the disappearing phase
      Rho=LRho(1)
      Mr=LMr(1)
      do j=1,comp
         Ix(j)=Lx(j,1)
      enddo

C     TransTemp is liquidus
c     xxx assume binary mixture
      TransTemp=0
      do i=1,11
         TransTemp=Liquidus(1,i)*Ix(1)**(i-1)+TransTemp
      enddo

c     EntMelt
      EntMelt=0
      do j=1,comp
         EntMelt=EntMelt+Ix(j)*CompEntMelt(j)
      enddo

C     KValue
      Temp=TransTemp
      Call KValue

C     PROPERTIES OF THE SOLID
      if (solid) then
c     density, Cp, term. cond
         do i=1,ST
            molvol=0
```

```
            SMr(i)=0
            SCp(i)=0
            SCond(i)=0
            do j=1,comp
c     assume no volume change during mixing
               molvol=molvol+Sx(j,i)*CompMr(j)/(1.0*SCompRho(j))
               SMr(i)=SMr(i)+Sx(j,i)*CompMr(j)
               SCp(i)=SCp(i)+SCompCp(j)*Sx(j,i)
               SCond(i)=SCond(i)+SCompCond(j)*Sx(j,i)
            enddo
            SRho(i)=SMr(i)/molvol

         enddo

c     XXX XXX XXX Alternative properties
         do i=1,ST
               SCp(i)=SCompCp(4)
               SRho(i)=SCompRho(4)
               SCond(i)=SCompCond(4)
         enddo
         EntMelt=CompEntMelt(4)
         TransTemp=293.2
c     harmonic averaging
         do i=3,ST-1
            S_BCond(i)=1/(
     &           1/SCond(I-1)*(S_B(i)-S(i-1))/(S(i)-S(i-1))+
     &           1/SCond(I)*(S(i)-S_B(i))/(S(i)-S(i-1)))
         enddo
         S_BCond(1)=SCond(1)
         S_BCond(2)=SCond(2)
         S_BCond(ST)=SCond(ST)

      endif

C     PROPERTIES OF THE LIQUID

c     density, Cp, term. cond.
```

```
      do i=1,LT
         molvol=0
         LMr(i)=0
         LCp(i)=0
         LRho(i)=0
         LCond(i)=0
         Di(i)=0
         do j=1,comp
c     assume no volume change during mixing
            molvol=molvol+Lx(j,i)*CompMr(j)/LCompRho(j)
            LMr(i)=LMr(i)+Lx(j,i)*CompMr(j)
            LCp(i)=LCp(i)+LCompCp(j)*Lx(j,i)
            LCond(i)=LCond(i)+LCompCond(j)*Lx(j,i)

c     Do(j,i)=tracer diffusion of comp j in mixture at cell i
c     model from wong:90
            D0(j,i)=(3.17E-4*LMr(i)*1000
     &           *(CompMr(j)*1000)**(-0.596)
     &           *exp(1/LTemp(i)*(-487.7-8.57*(LMr(i)*1000)
     &           +0.009*(LMr(i)*1000)**2)))
     &           /100/100
c     Darken approx (p.611 Reid:87, assuming alpha=1)
            Di(i)=Di(i)+Lx(j,i)*D0(j,i)

         enddo

C     XXX XXX XXX Alternative diffusion coeffisient XXX XXX
c     xxx Quick Difffusion xxx
         Di(i)=100000*Di(i)

         LRho(i)=LMr(i)/molvol
         A(i)=Di(i)*LRho(i)/(1.0*LMr(i))
      enddo

c     harmonic averaging
      do i=3,LT-1
```

```
          A_B(i)=1/(
     &         1/A(I-1)*(L_B(i)-L(i-1))/(L(i)-L(i-1))+
     &         1/A(I)*(L(i)-L_B(i))/(L(i)-L(i-1)))

          L_BCond(i)=1/(
     &         1/LCond(I-1)*(L_B(i)-L(i-1))/(L(i)-L(i-1))+
     &         1/LCond(I)*(L(i)-L_B(i))/(L(i)-L(i-1)))
          enddo

          A_B(1)=A(1)
          A_B(2)=A(2)
          A_B(LT)=A(LT)
          L_BCond(1)=LCond(1)
          L_BCond(2)=LCond(2)
          L_BCond(LT)=LCond(LT)

          return
          end

CCCCCCCCCCCCCCCCCCCCCCCCCCCCCCCCCCCCCCCCCCCCCCCCCCCCCCCCCCCCCCCCCCCCCCCCCCCCCCC
          subroutine Temperature
c         calculates the temperature profile in the liquid and solid phases
CCCCCCCCCCCCCCCCCCCCCCCCCCCCCCCCCCCCCCCCCCCCCCCCCCCCCCCCCCCCCCCCCCCCCCCCCCCCCCC
          implicit none
          include 'neumanndata.for'
          integer i,j

C         SOLID
          if (solid) then
             STemp(ST)=TransTemp

C         Assign values to the matrix
             Alfa(1)=0
             Beta(1)=0
             D(1)=1
             C(1)=BottomTemp
             Phi(1)=BottomTemp
```

```
          do i=2,ST-1
             Beta(i)=S_BCond(i)/(S(i)-S(i-1))
             Alfa(i)=S_BCond(i+1)/(S(i+1)-S(i))
             C(i)=SCp(i)*SRho(i)*(S_B(i+1)-S_B(i))*STemp(i)
     &            /(SMr(i)*dt)
             D(i)=Alfa(i)+Beta(i)+C(i)/STemp(i)
             Phi(i)=STemp(i)
          enddo
          Alfa(ST)=0
          Beta(ST)=0
          D(ST)=1
          C(ST)=STemp(ST)
          Phi(ST)=STemp(ST)
          N=ST

C     Solve the matrix
          call Solve

C     Phi is Stemp here:
          do i=1,St
             Stemp(i)=Phi(i)
          enddo
       endif

C     LIQUID

       if (solid) then
          LTemp(1)=TransTemp
       else
          LTemp(1)=BottomTemp
       endif

C     Assign values to the matrix
       Alfa(1)=0
       Beta(1)=0
       D(1)=1
       C(1)=LTemp(1)
```

```
      Phi(1)=LTemp(1)
      do i=2,LT-1
         Beta(i)=L_BCond(i)/(L(i)-L(i-1))
         Alfa(i)=L_BCond(i+1)/(L(i+1)-L(i))
         C(i)=LCp(i)*LRho(i)*(L_B(i+1)-L_B(i))*LTemp(i)
     &        /(LMr(i)*dt)
         D(i)=Alfa(i)+Beta(i)+C(i)/LTemp(i)
         Phi(i)=LTemp(i)
      enddo
      Alfa(LT)=0
      Beta(LT)=0
      D(LT)=1
      C(LT)=TopTemp
      Phi(LT)=TopTemp
      N=LT

C     Solve the matrix
      call Solve

C     Phi is Ltemp here:
      do i=1,Lt
         Ltemp(i)=Phi(i)
      enddo

      return
      end

CCCCCCCCCCCCCCCCCCCCCCCCCCCCCCCCCCCCCCCCCCCCCCCCCCCCCCCCCCCCCCCCCCCCCCCCCCCC
      subroutine FilePres
c     Final presentation of data to files
CCCCCCCCCCCCCCCCCCCCCCCCCCCCCCCCCCCCCCCCCCCCCCCCCCCCCCCCCCCCCCCCCCCCCCCCCCCC
      implicit none
      include 'neumanndata.for'
      integer i,j
      character*20 fil,phase
      character*2 PresChar
      real MeltTemp,FreezTemp
```

```
      Presno=Presno+1
      PresChar=char(48+Presno/10)//char(48+presno-10*(presno/10))

C     LCOMP
      do j=1,comp
         fil='LComp'//char(48+j)//PresChar//'.dat'
         open(10,file=fil,status='unknown')
         write(10,*) 'Time:',Time
         write (10,100) 'Position','Lx'//char(j+48)
         do i=1,LT
            write(10,200) L(i),Lx(j,i)
         enddo
         close(10)
 100     format(A10,3x,A10)
 200     format(1x,2E15.6)
      enddo

C     SComp
      if (solid) then
         do j=1,comp
            fil='SComp'//Char(48+j)//PresChar//'.dat'
            open(10,file=fil,status='unknown')
            write(10,*) 'Time:',Time
            write (10,300) 'Position','Sx'//char(48+j)
            do i=1,ST
               write(10,400) S(i),Sx(j,i)
            enddo
            close(10)
 300        format(A10,3x,A10)
 400        format(1x,2E15.6)
         enddo
      endif


C     SCond
      if (solid)then
```

```
         open(10,file='SCond'//PresChar//'.dat',status='unknown')
         write(10,*) 'Time:',Time
         write (10,500) 'Position','SCond'
         do i=1,ST
            write(10,600) S(i),SCond(i)
         enddo
         close(10)
 500     format(A10,3x,A10)
 600     format(1x,2E15.6)
      endif

C     LCond
      open(10,file='LCond'//PresChar//'.dat',status='unknown')
      write(10,*) 'Time:',Time
      write (10,700) 'Position','LCond'
      do i=1,LT
         write(10,800) L(i),LCond(i)
      enddo
      close(10)
 700  format(A10,3x,A10)
 800  format(1x,2E15.6)


C     STemp
      if (solid) then
         open(10,file='STemp'//PresChar//'.dat',status='unknown')
         write(10,*) 'Time:',Time
         write (10,900) 'Position','STemp'
         do i=1,ST
            write(10,1000) S(i),STemp(i)
         enddo
         close(10)
 900     format(A10,3x,A10)
 1000    format(1x,2E15.6)
      endif

C     LTemp
```

```
      open(10,file='LTemp'//PresChar//'.dat',status='unknown')
      write(10,*) 'Time:',Time
      write (10,1100) 'Position','LTemp'
      do i=1,LT
         write(10,1200) L(i),LTemp(i)
      enddo
      close(10)
 1100 format(A10,3x,A10)
 1200 format(1x,2E15.6)

C     S_BCond
      if (solid) then
         open(10,file='S_BCond'//PresChar//'.dat',status='unknown')
         write(10,*) 'Time:',Time
         write (10,1300) 'Position','S_BCond'
         do i=1,ST
            write(10,1400) S(i),S_BCond(i)
         enddo
         close(10)
 1300    format(A10,3x,A10)
 1400    format(1x,2E15.6)
      endif

C     L_BCond
      open(10,file='L_BCond'//PresChar//'.dat',status='unknown')
      write(10,*) 'Time:',Time
      write (10,1500) 'Position','L_BCond'
      do i=1,LT
         write(10,1600) L(i),L_BCond(i)
      enddo
      close(10)
 1500 format(A10,3x,A10)
 1600 format(1x,2E15.6)

C     SRho
      if (solid) then
         open(10,file='SRho'//PresChar//'.dat',status='unknown')
```

```
         write(10,*) 'Time:',Time
         write (10,1700) 'Position','SRho'
         do i=1,ST
            write(10,1800) S(i),SRho(i)
         enddo
         close(10)
 1700    format(A10,3x,A10)
 1800    format(1x,2E15.6)
      endif

C     LRho
      open(10,file='LRho'//PresChar//'.dat',status='unknown')
      write(10,*) 'Time:',Time
      write (10,1900) 'Position','LRho'
      do i=1,LT
         write(10,2000) L(i),LRho(i)
      enddo
      close(10)
 1900 format(A10,3x,A10)
 2000 format(1x,2E15.6)

      return
      end

CCCCCCCCCCCCCCCCCCCCCCCCCCCCCCCCCCCCCCCCCCCCCCCCCCCCCCCCCCCCCCCCCCCCCCCCCCCCCCC
      subroutine onscreenpres
C     provides onscreen presentation
CCCCCCCCCCCCCCCCCCCCCCCCCCCCCCCCCCCCCCCCCCCCCCCCCCCCCCCCCCCCCCCCCCCCCCCCCCCCCCC
      implicit none
      include 'neumanndata.for'
      write(*,*),'time since start of simulation (s) : ',dt*iter
      if (solid) then
         write(*,*),'ks*dt/dx=',S_BCond(ST)*(TransTemp-STemp(ST-1))/
     &        (S(ST)-S(ST-1))
         write(*,*),'kl*dt/dx=',L_BCond(1)*(LTemp(2)-TransTemp)/
     &        (L(2)-L(1))
         write(*,*) 'TransTemp:',TransTemp
```

```
      endif
      return
      end

CCCCCCCCCCCCCCCCCCCCCCCCCCCCCCCCCCCCCCCCCCCCCCCCCCCCCCCCCCCCCCCCCCCCCCC
      subroutine TempPres
C     provides presentation of data during run
CCCCCCCCCCCCCCCCCCCCCCCCCCCCCCCCCCCCCCCCCCCCCCCCCCCCCCCCCCCCCCCCCCCCCCC
      implicit none
      include 'neumanndata.for'

      if ((mod(iter,RunTime).eq.0).or.((iter.eq.1).or.
     &     (iter.eq.iterations))) then

c     Presentation to screen :
         write (*,*) 'iter:',iter,' xmp:',
     &        interface*1000,' t(s)',dt*iter,
     &        ' Tmp:',TransTemp
         Write(*,*) 'x(1,1):',Lx(1,1), ' s(1,ST):',SX(1,ST),' k(1)',k(1)
         Write(*,*)

c     Presentation to file:
         write(20,100) dt*iter,char(9),interface*1000
 100     format (E15.6,A1,E15.6)

      endif
      return
      end

CCCCCCCCCCCCCCCCCCCCCCCCCCCCCCCCCCCCCCCCCCCCCCCCCCCCCCCCCCCCCCCCCCCCCCC
      subroutine TwoPhaseCheck
C     Is called if the cell only consists of one phase,
C     checks if the lower cell change phase
CCCCCCCCCCCCCCCCCCCCCCCCCCCCCCCCCCCCCCCCCCCCCCCCCCCCCCCCCCCCCCCCCCCCCCC
      implicit none
      include 'neumanndata.for'
```

```
c     If freezing has started:
      if (LTemp(2).lt.TransTemp) then
         interface=L(2)
         LTemp(1)=TransTemp
         LTemp(2)=LTemp(3)
         solid=.true.
         call SolidInit
      endif

      return
      end

CCCCCCCCCCCCCCCCCCCCCCCCCCCCCCCCCCCCCCCCCCCCCCCCCCCCCCCCCCCCCCCCCCCCCCCCCCCCCCC
      subroutine SolidInit
C     Initializes the variables in the solid phase
CCCCCCCCCCCCCCCCCCCCCCCCCCCCCCCCCCCCCCCCCCCCCCCCCCCCCCCCCCCCCCCCCCCCCCCCCCCCCCC
      implicit none
      include 'neumanndata.for'
      integer i,j
      real ds,dTemp,sum

c     temperature, assume linear gradient initially
      STemp(1)=BottomTemp
      dTemp=(TransTemp-BottomTemp)/(ST-1)
      do i=2,ST-1
         STemp(i)=STemp(i-1)+dTemp
      enddo
      STemp(ST)=TransTemp

c     ensure no negative gradients in the liquid phase
      do i=1,LT
         if (LTemp(i).lt.TransTemp) LTemp(I)=TransTemp
      enddo

c     composition, no  massconservation ! xxx
      do i=1,ST
         do j=1,comp
```

```
            Sx(j,i)=K(j)*Lx(j,1)
         enddo
      enddo
c     ensure sigma sx=1:
      do i=1,ST
         sum=0
         do j=1,comp
            sum=Sx(j,i)+sum
         enddo
         do j=1,comp
            Sx(j,i)=Sx(j,i)/sum
         enddo
      enddo

c     grid
      call grid

      return
      end

CCCCCCCCCCCCCCCCCCCCCCCCCCCCCCCCCCCCCCCCCCCCCCCCCCCCCCCCCCCCCCCCCCCCCCCCCCCCCCC
      subroutine Solve
C     solves a tridiagonal matrix using the notation from
C     chapter 7 of Versteeg & Malalasekera (1995
CCCCCCCCCCCCCCCCCCCCCCCCCCCCCCCCCCCCCCCCCCCCCCCCCCCCCCCCCCCCCCCCCCCCCCCCCCCCCCC
      implicit none
      include 'neumanndata.for'
      integer i,j
      Real A(maxt),CMerk(maxt)

      CMerk(1)=Phi(1)
      A(1)=0
      do i=2,n-1
         A(i)=alfa(i)/(D(i)-Beta(i)*A(i-1))
         Cmerk(i)=(Beta(i)*CMerk(i-1)+C(i))/(D(i)-Beta(i)*A(i-1))
      enddo
```

```
      do i=n-1,2,-1
         Phi(i)=A(i)*Phi(i+1)+CMerk(i)
      enddo

      return
      end

CCCCCCCCCCCCCCCCCCCCCCCCCCCCCCCCCCCCCCCCCCCCCCCCCCCCCCCCCCCCCCCCCCCCCCCCCCCCCCC
      subroutine Composition
C     Determines the composition
CCCCCCCCCCCCCCCCCCCCCCCCCCCCCCCCCCCCCCCCCCCCCCCCCCCCCCCCCCCCCCCCCCCCCCCCCCCCCCC
      implicit none
      include 'neumanndata.for'
      integer i,j,m
      real LCons(LT),Sxn(comp),SRhon,SCons(Comp),SMrn,MolVol
      real SConsn(comp),sum,SG(ST),ds,dsx,SGx(comp,ST)

C     LIQUID

c     neccesary parameters:
      molvol=0
      SMrn=0
      do j=1,comp
         Sxn(j)=K(j)*Lx(j,1)
         MolVol=MolVol+Sxn(j)*CompMr(j)/(1.0*SCompRho(j))
         SMrn=SMrn+Sxn(j)*CompMr(j)
      enddo
      SRhon=SMrn/MolVol
      do j=1,comp
         SConsn(j)=Sxn(j)*SRhon/SMrn
      enddo


c     Lcons is used as phi
      do j=1,comp
         do i=1,LT
            LCons(i)=LRho(i)*Lx(j,i)/(1.0*LMr(i))
```

```
            Phi(i)=LCons(i)
         enddo

C     bottom cell (2)
         D(1)=1
         Beta(1)=0
         Alfa(1)=0
         C(1)=phi(1)
         D(2)=(L_B(3)-L_B(2))/dt + dxmp*SRhon*K(j)*LMr(2)/
     &        (dt*SMrn*LRho(2)) + A_B(3)*CompMr(j)/
     &        ((L(3)-L(2))*LRho(2))
         Beta(2)=0
         Alfa(2)=A_B(3)*CompMr(j)/((L(3)-L(2))*LRho(3))
         C(2)=(L_B(3)-L_B(2))*LCons(2)/dt

C     inner cells
         do i=3,LT-1
            Beta(i)=A_B(i)*CompMr(j)/((L(i)-L(i-1))*LRho(i-1))
            alfa(i)=A_B(i+1)*CompMr(j)/((L(i+1)-L(i))*LRho(i+1))
            D(i)=(L_B(i+1)-L_B(i))/dt+
     &           A_B(i+1)*CompMr(j)/((L(i+1)-L(i))*LRho(i)) +
     &           A_B(i)*CompMr(j)/((L(i)-L(i-1))*LRho(i))
            C(i)=(L_B(i+1)-L_B(i))*LCons(i)/dt
         enddo

C     top cell
         Beta(LT)=0
         Alfa(LT)=0
         D(LT)=1
         C(LT)=LCons(LT)

c     solve
         N=LT
         call Solve

c     let Lcons=phi
         Lcons(1)=phi(2)
```

```
         do i=2,LT
            Lcons(i)=Phi(i)
         enddo

c     Provisorily calculation of Lx
         do i=1,LT
            Lx(j,i)=LCons(i)*LMr(i)/LRho(i)
         enddo

      enddo                        ! component j

C     Need to calculate mole fractions to ensure that sigma Lx(i)=1
      do i=1,LT
         sum=0
         do j=1,comp
            sum=Lx(j,i)+sum
         enddo
         do j=1,comp
            Lx(j,i)=Lx(j,i)/sum
         enddo
      enddo

C     SOLID

c     need the old grid
      ds=(interface-dxmp)/(float(ST-2))
      SG(1)=0
      SG(2)=SG(1)+0.5*ds
      do i=3,ST-1
         SG(i)=SG(i-1)+ds
      enddo
      SG(ST)=SG(ST-1)+0.5*ds

      do j=1,comp
         Sx(j,ST)=Lx(j,1)*K(j)
      enddo
```

```
      do i=2,ST-1

c     newly added solid:
         if (S(i).gt.SG(ST)) then
            if (S(i-1).gt.SG(ST)) then
               do j=1,comp
                  Sx(j,i)=K(j)*Lx(j,1)
               enddo
            else
               do j=1,comp
                  dsx=Lx(j,i)*K(j)-Sx(j,ST)
                  ds=s(I+1)-SG(ST)
                  Sx(j,i)=Sx(j,ST)+dsx/ds*(S(i)-SG(ST))
               enddo
            endif
         else
c     reposition the old compositions
            m=1
 10         m=m+1
            if (SG(m).lt.S(i)) goto 10
            do j=1,comp
               dsx=SX(j,m)-Sx(j,m-1)
               ds=SG(m)-Sg(m-1)
               sx(j,i)=Sx(j,m-1)+dsx/ds*(S(i)-SG(m-1))
            enddo
         endif
      enddo

C     Need to calculate mole fractions to ensure that sigma Sx(i)=1
      do i=1,ST
         sum=0
         do j=1,comp
            sum=Sx(j,i)+sum
         enddo
         do j=1,comp
            Sx(j,i)=Sx(j,i)/sum
         enddo
```

```
      enddo

      return
      end

CCCCCCCCCCCCCCCCCCCCCCCCCCCCCCCCCCCCCCCCCCCCCCCCCCCCCCCCCCCCCCCCCCCCCCCCCCCCCCC
      subroutine KValue
C     Calculate the Kvalue for each component
CCCCCCCCCCCCCCCCCCCCCCCCCCCCCCCCCCCCCCCCCCCCCCCCCCCCCCCCCCCCCCCCCCCCCCCCCCCCCCC
      implicit none
      include 'NeumannData.for'
      integer j
      real DeltaCp,Tt,Hmp

      call gamma

C     Expression for K:
      do j=1,comp
         DeltaCp=LCompCp(j)-SCompCp(j)
         Tt=CompTransTemp(j)
         Hmp=CompEntMelt(j)
         K(j)=Lgamma(j)/SGamma(j)*exp(
     &        Hmp/(R*Tt)*(Tt/Temp-1)+DeltaCp/R*
     &        (1-Tt/Temp+log(Tt/Temp)))
      enddo
      return
      end

CCCCCCCCCCCCCCCCCCCCCCCCCCCCCCCCCCCCCCCCCCCCCCCCCCCCCCCCCCCCCCCCCCCCCCCCCCCCCCC
      subroutine gamma
C     Calculates activity coefficients
CCCCCCCCCCCCCCCCCCCCCCCCCCCCCCCCCCCCCCCCCCCCCCCCCCCCCCCCCCCCCCCCCCCCCCCCCCCCCCC
      implicit none
      include 'NeumannData.for'
      integer j,i,kl,ks
      real top(comp),bottom,fi(comp),lngamma(comp)
      real term(2),lambda(comp,comp),li(comp)
```

```
      real alf(Comp,Comp),VapHeat(comp),inter(comp,comp)
      real topklsum,bunnklsum

      do j=1,comp
         top(j)=Lx(j,1)*(LiqMolVol(j)**(1.0/3.0)
     &        -WaalsVol(j)**(1.0/3.0))**(3.3)
      enddo
      bottom=0

      do j=1,comp
         bottom=bottom+top(j)
      enddo

      do j=1,comp
         fi(j)=top(j)/bottom
         lngamma(j)=log(fi(j)/Lx(j,1))+1-fi(j)/Lx(j,1)
         lgamma(j)=exp(lngamma(j))
      enddo

C     SOLID:

C     Heat of vaporization
      do j=1,comp
         VapHeat(j)=0.001*VapHeatPar(j,1)*(1-Temp/CritTemp(j))
     &        **(VapHeatPar(j,2))
      enddo

C     l
      do j=1,comp
         li(j)=1.270*Cno(j)+1.98
      enddo


c     alfa
      do j=1,comp-1
         do i=j+1,comp
            alf(i,j)=0.01501-73.98*(li(i)-li(j))**2/(li(j)**3)
```

```
         enddo
      enddo

c     lambda
      do j=1,comp
         lambda(j,j)=-2.0/6.0*((CompEntMelt(j)+VapHeat(j)
     &        +CompSSEnt(j))-R*Temp)
      enddo

      do j=1,comp-1
         do i=j+1,comp
            lambda(i,j)=lambda(j,j)*(1+alf(i,j))
         enddo
      enddo


c     inter
      do i=1,comp
         inter(i,i)=1
      enddo
      do j=1,comp
         do i=1,comp
            if (i.lt.j) then
               ks=i
               kl=j
            else
               ks=j
               kl=i
            endif
            inter(i,j)=exp(-(lambda(kl,ks)-lambda(i,i))/(R*Temp))
         enddo
      enddo

c     sgamma
      if (.not.(solid)) then
         do j=1,comp
            Sx(j,ST)=Lx(j,ST)
```

```
         enddo
      endif

      do i=1,comp

c     term1
         term(1)=0
         do j=1,comp
            term(1)=term(1)+(Sx(j,ST)*inter(i,j))
         enddo
         term(1)=log(term(1))

c     term2
         term(2)=0
         do j=1,comp
            topklsum=0
            bunnklsum=0
            do kl=1,comp
               topklsum=topklsum+Sx(kl,ST)*Inter(j,kl)
               bunnklsum=bunnklsum+Sx(kl,ST)*Inter(j,kl)
            enddo              ! kl
            term(2)=term(2)+Sx(j,ST)*(Inter(j,i)-topklsum)/bunnklsum
         enddo                  ! j

         lngamma(i)=-term(1)-term(2)
         sgamma(i)=exp(lngamma(i))
      enddo                     !i

      return
      end
```

H.2 Global Variables

```
C*****************************************************************
C   GLOBAL VARIABLES
C*****************************************************************
      integer Maxt,Maxcomp
      parameter (maxt=10000,maxcomp=6)
c     maxt; maximum # of liquid or solid calc. cells
c     maxcomp; maximum # of componets

      integer iterations, iter, RunTime,N,PresNo
      common/counters/iterations,iter,runtime,N,PresNo
C     iterations; total # of iterations
C     iter; current iteration
c     RunTime; iterations between dumping of runtime data
C     N; Number of equations to be solved during TDMA
C     PresNo;Presentation #

      real time, dt
      common/timecounters/time,dt
C     time; current time since start of calculation
C     dt; timestep

      integer LT,ST,comp
      common/geoint/LT,ST,comp
c     LT; total # of liquid calc. cells
C     ST; total # of solid calc. cells
c     comp; total # of components

      real H,L(maxt),S(maxt),L_B(maxt),S_B(maxt),interface,dxmp
      common/georeal/H,L,S,L_B,S_B,interface,dxmp
C     H; total lenght of exp. cell
c     L(i);position of midpoint in liquid cell # i
c     S(i);position of midpoint in solid cell # i
c     L_B(i);position of bottom in liquid cell # i
```

```
c     S_B(i);position of bottom in solid cell # i
C     interface position of liquid-solid interface
C     dxmp; change in interface during a timestep

      real LTemp(maxt),STemp(maxt),InitTemp,TopTemp,BottomTemp
      common/Tempvar/LTemp,STemp,InitTemp,TopTemp,BottomTemp
C     T(i);temperature in cell # i
C     LTemp(i);Temperature of liquid cell # i
C     STemp(i);Temperature of solid cell # i
C     InitTemp; Initial temperature of cell
c     TopTemp; temperature of top plate
c     BottomTemp; temperature of lower plate

      real lx(maxcomp,maxt),sx(maxcomp,maxt),z(maxcomp)
      common/comp/lx,sx,z
c     lx(j,i); molar fraction of component j in liquid cell # i
c     sx(j,i); molar fraction of component j in solid cell # i
c     z(i); molar fraction of component i in feed

      real LCompCp(maxcomp),SCompCp(maxcomp),SCp(Maxt),LCp(Maxt)
      Common/Cpvar/LCompCp,SCompCp,SCp,LCp
C     LCompCp(j);Heat capacity of pure liquid component j
C     SCompCp(j);Heat capacity of pure solid component j
C     SCp(i);Heat capacity in solid cell # i
C     LCp(i);Heat capacity in liquid cell # i

      real CompTransTemp(maxcomp),TransTemp
      Common/MeltPtvar/CompTransTemp,TransTemp
c     CompTransTemp(j); temperature of solid-liquid transition of comp.(j) (me
C     TransTemp;Temperature of solid-liquid transition at interface

      real CompEntMelt(maxcomp),EntMelt,CompSSEnt(maxcomp)
      Common/EntMeltVar/CompEntMelt,EntMelt,CompSSEnt
c     CompEntMelt(j); Entalphy of melting of component j
c     EntMelt(i);Entalphy of melting at interface
c     CompSSEnt(maxcomp), Solid-Solid Entalphy
```

```
      real CompMr(maxcomp),LMr(Maxt),SMr(Maxt),Mr
      Common/Mrvar/CompMr,LMr,SMr,Mr
C     CompMr(j); Molecular mass of component j
C     LMr(i); mol average molecular mass in liquid cell i
c     SMr(i); mol average molecular mass in solid cell i
C     Mr;  mol average molecular mass of the dissap. phase at the interf.

      real LCompRho(maxcomp),SCompRho(maxcomp),LRho(maxt),SRho(maxt)
      Common/Rhovar/LCompRho,SCompRho,LRho,SRho
C     LCompRho(j); Density of pure liquid component j
C     SCompRho(j); Density of pure solid component j
C     LRho(i); Density in liquid cell # i
C     SRho(i); Density in solid cell # i

      Real LCompCond(maxcomp),SCompCond(maxcomp)
      Common/CompCondvar/LCompCond,SCompCond
C     LCompCond(j);Liquid thermal conductivity of pure component j
C     SCompCond(j);Solid thermal conductivity of pure component j

      Real LCond(Maxt),SCond(Maxt),S_BCond(Maxt),L_BCond(Maxt)
      Common/CompCondvar/LCond,SCond,S_BCond,L_BCond
C     LCond; termal conductivity in liquid cell i
C     SCond; thermal conductivity in solid cell i
C     L_BCond(i);termal conductivity at bottom of liquid cell i
C     S_BCond(i);termal conductivity at bottom of solid cell i

      Logical solid
      Common/Logical/solid
C     Solid; true if solid phase exists

      real Alfa(maxt),Beta(maxt),Phi(maxt),D(maxt),C(maxt)
      common/Thomas/Alfa,Beta,Phi,D,C
C     parameters used in the Thomas algorithm
C     same notation as in chapter 7 of Versteeg & Malalasekera (1995)

      real Temp,Rho,CritTemp(MaxComp)
      common/EnvelopeTemp/Temp,Rho,CritTemp
```

```
c     Temp; Temperature which is considered  in phase calc.
C     Rho; Desity of the dissap. phase at the interphase
C     CritTemp;Critical temperature

      real K(MaxComp),VapHeatPar(MaxComp,2)
      common/equlibria/K,VapHeatPar
c     K(j); ratio between solid and liquid molfraction of component
C     VapHeatPar; Parameters needed to calc. heat of vaporization

      real R
      parameter(R=8.314510)
C     R;Gas Constant, Jmol^-1K^-1

      real A_B(MaxT)
      common/diff/A_B
C     A_B; parameter used in calc of diffusion=D*rho/Mr (between cells)

      real Waalsvol(MaxComp),LiqMolVol(Maxcomp),Cno(MaxComp)
      common/activitcoeff/WaalsVol,LiqMolVol,Cno
c     WaalsVol; van der Waals volume from Daubert:89
c     LiqMolVol; Liq. molar volume from daubert:89
c     Cno; Number of C-atoms

      real lgamma(MaxComp),sgamma(MaxComp)
      common/gammavalue/lgamma,sgamma
c     lgamma(j); liquid activity coefficient of component j
c     sgamma(j); solid activity coefficient of component j

      real liquidus(Maxcomp,11),solidus(maxComp,11)
      common/liqsol/liquidus,solidus
c     parameters to calculate the liquidus and solidus lines
```